ATTACHMENT B: AREA OF REVIEW AND CORRECTIVE ACTION PLAN [40 CFR 146.84(B)] CTV II

Table of Contents

Document Version History

Version	Submission Date	File Name	Description of Change
1	5/3/2022	Att B – AoR_CA CTV II	Original submission as part of CTV II storage project
2	8/4/2022	Att B – AoR_CA CTV II V2	Updated submission to address EPA Administrative review request for additional information dated 6/9/2022.
3	12/14/2022	Att B – AoR_CA CTV II V3	Updated submission to address EPA Administrative review request for additional information dated 9/21/2022, and for project expansion from two to five injectors
4	2/2/2023	Att B – AoR_CA CTV II V3.1	Updated to address EPA request
5	2/13/2023	Att B – AoR_CA CTV II V3.2	Updated to address EPA request
6	2/28/2024	Att B – AoR_CA CTV II V6	Revised based on EPA comment
7	11/26/2024	Att B - AoR CA CTV II V7	Response to August 29, 2024 EPA Comments
8	5/23/2025	Att B - AoR CA CTV II V8	Response to March 26, 2025 EPA Comments

Facility Information

Facility name: CTV II

Facility contact: Faisal Latif/Storage Development Manager
(661) 412-5000/Faisal.Latif@crc.com

Well location: Union Island Gas Field, San Joaquin County, CA
37.868/–121.420

1. Computational Modeling Approach

Computational modeling workflow begins with development of a three-dimensional (3D) representation of subsurface geology that leverages well data (bottom and surface hole location, wellbore trajectory, well logs, etc.) for rendering structural surfaces into a geocellular grid, and seismic information to map faults and flow barriers. Grid attributes include porosity, permeability, and facies distributions of reservoir lithologies by subzone, as well as observed fluid contacts and saturations for each fluid phase. This geologic model is often referred to as a static model, as it reflects the reservoir at a single moment. Carbon TerraVault Holdings LLC (CTV) licenses Schlumberger Petrel, an industry-standard geocellular modeling software platform, for building and maintaining static models. The static model becomes dynamic with the addition of the following:

- Fluid properties such as density and viscosity for each hydrocarbon and water phase
- Liquid and gas relative permeability
- Capillary pressure data
- Proposed injection well locations, completions, injection rates, and injection pressure over the life of the project

- Field pressure history
- Fluid geochemical analysis
- Rock and fluid compressibility

Results from the dynamic computational model are used to establish the area of review (AoR), the 'region surrounding the geologic sequestration project where underground sources of drinking water (USDWs) may be endangered by the injection activity' (EPA 75 FR 77230). In the case of the CTV II storage project, the AoR encompasses the maximum areal extent of the carbon dioxide (CO_2) plume (e.g., supercritical, liquid, or gaseous) plus a buffer zone, and this provides confidence that the corrective action well review and potential impact to the USDW is conservative and has been appropriately evaluated. Reservoir pressure will be at or below the initial/discovery pressure, minimizing the already minor potential for induced seismicity and ensuring no elevated pressure following injection.

1.1 Model Background

Computational modeling was completed using the Computer Modeling Group (CMG) Equation of State Compositional Simulator (GEM). GEM is capable of modeling enhanced oil recovery, chemical EOR, geomechanics, unconventional reservoir, geochemical EOR, and carbon capture and storage. GEM can model flow of three components (gas, oil, and aqueous) and multi-phase fluids, and can predict phase equilibrium compositions, densities, and viscosities of each phase. GEM incorporates all the physics associated with handling of relative permeability as a function of interfacial tension (IFT), velocity, composition, and hysteresis. Computational modeling for the CO_2 plume used the Peng-Robinson Equation of State, and the solubility of CO_2 in water is modeled by Henry's law. The Peng-Robinson Equation of State establishes the interaction/ solubility of CO_2 and residual gas in the reservoir. Solubility of CO_2 in aqueous phase was modeled by Henry's law as a function of pressure, temperature, and salinity.

1.2 Governing Equations

In CMG GEM, mass transfer includes solving the equations of volume constraint equations, component flow equations, and phase equilibrium equations.

1.2.1 Flow Equations

The material-balance finite-difference equations for the components in the oil and gas phases, and for the water component are:

$$\psi_i \equiv \Delta T_o^m y_{io}^m \left(\Delta p^{n+1} - \gamma_o^m \Delta D\right) + \Delta T_g^m y_{ig}^m \left(\Delta p^{n+1} + \Delta P_{cog}^m - \gamma_g^m \Delta D\right)$$

$$+ q_i^m - \frac{V}{\Delta t} \left[N_i^{n+1} - N_i^n \right] = 0 \qquad i = 1, ..., n_c$$

(Eq-1)

$$\psi_{n_c+1} \equiv T_w^m \left(\Delta p^{n+1} - \Delta P_{cwo}^m - \gamma_w^m \Delta D\right) + q_{n_c+1}^m - \frac{V}{\Delta t}\left[N_{n_c+1}^{n+1} - N_{n_c+1}^n\right] = 0 \quad \text{(Eq-2)}$$

where $N_i (i = 1, \ldots, n_c)$ = the moles of Component *i* per unit of grid block volume
N_{n_c+1} = the moles of water per unit of grid block volume
n = old time level
n+1 = current time level

The N_is are related to porosities, phase molar densities, saturations, and compositions as follows:

$$N_i = \phi\left(\rho_o S_o y_{io} + \rho_g S_g y_{ig}\right) \qquad i = 1, ..., n_c \quad \text{(Eq-3)}$$

$$N_{n_c+1} = \phi \rho_w S_w \quad \text{(Eq-4)}$$

1.2.2 Phase-Equilibrium Equations

If the hydrocarbon system is in the two-phase region at a given *p*, *T* and $N_i (i = 1, \ldots, n_c)$, the phase compositions and splits can be obtained by solving the thermodynamic-equilibrium equation:

$$\mathbf{g}_i \equiv \ln f_{ig} - \ln f_{io} = 0 \qquad i = 1, ..., n_c \quad \text{(Eq-5)}$$

for N_{ig}, the moles of Component *i* in the gas phase. The moles of Component *i* in the oil phase, N_{io}, can be obtained as follows:

$$N_{io} = N_i - N_{ig} \qquad i = 1, ..., n_c \quad \text{(Eq-6)}$$

1.2.3 Saturation Equation

The saturations are related to N_i and $\rho_m (m = o,g,w)$ through the following equations:

$$S_w = N_{n_c+1} / \left(\phi \rho_w\right) \quad \text{(Eq-7)}$$

$$S_o = (1 - S_w) \frac{N_o/\rho_o}{N_o/\rho_o + N_g/\rho_g} \quad \text{(Eq-8)}$$

$$S_g = (1 - S_w)\frac{N_g/\rho_g}{N_o/\rho_o + N_g/\rho_g} = 1 - S_w - S_o$$

(Eq-9)

1.2.4 Mole or Volume Consistency Equations

Mole or volume consistency equations include the following:

$$\psi_p \equiv \sum_{i=1}^{n_c+1} N_i^{n+1} - \phi^{n+1}(\rho_o S_o + \rho_g S_g + \rho_w S_w)^{n+1} = 0$$

(Eq-10)

Nomenclature for the mass transfer equations is listed below:

D	depth
f_{ij}	fugacity of component i in phase j
F	function
$\mathbf{g}$	phase-equilibrium function
n_b	number of gridblocks
n_c	number of components
N_i	moles of component i per unit block volume
p	pressure
P_{cog}	oil-gas capillary pressure
P_{cwo}	water-oil capillary pressure
q	injection/production rate
t	time
T_j	transmissibility of phase j
V	gridblock volume
y_{ij}	mole fraction of component i in phase j
γ	specific gravity or gravity term in flow equation
Δt	timestep
ρ_m	molar density of phase m
ϕ	porosity
ψ	function

(k)	iteration level
n	old time level
n+1	new time level
i	component
j	phase
o	oil
g	gas
w	water

GEM can also handle non-isothermal reservoir condition, which involves development of an energy equation to calculate temperature distribution in the reservoir for the compositional processes where reservoir temperature could change with time (e.g., when the injected fluid is at a different temperature than the one prevailing in the reservoir). This includes solving the energy balance equation and mass transfer equations simultaneously.

1.2.5 Energy Balance Equation

The energy balance equation involving convection, conduction and heat losses to the surroundings is:

$$\psi_T \equiv \Delta T_o^m H_o^m \left(\Delta p_o^{n+1} - \tilde{\rho}_o^m g \Delta D\right) + \Delta T_g^m H_g^m \left(\Delta p_o^{n+1} + \Delta P_{cog}^m - \tilde{\rho}_g^m g \Delta D\right)$$

$$+\Delta T_w^m H_w^m \left(\Delta p_o^{n+1} - \Delta P_{cwo}^m - \tilde{\rho}_w^m g \Delta D\right) + \Delta \tau_c^m \Delta T^{n+1} + Q_{loss} + \sum_k H_k^{n+1} q_k^{n+1}$$

$$-\frac{V}{\Delta t}\left[\phi^{n+1}\left(\sum_k \rho_k^{n+1} S_k^{n+1} U_k^{n+1}\right) - \phi^n \left(\sum_k \rho_k^n s_k^n U_k^n\right)\right]$$

$$-\frac{V}{\Delta t}\left[\left(1-\phi_0\right) c_R \tilde{\rho}_R \left(T^{n+1} - T^n\right)\right] \;=\; 0, \;\; k = o, g, w \qquad \text{(Eq-11)}$$

where

c_R = heat capacity of rock

H_k = molar enthalpy of Phase k(k = o,g,w)

S_k = saturation of Phase k(k = o,g,w)

Q_{loss} = heat loss rate to the (over/underburden) surroundings

T = temperature

ϕ = Porosity (0 = initial; n+1 = current timestep; n = previous timestep)

U_k = H_k - p/p_k; molar internal energy of Phase k

$\tilde{\rho}_R$ = Rock mass density

τ_c = total thermal conductivity of rock and fluids

1.2.6 Enthalpy Calculations

The enthalpy of the water phase is calculated from a look-up of the steam table. The oil and gas enthalpies are calculated from an EOS as follows.

The excess enthalpy for a fluid, which is the difference of the enthalpy at p and T and the ideal gas enthalpy at zero pressure and T, can be calculated from an EOS:

$$\Delta H^E = H - H^* = RT\,(Z-1) + \int_{\infty}^{v} \left[T\left(\frac{\partial p}{\partial T}\right)_v - p \right] dv \qquad \text{(Eq-12)}$$

where

R = universal gas constant

v = molar volume

Z = compressibility factor

The above quantity is also referred to as enthalpy departure. Using Equation 12, the following equation can be derived to calculate enthalpy departure for the SRK or PR EOS:

$$\Delta H^E = RT\,(Z-1) + \frac{T\,(\partial a/\partial T) - a}{b\,(\delta_2 - \delta_1)} \ln\left(\frac{v+\delta_2 b}{v+\delta_1 b}\right) \qquad \text{(Eq-13)}$$

where

$\delta_1 = 1 - \sqrt{2}$; $\delta_2 = 1 + \sqrt{2}$ for the PR EOS, and

$\delta_1 = 0$; $\delta_2 = 1$ for the SRK EOS

and a and b are EOS parameters.

1.2.7 Heat Loss Calculation

The heat loss to the overburden and underburden is calculated using the method of Vinsome and Westerveld (1980). They assumed a temperature profile in the overburden and underburden of the form:

$$T(t,z) = (\theta - \theta^0 + b_1 z + b_2 z^2) \exp(- z / d) + \theta^0) \quad \text{(Eq-14)}$$

where

$T(t,z$ = over/underburden temperature at time t at a distance z from the reservoir boundary

b_1, b_2 = time-dependent parameters

d = thermal diffusion length

θ = temperature in the boundary grid block

θ^0 = initial temperature in boundary grid block

The diffusion length is taken as:

$$d = \frac{\sqrt{\eta t}}{2} \quad \text{(Eq-15)}$$

where η is the thermal diffusivity

$$\eta = \frac{\kappa_R}{c_R \tilde{\rho}_R} \quad \text{(Eq-16)}$$

where

c_R = rock heat capacity

$\tilde{\rho}_R$ = mass density of rock

κ_R = rock thermal conductivity

Vinsome and Westerveld (1980) derived the following expression for b_1 and b_2 and the heat loss rate:

$$b_1^{n+1} = \frac{\dfrac{\eta \Delta t \left(\theta^{n+1} - \theta^0\right)}{d^{n+1}} + \xi^n - \dfrac{\left(d^{n+1}\right)^3 \left(\theta^{n+1} - \theta^n\right)}{\eta \Delta t}}{3(d^{n+1})^2 + \eta \Delta t} \qquad \text{(Eq-17)}$$

$$b_2^{n+1} = \frac{2b_1^{n+1}\left(d^{n+1}\right) - \left(\theta^{n+1} - \theta^0\right) + \dfrac{\left(d^{n+1}\right)^2 \left(\theta^{n+1} - \theta^n\right)}{\eta \Delta t}}{2(d^{n+1})^2} \qquad \text{(Eq-18)}$$

$$\xi^n = \left[\left(\theta - \theta^0\right) d + b_1 d^2 + 2b_2 d^3\right]^n \qquad \text{(Eq-19)}$$

$$Q_{loss} = \kappa_R A \left[\frac{\left(\theta^{n+1} - \theta^0\right)}{d^{n+1}} - b_1^{n+1}\right] \qquad \text{(Eq-20)}$$

where A is the cross-sectional area for heat loss to the overburden/underburden.

1.2.8 Well Model

Each injector was incorporated into the dynamic model using the well model. The injection well model correlates the reservoir flow rate of phase j (j=g(gas), w(water)) to the wellbore bottom-hole pressure (P_{bh}) and the pressure at grid point via the following relationship:

$$Q_j = \sum_l WI_l \, \lambda_{T,l} (p_{bh} - p_{o,i}) \qquad j = g, w \qquad \text{(Eq-21)}$$

$$WI = 2\pi \ \text{ff} \ kh \frac{wfrac}{\ln\left(r_e / r_w\right) + S} \qquad j = g, w \qquad \text{(Eq-22)}$$

where Q_j = flow rate of phase j(j = g,w) at reservoir conditions (cubic meters per day [m^3/d] or cubic feet per day [ft^3/d])
p_{bh} = bottom-hole pressure (kiloPascals [kPa] or pounds per square inch, actual [psia])
$p_{o,i}$ = pressure of ith grid block containing the well (kPa or psia)
$W_{Ij,1}$ = well injectivity index for phase j(j = g,w) to layer 1
w_{frac} = well fraction, governed by areal geometry
k = effective permeability in the plane perpendicular to the well direction
h = gridblock thickness in well direction (meters or feet)
λT = total mobility of the fluid in the well block. The relative permeabilities are calculated using the gridblock saturation
r_w = wellbore radius (meters or feet)
r_e = effective radius (meters or feet)
A_i = area of i-th gridblock perpendicular to well direction (square meters [m^2] or square feet [ft^2])
CC = geometric factor
S = skin factor (dimensionless)
ff = fraction of completion of the well in the gridblock
$\sum_l$ = summation over all layers

The well model is a generalization of the well model proposed by Peaceman (1987) and Peaceman (1983) for square and non-square gridblocks. The mobility treatment follows the suggestion of Chappelear and Williamson (1981). In addition, the geometric factor allows the determination of the equivalent radius from both the geometry of the gridblock and the location of the well in the grid block.

1.3 CO_2 Plume and Storage Volume

The dynamic model simulates the potential quantity of CO_2 stored, and simulates lateral and vertical movement of the CO_2 to define the AoR. The simulator predicts the evolution of the CO_2 plume by:

- Incorporating complex reservoir geometry and wells and using a full field static geological 3D characterization of the reservoir incorporating lithology, saturation, porosity, permeability, and seismic interpretation.
- Forecasting the CO_2 plume movement and growth by inputting the operating parameters into simulation (injection pressure and rates).
- Assessing the movement of CO_2 after injection ceases and allowing the plume to reach equilibrium, including pressure equilibrium and compositions in each phase.

The CMG GEM software has been used in numerous CO_2 sequestration peer-reviewed papers, including Nghiemw et al. (2004), Zhang et al. (2014), and Tran et al. (2009).

1.4 Site Geology and Hydrology

The Union Island Gas Field is a northeast-southwest trending faulted anticlinal structure located at the southern end of the Sacramento Basin of California. Historical and current gas production is sourced from the Late Cretaceous Winters Formation in the footwall along a regional reverse fault, the Stockton Arch fault. As described in **Attachment A: Narrative**, the Winters Formation is the proposed Injection Zone. Different gas-water contacts observed at the time of the field's discovery indicate a flow barrier exists within the Injection zone, between the northern and southern halves of the field. The reservoir sands were deposited as a series of coalesced channels at the base of the slope on the upper channelized portion of a sandy suprafan. The Injection Zone reservoir is present across the entire project area and is offset by the Stockton Arch fault, as shown in **Figure B-1**.

The Injection Zone is bound above by the Starkey-Sawtooth Shale and below by the Delta Shale. The Delta Shale Formation consists of an approximately 157-foot shale barrier. This shale has an average permeability of 0.04 millidarcies (mD) and porosity of 14.7 percent. The Starkey-Sawtooth Shale has an average gross thickness of over 2,200 feet and a very low matrix permeability, which makes it a competent Upper Confining Zone in preventing the upward migration of fluids.

The Injection Zone reservoir was discovered in the 1970s, and has been developed with primary production (**Table B-1**). Over 50 years, reservoir pressure has declined from 5,040 pounds per square inch (psi) to 1,200 psi, indicating a closed reservoir with limited water influx and/or connection to an aquifer (DOGGR, 1998; Leong and Tenzer, 1994).

Well data, open-hole well logs, and core data (**Figure B-2**) define the subsurface geological characteristics of stratigraphy, lithology, and rock properties. Reservoir performance information (production rates and volumes, reservoir and wellbore pressures) complements the static characterization by adding the dynamic components, such as reservoir continuity and hydrogeology.

1.5 Model Domain

A static geological model developed with Schlumberger Petrel was the computational modeling input. Model domain information is summarized in **Table B-2**.

The geocellular grid was initially built with uniformly spaced 100-foot by 100-foot cells throughout the 36.9-square mile model area (**Figure B-3a**). This was then upscaled to 200 feet by 200 feet for the dynamic modeling based on grid designing. These grid dimensions allow for adequate resolution of plume development as demonstrated by a grid refinement sensitivity analysis, which includes 10 areas around each injector, refining the current grid from 200 feet by 200 feet to 40 feet by 40 feet and maintaining the vertical resolution. Results show 1 percent difference for storage volume, plume boundary with minor difference and maximum injection pressure for local grid refinement model approximately 10 percent lower. This demonstrates that the submitted case is conservative. Finer resolution for the grid will prevent the simulation from running efficiently, and a coarser grid may not adequately simulate plume movement.

Horizontal grid size is important to ensure that the model represents the geologic structure, optimizes well locations, maintains volumetric balance, describes flow units properly, and calculates fluid flow in an appropriate way. Property upscaling maintained the volumetric and geologic heterogeneity, including net-to-gross (NTG), permeability, porosity, and end points. NTG is volume-weighted arithmetic average, permeability is a volume-weighted geometric average, and porosity is a volume- and NTG-weighted arithmetic average. The 100-foot by 100-foot (horizontal) by 5-foot vertical fine geologic static grid was chosen to capture significant heterogeneity aerially and vertically that ensures accurate upscaling of log data and distribution of reservoir properties in the static model (**Figure B-3a**). Based on a smaller sector model sensitivity analysis, from 100 feet by 100 feet upscaled to 200 feet by 200 feet, storage volume reduced by 3.6 percent, plume boundary differences were minor, and maximum injection pressure increased slightly. The 200-foot by 200-foot by 9-foot (averaged, 5 to 14 feet by proportional layering methodology) coarser dynamic model grid maintains important features of the fine geomodel grid, and allows for reasonable computational time. The predicted storage volume, reservoir pressure, and plume boundary were similar for sensitivity analyses testing a finer grid. **Figure B-4** shows a comparison of fine resolution model data and the associated upscaled dynamic model data.

The geologic model was populated with properties using petrophysical modeling algorithms available in Petrel. Properties were distributed in the model by upscaling the well log data to the grid cells that the wells intersect. The upscaled data were then distributed between wells using sequential gaussian simulation (SGS). SGS is a stochastic estimation algorithm based on the Geostatistical Software Library (GSLIB) developed at Stanford University (Deutsch and Journel, 1997). SGS uses well data, data distribution, variograms, and trends to estimate property values between wells.

Preferential flow pathways are primarily caused by reservoir heterogeneity, especially for permeability. The current dynamic fluid flow model captures this heterogeneity by incorporating geologic property variability (facies, porosity, permeability) based on well logs and guided by realistic spatial trends (variograms) away from the wells. This heterogeneity captures preferential flow pathways within the model.

The influence of grid orientation on fluid flow is more pronounced at high mobility ratio conditions. To optimize performance prediction, grid orientation should account for the principle direction of fluid flow and along the principal axes of the permeability. Considering the structure difference to the north and south, fault orientation, and boundary conditions, the project grid was designed to align west to east. In order to investigate the grid orientation effect, a nine-point spatial discretization sensitivity case was conducted. This sensitivity run indicated 5 percent increased storage compared to the base case, and plume boundary acreage reduced by 0.1 percent. This confirmed that the base case is conservative.

Model boundaries were defined to include the entire footwall portion of the Injection Zone's anticlinal structure that is bound to the east by the Stockton Arch fault (**Figure B-3a**). To the north, transition of the Winters to a predominantly shaley section is implemented as a closed boundary (**Figure B-2**). The flow barrier identified at discovery is modeled by a material property boundary and partially separates the northern and southern portions of the field.

An average vertical cell height of 5 feet was used initially over the model domain to generate grid layers within the geomodel as shown in **Figure B-5**. The average 5-foot cell height provides the vertical resolution necessary to capture significant lithologic heterogeneity (sand versus shale), which helps to ensure accurate upscaling of log data and distribution of reservoir properties in the static model. To optimize run times and make the dynamic model run more efficiently, some vertical upscaling was done for the dynamic flow model such that vertical thickness within the model depends on the vertical proportion of each sandy body. Final cell thickness ranges from 5 to 14 feet, with an average height of 9 feet. **Figure B-6** shows a comparison of open-hole log data and the associated upscaled logs for a well within the AoR.

Current assumed caprock is water-saturated without pressure depletion. A mechanistic model was built to evaluate CO_2 leakage to caprock because of pressure elevation with CO2 injection (**Figure B-3b)**. The model includes caprock and the Winters Injection Zone. Winters properties are the same as the full field model. Starkey-Sawtooth confining zone properties are based on Lathrop shale samples MICP data. Average permeability is 0.00098 mD and entry pressure is 1,491 psi. Model results show 5 feet of CO_2 leakage vertically from Injection Zone to caprock near the injector (**Figure B-3b)**. The total leakage is around 0.002 percent over total injection mass.

The Injection Zone/Confining Zone interface is treated as a no-flow boundary during full field dynamic modeling based on caprock sensitivity results. During pre-operational testing, more site-specific caprock input data will be collected, the model will be updated, and the AoR will be reevaluated.

1.6 Porosity and Permeability

Wireline log data were acquired with measurements that include but are not limited to spontaneous potential, natural gamma ray, borehole caliper, compressional sonic, resistivity, neutron porosity, and bulk density. **Table B-3** summarizes the computational model input parameters and sources.

Formation porosity is determined one of two ways: from bulk density using 2.65 gram per cubic centimeter (g/cc) matrix density as calibrated from core grain density and core porosity data, or from compressional sonic using 55.5 microseconds per foot (µsec/ft) matrix slowness and the Raymer-Hunt equation.

Volume of clay is determined by spontaneous potential, and is calibrated to core data.

Log-derived permeability is determined by applying a core-based transform that uses capillary pressure porosity and permeability along with clay values from X-ray diffraction (XRD) or Fourier transform infrared (FTIR) analysis. Core data from two wells with 13 data points were used to develop a permeability transform (**Figure B-7**). An example of the transform from core data is illustrated in **Figure B-8**.

Figure B-9 shows porosity and permeability histograms for the Injection Zone. Porosity is derived from open-hole well log analysis and permeability is a function of porosity and clay

volume. **Figures B-10a and B-10b** show the distribution of permeability and porosity using Sequential Gaussian simulation (kriging) within the static model. Reservoir quality is the highest at the top of the faulted anticline.

1.7 Constitutive Relationships and Other Rock Properties

The proposed Injection Zone reservoir has a gas cap underlain by a basal water zone. Contacts for gas and water depths are derived from open-hole well logs and production analysis and verified through simulation and history matching. Single values for the saturation have been assumed for the computational model study for the regions above and below the gas-water contact at the start of CO_2 injection. **Table B-4** shows the reservoir contacts and saturations used in the computational model.

With only gas and water present in the reservoir, one set of two-phase relative permeability relationships is needed to determine the flow characteristics of each component and/or phase, where K_{rw} (water relative permeability) and K_{rg} (gas relative permeability) are functions of gas saturation.

Relative permeability and capillary pressure were derived from special core analysis from the specific site. Two samples from Sonol Securities 6 were used to normalize, average, and denormalize the relative permeability. The gas/water RPM Corey model used to match the laboratory data. Parameters used included:

- s_{gc} = 0.00 fraction, connate gas saturation
- s_{gcrit} = 0.05 fraction, critical gas saturation
- K_{rw} at s_{gc} = 0.447
- Residual water saturation = 0.54, scale up to 0.34 during dynamic modeling
- K_{rg} at residual water saturation = 0.32
- Gas relative permeability curvature to water = 2.6
- Water relative permeability curvature to gas displacement = 3.5

The computational flow model incorporated the effect of hysteresis on gas relative permeability. Maximum trapping gas saturation of 0.25 is assumed. Imbibition and scanning curves are calculated by the Land's method. The Land's constant C is calculated using the following equation:

$$C = \frac{1}{S_{grmax} - S_{gcrit}} - \frac{1}{S_{gmax} - S_{gcrit}} \quad \text{(Eq-23)}$$

The trapping function is:

$$S_{grh} = \frac{S_{gh} - S_{gic}}{1 + C\,(S_{gh} - S_{gic})} \qquad \text{(Eq-24)}$$

where S_{gic} = critical reversal gas saturation for trapping
S_{gcrit} = critical gas saturation.
S_{gh} = the value of S_g when the shift to imbibition occurs
S_{grh} = maximum trapped gas saturation corresponding to reversal saturation S_{gh}
S_{grmax} = maximum trapped gas saturation
S_{gmax} = Maximum saturation

Capillary pressure data were obtained from Sonol Securities 5, which is close to Sonol Securities 6. Two representative samples used for capillary curve generation measured by Centrifuge methods. Laboratory-tested capillary pressure was converted to reservoir condition, averaged by J-function, and then the capillary pressure curve was derived based on the average permeability and porosity. Both the relative permeability curve and capillary pressure were scaled up to the residual water saturation of 0.34 based on field development and published data.

There are two facies defined in the model: sand and shale. Only one set of relative permeability and capillary pressure curves was used for each facies. **Figures B-11a and B-11b** show the relative permeability curves (Reference case, Case J, and Case K). **Figure B-12** shows the capillary pressure curve used in the computational model.

During pre-operational tests, more core will be collected, more special core analysis will be acquired, and the model will be updated accordingly. Also, as discussed below, several sensitivity analyses were conducted to investigate the uncertainty related to these parameters.

1.8 Mineralization

Previous studies into reactive transport modeling and geochemical reaction in carbon capture and storage (CCS) have shown that the amount of CO_2 trapped by mineralization reactions is extremely small over a 100-year post-injection time frame (IPCC, 2005) for sandstone reservoirs. For the sake of computational efficiency and the minor expected effect on the AoR, reactive transport was not included as a part of the compositional simulation modeling.

Potential geochemical reactions of the Injection Zone, Confining Zone, and formation fluids with the injectate streams being considered were modeled using PHREEQC (ph-REdox-Equilibrium), the U.S. Geological Survey (USGS) geochemical modeling software. Details on the modeling procedure and results are provided in the Section 2.8.3 of **Attachment A**, and in **Appendix 3: CTV II Geochemical Modelin**g. The modeling indicates, as expected, that as the formations are stable quartz dominated mineralogy, the effect of geochemical reactions with the injectate will be minor, with a predicted net molar mass increase (precipitation) of 1.5 to 2 percent, which is not expected to have a major impact on porosity or permeability in the Injection Zone or Upper Confining Zone.

1.9 Boundary Conditions

Model boundaries were defined to include the entire footwall portion of the Injection Zone that is bound to the east by the Stockton Arch fault (**Figure B-3**). To the north, transition of the Winters to a predominantly shaley section is implemented as a closed boundary (**Figure B-2**). The northern boundary of the model is based at the 0-foot net sand line as mapped in a regional study by the California Geological Survey (Downey, 2010). Because this boundary is based on the mapped extent of the Winters sands, other locations for the northern boundary were not considered. The lack of aquifer support in the field's production history also suggests a close boundary to the north.

The flow barrier identified at discovery is modeled as a material property boundary and partially separates the northern and southern portions of the field. The Winters Formation at Union Island is a 300-foot-thick lobe of Winters sand with a complex series of sand filled channels with rapid lateral and vertical stratigraphic changes (Hill, 1979). The internal barrier in the field is due to these stratigraphic changes, which have a major effect on the hydrocarbon accumulation in this field. For the simulation model, the partial flow barrier presented in **Figure B-13** has a transmissibility multiplier of 0 and does not extend to the western edge of the model boundary. Based on a sensitivity analysis removing the partial flow barrier, the storage volume increases approximately 4.5 percent and the plume is contained within the submitted AoR. Therefore, the reference case is considered conservative (resulting in a larger CO_2 plume).

No-flow boundary conditions were applied to the edges of reservoir in the computational flow modeling. These conditions were based on the following:

- The Upper Confining Zone is continuous through the area, has a low permeability (0.00098 mD based on Lathrop shale samples MICP data), and has confined oil and gas operations (see Section 2.4 of **Attachment A**).
- Stockton Arch fault is assumed to be sealing (see **Attachment A**).
- North edge net thickness zeros out because of facies change.
- Performance data from operating the field indicates limited active aquifer including
  - Material balance (MBAL) analysis.
  - Historical production data (**Figure B-14**) show limited water production.
  - Pressure in the reservoir is currently at 1,200 psi from a discovery pressure of 5,040 psi, demonstrating limited aquifer influx (DOGGR, 1998; Leong and Tenzer, 1994).

1.10 Initial Conditions

The initial conditions at the time of CO_2 injection were established based on information gained over time as the reservoir was developed for gas production. The model was initialized based on the most recent pressure data of 1,200 psi in the reservoir gas cap from well Pool B-2 based on pressure and temperature gradient survey in 2022, which matches well with material balance based on the field production since 1972. Minor gas production occurred after this measurement

and the field has completely shut down since June 2023. Additional pressure data will be gathered during the pre-operational testing phase to confirm that the pressure in the gas cap is as expected, and AoR modeling will be updated if necessary. During initialization, the model was used to calculate each point reservoir pressure based on the depth and fluid density. Initial conditions for the model are given in **Table B-5**. Base case simulations do not include a geothermal gradient. A sensitivity analysis incorporating a geothermal gradient of 0.0159561°F/foot was conducted, and results were found to be similar to the base case, which has storage volume and plume size reducing by around 1 percent.

1.11 Operational Information

Details on the model-assumed injection operation are presented in **Table B-6**. Injection wells were assumed to be perforated throughout the entire thickness of the injection zone in each location. All injection wells are constant-rate controlled subject to a maximum allowable injection pressure. Additionally, injection will stop once the reservoir pressure reaches 4,500 psi, as discussed in Section 1.12.

1.12 Fracture Pressure and Fracture Gradient

In the past, produced water from the field had been injected into the Mokelumne Formation by well GALLI 1. The Class II permit approved maximum operating pressure gradient for that zone was 0.80 psi per foot (psi/ft). A 0.7 psi/ft fracture gradient is currently assumed for the Injection Zone. CTV will conduct a step rate test in the injection zone as part of the pre-operational testing plan to confirm this fracture pressure gradient.

At this time, no fracture gradient information has been found for the Upper Confining Zone. CTV will conduct a step rate test for the Upper Confining Zone per the pre-operational testing plan.

The currently assumed maximum injection pressures for the injection wells, calculated at the top perforation using a 0.7 psi/ft fracture gradient and a 10 percent safety factor per EPA guidance, are shown in **Table B-7**. The average operating conditions of the injectors are also shown, and CTV will ensure that the wells never cross the maximum injection pressures. Further details can be found in **Appendix 4: Operational Procedures**.

1.13 Time Steps

Adaptive time-stepping control was used during simulation, and the time step duration was between a minimum of 0.00001 day to maximum of 31 days.

2. Computational Modeling Results

2.1 Predictions of System Behavior

Computational modeling cases were run using two injectate streams representing potential injectate compositions from different sources. Details of the injectate composition are covered in Section 7.2 of **Attachment A**.

2.1.1 Carbon Dioxide Plume

Maps (**Figures B-15a and B-15b**) and cross sections (**Figures B-16a and B-16b**) show the computational modeling results and development of the CO_2 plume at different time-steps for two injectate composition scenarios (see injectate composition discussion in Section 7.2 of **Attachment A**). **Figures B-17a through B-17e** display cross section diagrams of the plume evolution for the 100 percent CO_2 injectate scenario at injection well locations. The boundaries of the AoR are defined with a 0.01 CO_2 global mole fraction cutoff of 100 years post-injection plus a buffer zone.

As shown in **Figures B-15a through B-16b**, the CO_2 extent is largely defined by the end of injection (Year 23.5). By Year 30 after the end of injection, for both Injectate 1 and Injectate 2, the plume is largely stabilized, with very little further movement seen in comparison to the 100-year post end of injection plume extent. There is minor movement from 50 to 100 years, mainly because the Injection Zone is a dry gas field and, with continued CO_2 injection, some dry gas accumulates at the reservoir upper boundary. After the CO_2 injection stops, pressure and composition equilibrate due to CO_2 buoyancy, and some CO_2 replaces the accumulated dry gas.

For both injectates, the majority of the CO_2 injectate remains as super-critical CO_2 (88 percent), with the remaining portion of the CO_2 dissolving in the formation brine over the simulated 100 years post-injection.

Figure B-18 shows the cumulative storage for each of the mechanisms for Injectate 1 and Injectate 2.

2.1.2 Simulated Pressure Increase

The 5-points method was used to calculate the average reservoir pressure near the injectors, which is pore volume weighted average pressure of the block containing each well's bottom-hole reference layer and four of its immediate neighboring blocks. **Figures B-19a through B-19c** show pressure at each injection well for the three injectate cases. **Figure B-20a** shows average reservoir pressure within the AoR. Pressure profiles are identical for the three injectates. Average pressure increases to a maximum (4,500 psi) at the end of the injection period, decreases by less than 10 percent from the peak value in the 10-year period following injection, and then remains essentially constant for the remainder of the simulation.

Figure B-21 displays a plan-view of pressure at time steps from 1 year of injection to 98 years after injection ends. **Figure B-22a** displays 3D pressure and pressure in cross-section view at each injection well. These figures show that there is no location that has reservoir pressure building back to original reservoir pressure, and all the pressure built up against the Stockton Arch fault is below 4,900 psi.

2.2 Model Validation

The Union Island Gas Field was discovered in 1972, and has been produced from the Winters Formation for around 50 years. This operational experience provides insight into the reservoir continuity. The plume model results were compared against the area of the reservoir that has

been depleted by gas production and against initial gas contacts. Historical cumulative gas production and CO_2 saturation distribution at 100 years post-injection align quite well (**Figure B-23**). This comparison confirms that the simulated CO_2 plume extent is consistent with areas where gas has previously been produced. **Figure B-22b** shows the trapped and dissolved CO_2 distribution at 100 years post injection for the 100 percent CO_2 injection case.

2.3 Sensitivity Analyses

The reference base case is considered a sufficiently realistic representation of the hydrogeologic structure and conditions at the proposed injection site suitable for delineating the AoR. Sensitivity analyses were performed to examine the impacts of various assumptions on the simulation results. Sensitivity scenarios listed in **Table B-8** were run varying major inputs to the simulation to see whether they have any significant impact on the AoR boundary. All cases were run with injection ceasing once the depleted reservoir had been pressured back up to 90 percent of discovery pressure (in addition to maximum allowable injection pressure control for each injector, which is based on 0.7 psi/ft frac gradient plus 10 percent safety factor). The results from the different scenarios were reviewed and showed varying final CO_2 storage amount but minimal impact to the AoR boundary.

Sensitivity analyses demonstrate that the AoR, as defined by the maximum extent of CO_2 plume plus a buffer, is consistent for a range of model assumptions. This provides confidence that the corrective action well review and potential impact to the USDW is conservative and has been appropriately evaluated.

2.3.1 CO_2 Injectate Effect on Plume and AoR Modeling Results

The compositional simulation model was run for the two simplified injectate compositions discussed in **Attachment A**, Section 7.2, and their results were also compared against a 100 percent CO_2 injectate case. The cumulative volume, rate, and injection duration for all three cases was similar for the simulations.

The Injection Zone CO_2 plume for Injectate 1 and Injectate 2 is consistent with the plume outline for 100 percent CO_2 injectate (**Figure B-24a**), with negligible difference between the three cases. The CO_2 plume outline was defined by a 0.01 global CO_2 mole fraction cutoff of 100 years post-injection for all three cases, which encompasses greater than 99 percent of the injected mass within the plume boundaries. Potential corrective action wells that fall within the CO_2 plume are the same for all three cases. The final AoR was delineated using final plume boundary plus 500 feet buffer. The final $scCO_2$ plume boundary is shown on **Figure B-24b**, overlaid with each other for the three scenarios. $scCO_2$ plume boundary is defined by 0.05 gas saturation cutoff 100 years post-injection.

Additionally, the average pore volume pressure within the approximate AoR boundary was plotted for the three cases and overlaid (**Figure B-20a**); the cumulative injection and injection rate are shown on **Figure B-20b**. Multiple scenarios were also run to test the effect of mixing Injectate 1 and Injectates 2 in different ratios on the AoR boundary and plume shapes. As expected, because the resulting mixed injectates were still high-purity CO_2 streams with impurity

concentrations in between those of Injectates 1 and 2, the plume shapes for these scenarios were within the envelope represented by the end point compositions. Near injector reservoir pressure data are shown on **Figures B-19a through B-19c**.

In summary, there is minimal effect of the minor components on the CO_2 plume shape and the AoR boundary for the proposed injectate compositions. As such, CTV's plume and AoR modeling for corrective action assessment is adequate for the expected injectate composition ranges. CTV will confirm that the properties of the injectate are consistent with the model inputs during the pre-operational phase. In addition, the AoR will be reviewed per Section 6.

2.3.2 Model Parameters and Boundary Conditions

As shown on **Table B-8**, major inputs with potential impacts on AoR delineation were included in the additional sensitivity analyses. These include permeability, porosity, reservoir compaction, phase trapping, relative permeability end points and shape, initial gas saturation, boundary condition, nine-point spatial discretization, geothermal gradient, and non-isothermal effects. For this dry gas reservoir, sector model work has shown that capillary pressure is not a very sensitive parameter based on the range of reasonable changes. Additionally, capillary pressure was changed by increasing 30 percent and reducing 30 percent based on base case for the full field model, which shows storage volume change of -1.8 percent to 1.9 percent and plume size change of -1.4 percent to 2.2 percent; therefore, it was not included in the analysis. All the following sensitivity analyses are based on 100 percent CO_2 injectate.

Sensitivity results are summarized in **Figures B-25 through B-28b**. Storage volume range is 19.3 MMT to 27.3 MMT; compared to reference case, storage volume change is less than 10 percent for most cases. Plume extent is within the submitted AoR, except for Case A with permeability multiplier by 3. Even Case A storage volume increased by only 4 percent, and plume size changed only 0.2 percent, with plume extent shifted to the northeast. Relative permeability end points have more impact on storage volume and less impact on plume size; relative permeability shapes have less impact on storage volume, but more impact on plume size. Case H, Case I, Case J, and Case K calculated plume boundaries are still within submitted AoR.

There are four cases with storage volume changes more than 10 percent, including Case L, Case O, Case B, and Case M. Case L and Case M both added gas saturation 0.05 and 0.03 between the current gas-water contact (GWC) to original GWC. These changes result in increases in storage volume of 13 to 20 percent, and plume size changes of 10 to 15 percent. Plume boundaries in each case are still within the submitted AoR. The reference case is the most conservative case, with the depleted dry gas reservoir and set initial gas saturation as zero between these two contacts. Case O includes the west side and south side pore volume multiplied by 10, and both storage volume and plume size will increase around 15 percent. Case B is permeability multiplied by 0.3, and in this case storage volume is reduced by 15 percent and plume size is reduced by 6 percent.

Overall, based on these sensitivity analyses, the submitted base reference case is considered conservative based on both the storage volume and plume boundary comparisons. The reference

case provides confidence that the corrective action well review and potential impact to the USDW are conservative and have been appropriately evaluated.

2.4 AoR Delineation

The critical threshold pressure calculation and results are discussed in **Appendix 10**. As the injection is in a depleted reservoir being repressured to remain below the discovery conditions, the largest CO_2 plume extent plus a buffer zone was used to determine the AoR. For both injectate scenarios, CO_2 was injected into the depleted Injection Zone until the reservoir pressure reached 90 percent of the discovery pressure of 5,040 psi.

Figure B-29 shows the AoR, injectors, and offset monitoring wells. These monitoring wells were selected to both track the plume and measure reservoir pressure to understand the pressure and CO_2 plume development:

- By integrating the reservoir pressure increase with the injected volume, CTV will complete a material balance to verify the pore volume and AoR edges.
- CO_2 plume and water contact will be calculated from monitoring well pressure, CO_2 saturation, and column height.

If the reservoir pressure increase associated with the injected volume does not follow the predicted trend from computational modeling, CTV will reassess the AoR.

3. Corrective Action

3.1 Tabulation of Wells within the AoR

Wells within the AoR are associated with exploration and development of the Winters Formation for gas production from 1972 onward. As such, there are sufficient records for wells drilled in the study area. There have been no undocumented historical wells found in the AoR.

CTV accessed internal databases, as well as California Geologic Energy Management Division (CalGEM) web-based databases (WellSTAR and Well Finder), to identify and confirm wells within the AoR.

Table B-9 provides the count of wellbores located within the AoR and their associated status. **Appendix 7** provides a complete list of the wellbores, including status, type, and a unique API-12 identifier. As required by 40 CFR 146.84(c)(2), the well table in **Appendix 7** describes each well type, construction, date drilled, location, measured depth, true vertical depth, completion record relative to the Injection zone, record of plugging, and requirement for corrective action, if necessary. Wells identified as “abandon” in Appendix 7 do not require additional corrective action; they will be routinely plugged back in compliance with CalGEM and EPA Class VI regulations. CTV also identifies well work to be completed during the pre-operational testing phase. **Figure B-30** shows locations of wells penetrating the Upper Confining Layer and the Injection Zone reviewed for corrective action.

3.2 Protection of USDW

For the CTV II Storage Project, CTV assessed the USDW protection by evaluating all wellbores that penetrate the Upper Confining Zone. All wells within the AoR meet the following criteria, ensuring the protection of the USDW:

- Surface or intermediate casing over the USDW
- If well is abandoned, cement plug across base of USDW
- Cement in the annulus:
  - Surface 2 or Intermediate casing: cement above the surface casing shoe.
  - Adequate annular cement within the confining Upper Confining Zone.

3.3 Wells Penetrating the Confining Zone

The depth of the Confining Zone in each of the wells penetrating the Upper Confining Zone was determined through open-hole well logs using the deviation survey. All wells in the AoR penetrate the Upper Confining Zone.

3.4 Injection Zone Isolation

Wells that will not be repurposed for the storage project that penetrate and are currently open in the Injection Zone will be abandoned prior to injecting CO_2. These wells have not been deemed deficient. The abandonment of these wells, shown in **Figure B-31**, is considered to be normal operating procedures to manage and minimize liabilities. Wellbores that meet these criteria are identified for abandonment in **Appendix 7**.

Appendix 8 provides the plugging procedure that will be used to abandon these wells along with well-specific plugging plan tables that identify the number of plugs, placement method, cement type, density, and volume for the wells to be abandoned during pre-operational testing. Additionally, the procedures achieve all requirements of CalGEM regulations for proper abandonment of oil and gas wells.

3.5 Corrective Action Assessment of Wells in AoR

The corrective action assessment included the generation of detailed casing diagrams for each wellbore, review of all perforations, assessment of well architecture (casing depths, annular cement, etc.), and determination of cement plug depths relative to key storage complex formation tops. Corrective action review for all wells in the AoR is summarized in **Appendix 7**.

The Brooks 10-1-RD1 is a sidetrack of the Brooks 10-1 original hole. The original hole was sidetracked by setting a cement plug from 5,648 to 6,246 feet measured depth (MD), and the well was suspended with drilling mud below the plug. CTV will reabandon the well and ensure isolation of the injection zone. CTV plans to reenter the section of the well beneath the plug from approximately 5,700 to 6,500 feet MD, clean out the original openhole as deep as possible,

and fill the well with Class G cement plugs to ensure isolation. Brooks 10-1 RD1 will then be abandoned to surface.

Pool B-1 RD1 is the idle sidetrack of Pool B-1, a wellbore within the AoR that will require corrective action. Originally sidetracked due to a drillpipe fish, there is no cement across the confining layer in this wellbore. CTV plans to reabandon the portion of the well below the fish by reentering the wellbore and filling the well with Class G cement plugs to ensure isolation. Pool B-1 RD1 will then be abandoned to surface.

Mobil Parcel X 1 is a dry hole abandonment well outside of the Union Island Gas Field boundary. With no gas shows during the drilling process, this well was abandoned with casing set above the confining layer and open hole drilled through the Injection Zone. Abandonment plugs were set within the casing, but no cement was laid across the confining layer. CTV plans to drill out abandonment plugs and reenter the open hole portion of the abandoned wellbore, filling the well with Class G Portland cement plugs to reestablish the confining layer and ensure isolation.

All corrective action wells are highlighted in **Figure B-30**. **Appendix 9** shows diagrams for the current well configurations and proposed corrective action on all three wells.

3.6 Plan for Site Access

CTV has obtained surface access rights for the duration of the project.

3.7 Corrective Action Schedule

Corrective action for all wells within the AoR will be completed before CO_2 is injected in the reservoir. This will ensure that CO_2 is confined to the injection zone for the entire AoR, protecting the overlying USDW and ensuring confinement. CTV will communicate a specific corrective action schedule to EPA prior to permit finalization.

Through time, if the plume development is not consistent with the predicted results, computational modeling will be updated to reassess the AoR. In this event, all wells in the updated AoR will be subject to the Corrective Action Plan and will be remediated if necessary.

4. Reevaluation Schedule and Criteria

4.1 AoR Reevaluation Cycle

CTV will reevaluate the above described AoR at a minimum every five years during the injection and post-injection phases, as required by 40 CFR 146.84 (e).

Simulation study results are reviewed when operating data is acquired. Preparation of necessary operational data for the review includes injection rates and pressures, CO_2 injectate concentrations, and monitoring well information (storage reservoir and overlying dissipation intervals).

Dynamic operating and monitoring data that will be incorporated into future reevaluation will include:

1. Pressure data from monitoring wells that constrain and define plume development.
2. CO_2 content/saturation from monitoring wells. This data may be acquired with direct aqueous measurements and cased hole log results that will constrain and define plume development.
3. Injection pressures and volumes. The injection pressures and volumes in the computational model are maximum values. If the actual rates are lower than expected, the plume will develop at a slower rate than expected and be reflected in the pressure and CO_2 concentration data in 1 and 2 above.
4. A review of the full suite of water quality data collected from monitoring wells in addition to CO_2 content/saturation (to evaluate the potential for unanticipated reactions between the injected fluid and the rock formation).
5. Review and submission of any geologic data acquired since the last modeling effort, including any additional site characterization performed for future injection wells.
6. Reevaluation modeling results will be compared with the most recent modeling (i.e., from the most recent AoR reevaluation). A report describing the comparison of the modeling results will be provided to the EPA with a discussion on whether the results are consistent.
7. Description of the specific actions that will be taken if there are discrepancies between monitoring data and prior modeling results (e.g., remodel the AoR, update all project plans, perform additional corrective action if needed, and submit the results to EPA).

Reevaluation results will be compared to the original results to understand dynamic inputs affecting plume development and static inputs that would impact injectivity and storage space. Static inputs that may potentially be considered to understand discrepancies between initial and reevaluation computational models could include permeability, sand continuity, and porosity. Although the AoR has been fully delineated, all inputs to the static and dynamic model will be reviewed.

As needed, CTV will review all of the plans that are impacted by a potential AoR increase such as Testing and Monitoring, Corrective Action, and Emergency and Remedial Response. If pressure increases are detected in the Mokelumne Formation or USDW, CTV may update the Testing and Monitoring Plan to include additional plume and pressure front monitoring or additional USDW monitoring wells. For corrective action, all wells potentially impacted by a changing AoR will be addressed immediately.

4.2 Triggers for AoR Reevaluations Prior to the Next Scheduled Reevaluation

An ad-hoc reevaluation prior to the next scheduled reevaluation will be triggered if any of the following occur:

- Changes in pressure or injection rate that are unexpected and outside three standard deviations from the average will trigger a new evaluation of the AoR.

- Difference between the computation modeling and observed plume development:
  - Unexpected changes in fluid constituents or pressure outside the Injection Zone that are not related to well integrity.
  - Reservoir pressures increase versus injected volume is inconsistent with computational modeling results with a variance more than ±10 percent from the Base Case Simulation.
  - Any other activity prompting a model recalibration.
- Seismic monitoring anomalies within two miles of the injection well that are indicative of:
  - The presence of faults near the confining zone that indicates propagation into the confining zone.
  - Events reasonably associated with CO_2 injection that are greater than M3.5.
- Exceeding 90 percent of the geologic formation fracture pressure in any injection or monitoring wells.
- Detection of changes in shallow groundwater chemistry (e.g., a significant increase in the concentration of any analytical parameter that was not anticipated by the AoR delineation modeling).
- Initiation of competing injection projects within the same injection formation within a 1-mile radius of the injection well (including when additional CTV injection wells come online).
- A significant change in injection operations, as measured by wellhead monitoring.
- Significant land-use changes that would impact site access.
- Any other activity prompting a model recalibration.

CTV will discuss any such events with the UIC Program Director as soon as possible to determine if an AoR reevaluation is required. If an unscheduled reevaluation is triggered, CTV will perform the steps described at the beginning of this section of the Plan within six months of the triggering event.

References

California Department of Conservation Division of Soil, Gas and Geothermal Resources (DOGGR). 1998. California Oil and Gas Fields. Volume III – Northern California.

Deutsch, C.V., & Journel, A.G. (1997). GSLIB: Geostatistical Software Library and User's Guide. Oxford University Press, New York.

Hill, 1979. California Well Sample Repository Special Publication No. 2: Display of Cores From The Winters Sand (Upper Cretaceous), Sacramento Valley California. May 7 – 12, 1979.

Leong, J.K., and J.R. Tenzer. 1994. Production Optimization of a Mature Gas Field. Paper presented at the SPE Western Regional Meeting, Long Beach, California.

Nghiemw, L., A. Shrivastavar, B. Kohse, and P. Sammon. 2004. *Simulation of CO_2 EOR and sequestration processes with a geochemical EOS compositional simulator*. Paper presented at the Canadian International Petroleum Conference, Calgary, Alberta. June 2004. https://doi.org/10.2118/2004-051

Tran, D., V. Shrivastava, L. Nghiem, and B. Kohse. 2009. *Geomechanical risk mitigation for CO_2 sequestration in saline aquifers*. Paper presented at the SPE Annual Technical Conference and Exhibition, New Orleans, Louisiana. October 2009. https://doi.org/10.2118/125167-MS

Zhang G., P. Lu, and C. Zhu. 2014. Model predictions via history matching of CO_2 plume migration at the Sleipner Project, Norwegian North Sea. *Energy Procedia* 63: 3000-3011. https://doi.org/10.1016/j.egypro.2014.11.323.

Vinsome, P.K.W. and J. Westervled. A simple method for predicting cap and base rock heat losses in thermal reservoir simulators. *JCPT* 19 (July 1980): 87-90.

Figures

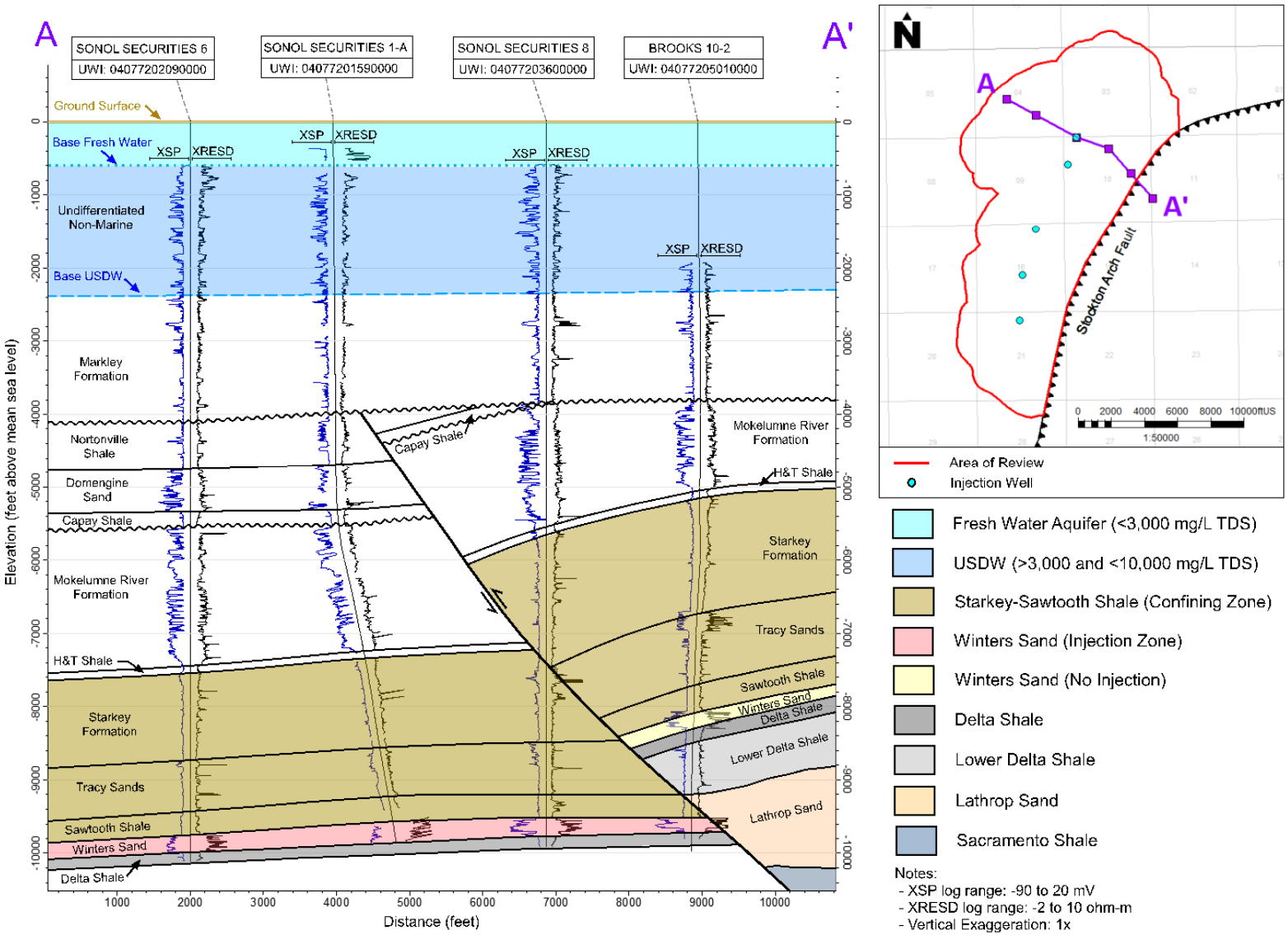

Figure B-1. Dip cross section showing stratigraphy and lateral continuity of major formations across the project area. Section is representative of formations and sand continuity at all five CO_2 injector locations.

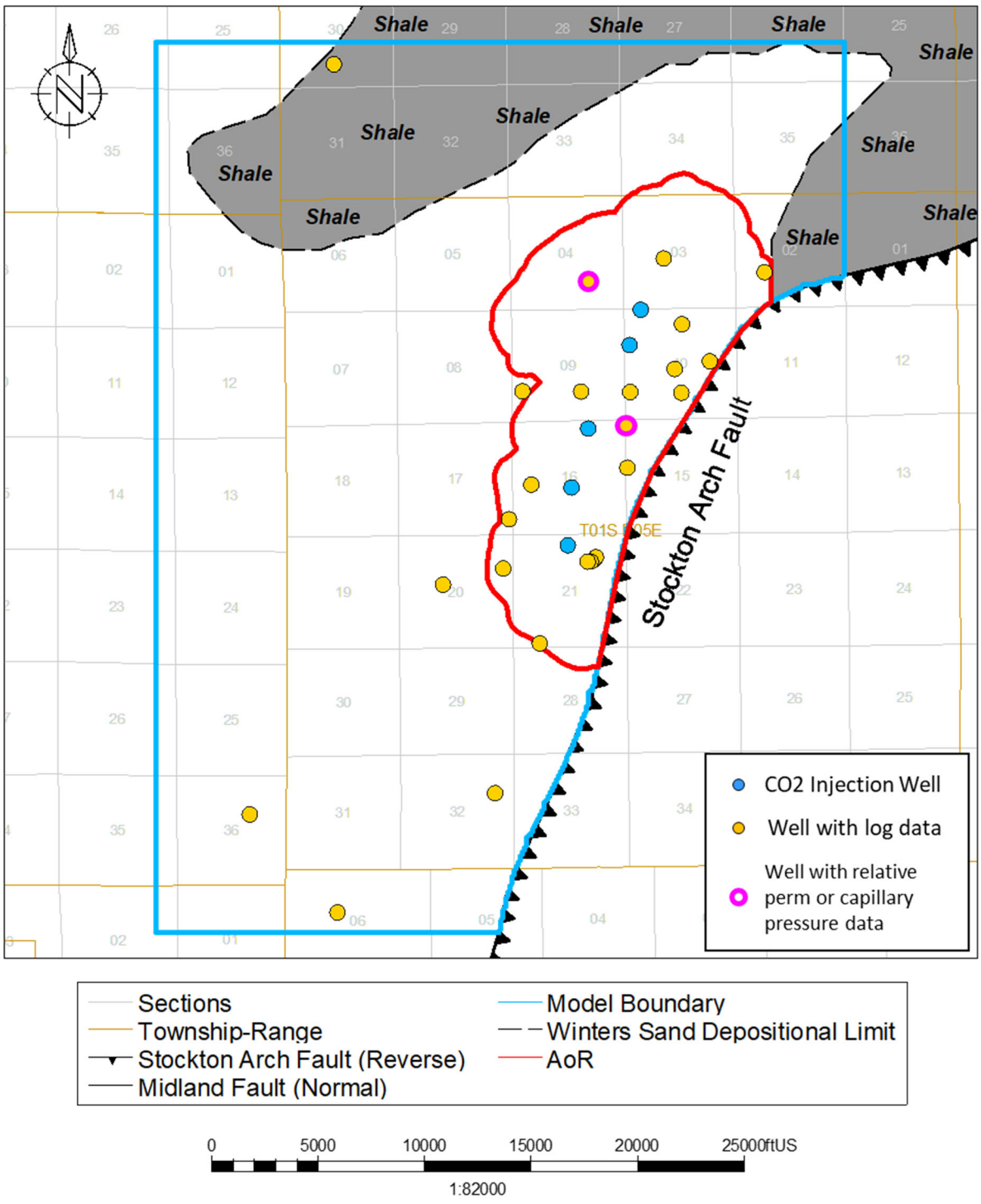

Figure B-2. Location of wells with open-hole log data and injection zone relative permeability or capillary pressure data used to develop the static and computational models.

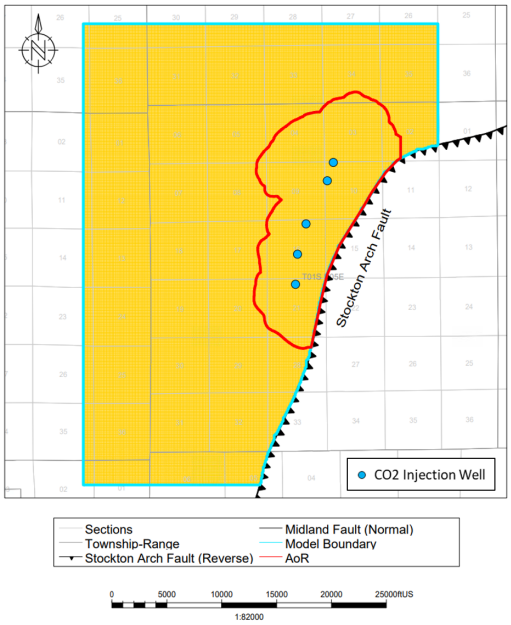

Figure B-3a. Plan view of the model boundary and geo-cellular grid used to define the project AoR.

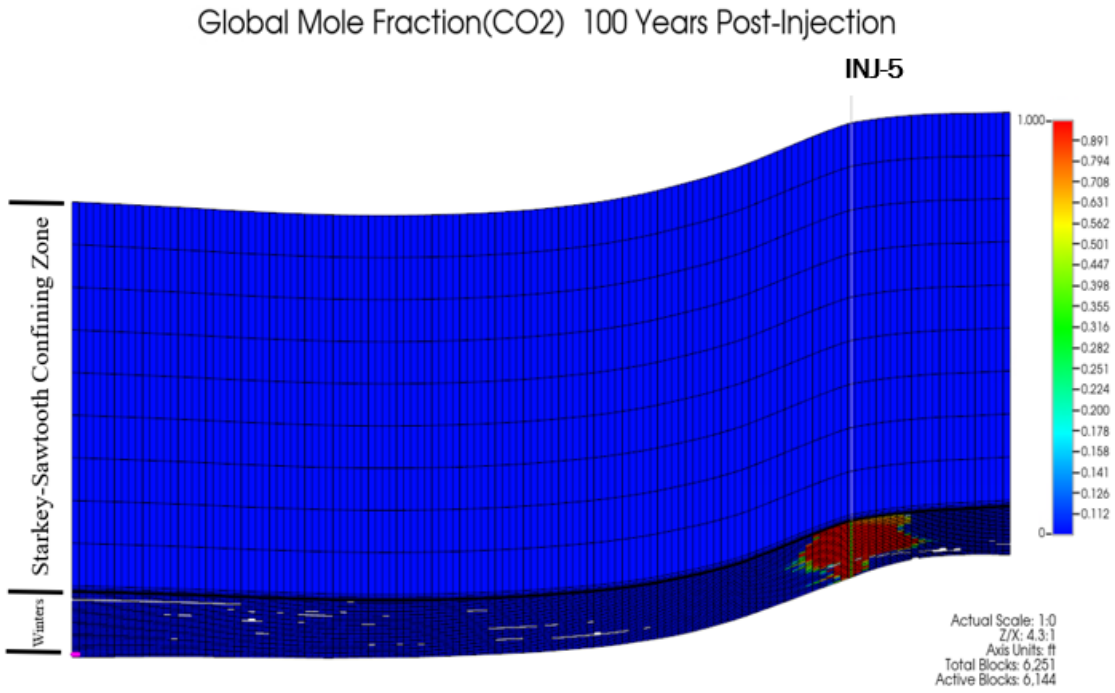

Figure B-3b. CO_2 global mole fraction distribution at 100 years post-injection for mechanistic model, including Starkey-Sawtooth confining zone and Winters Injection Zone.

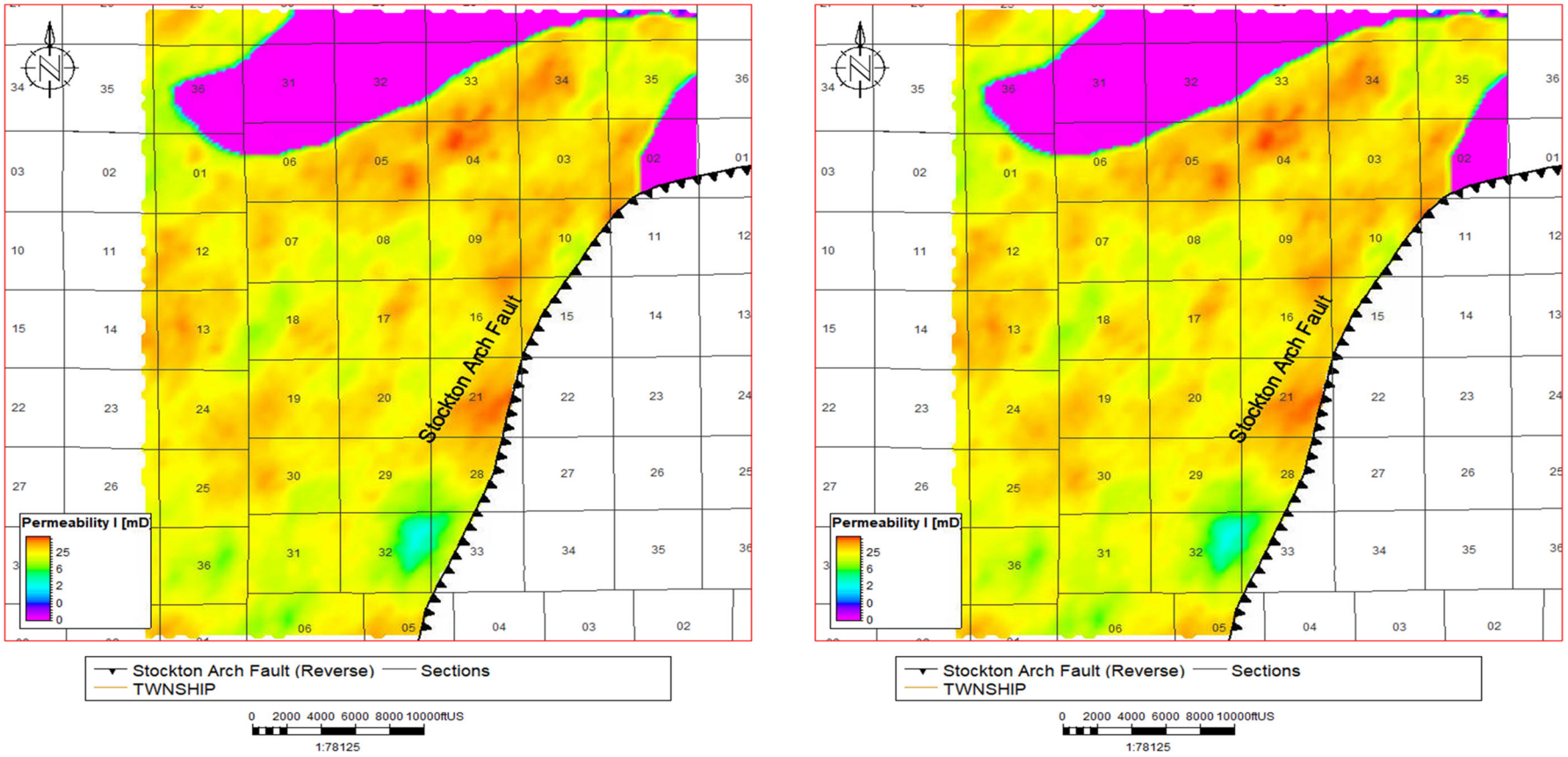

Figure B-4. Geological model permeability distribution for grid size 100 feet x 100 feet x 5 feet (left) and grid size 200 feet x 200 feet x 9 feet (right).

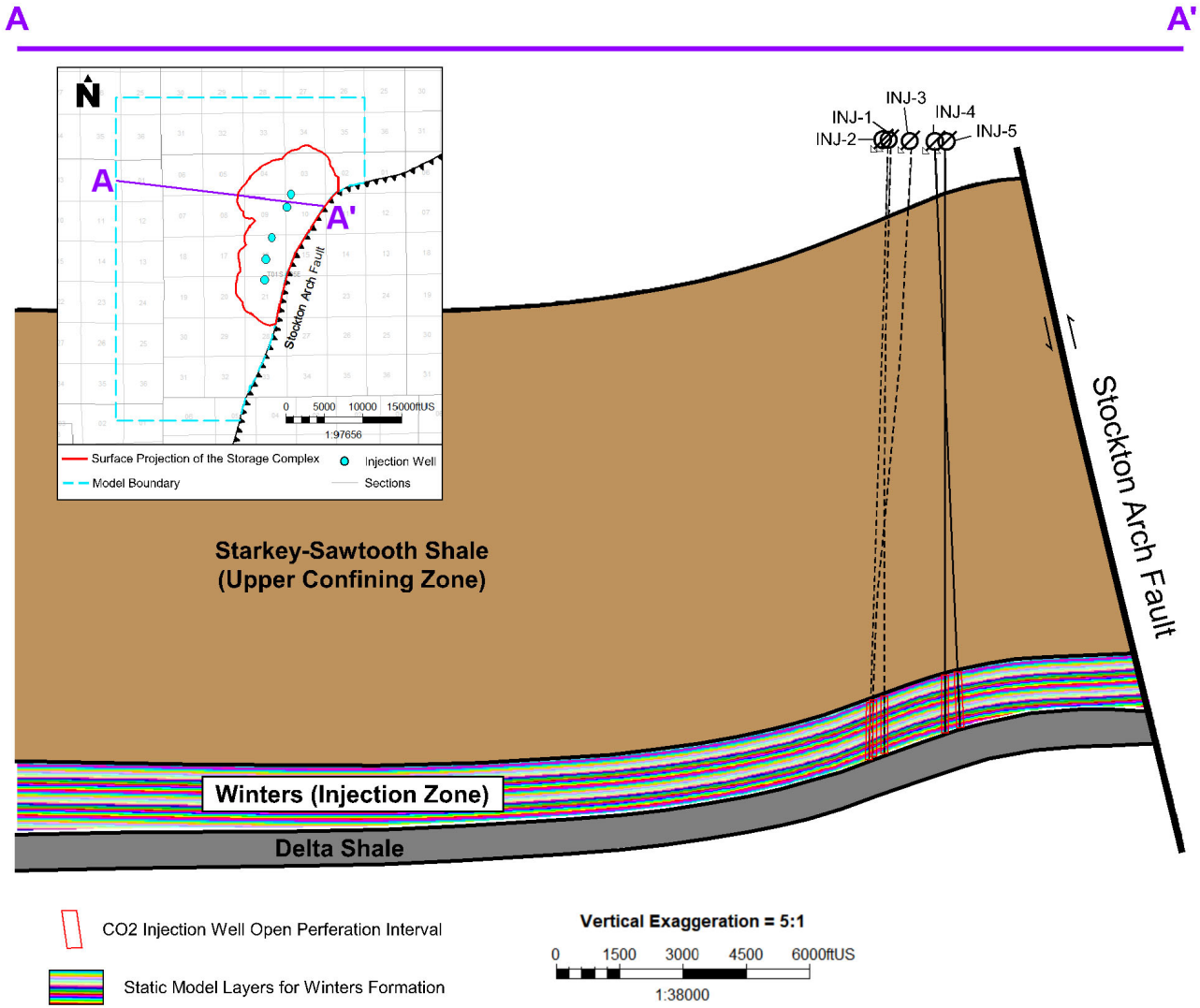

Figure B-5. Dip section showing static model layering for the injection zone with all injectors projected onto section to show relative depth in reservoir structure. Section is representative of all injector locations.

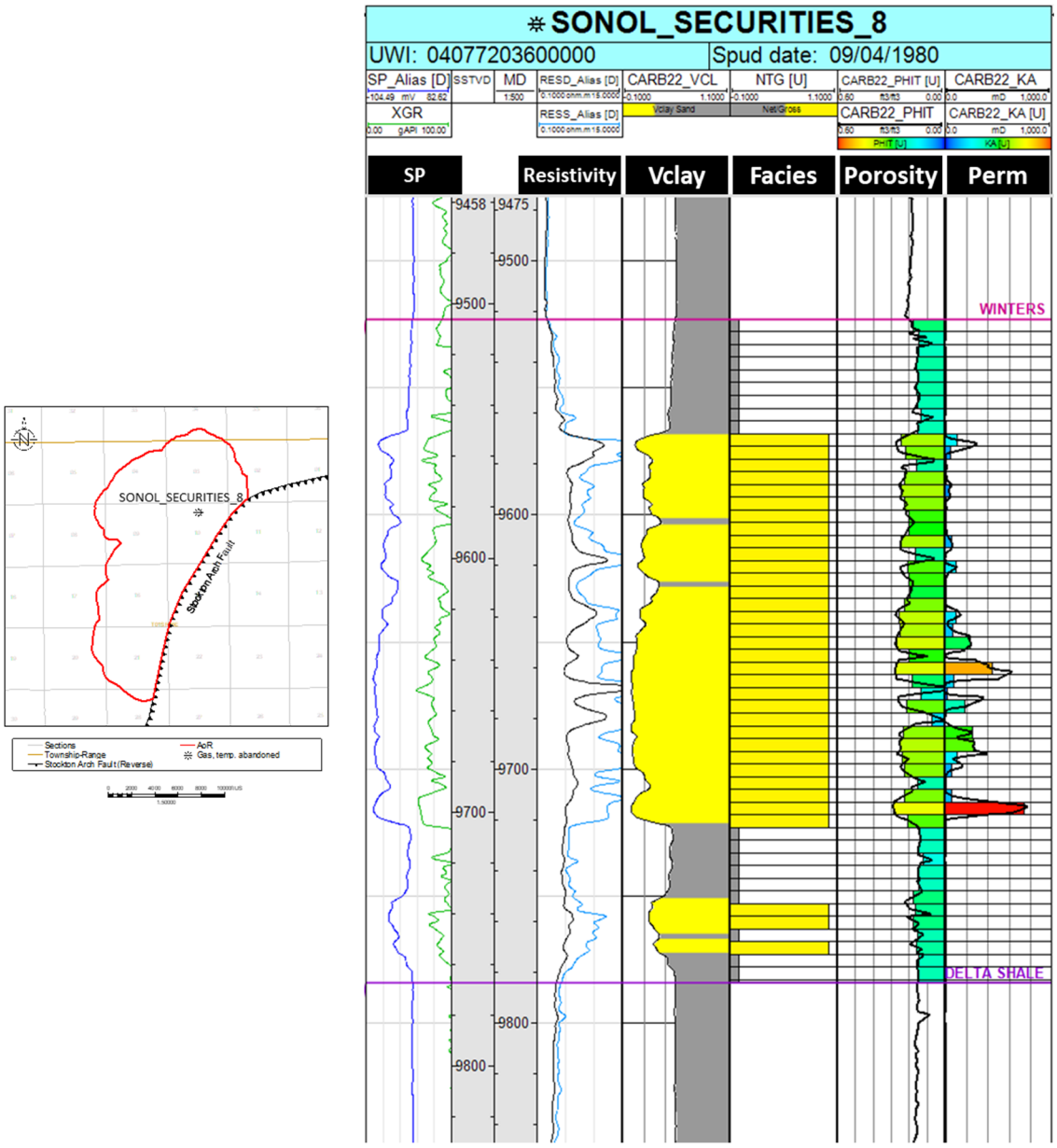

Figure B-6. Well "Sonol Securities 8" upscaled logs versus open-hole logs.

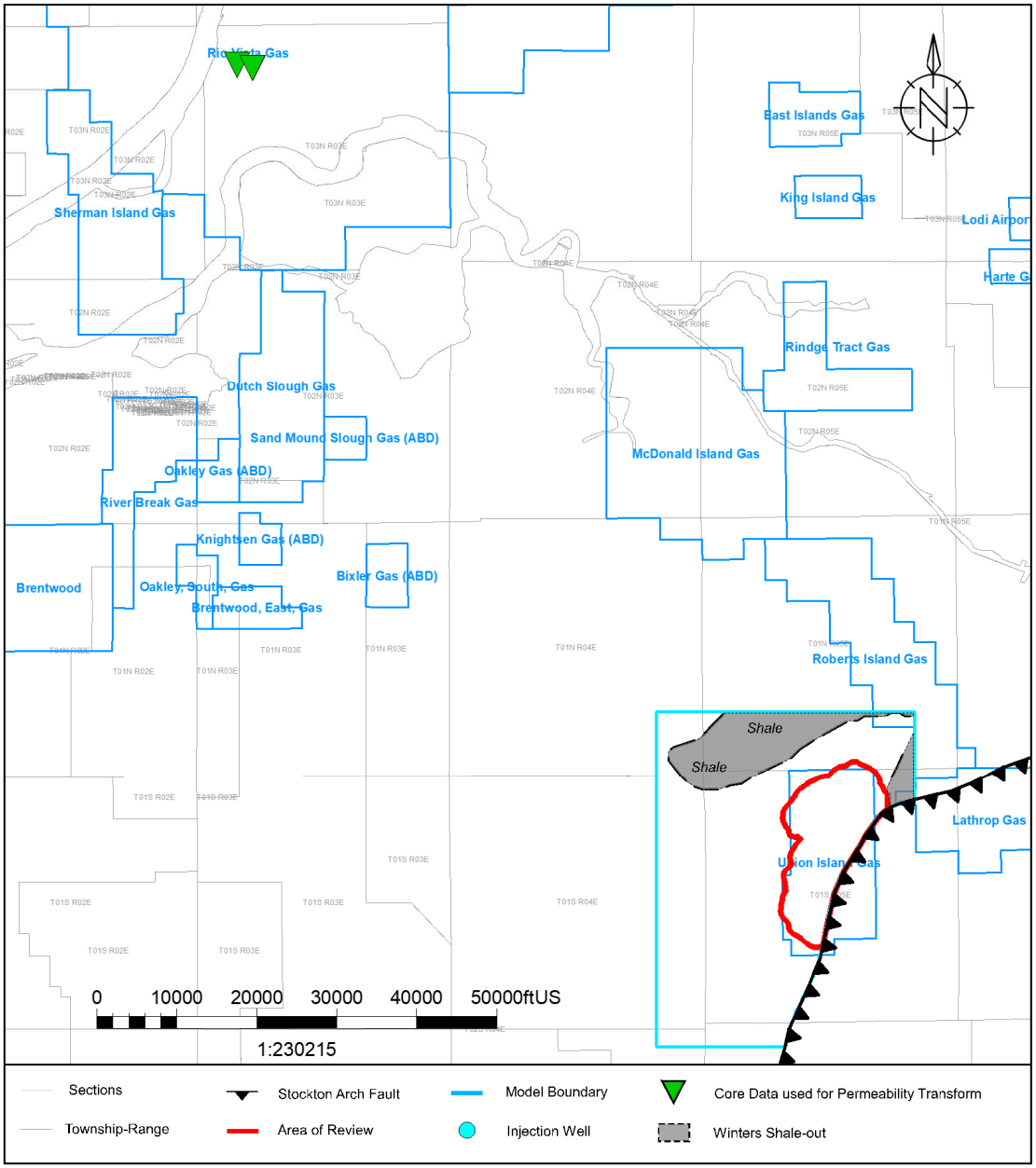

Figure B-7. Locations of wells with core data used for permeability transform. Wells are RVGU_215 on the west and RVGU_209 on the east.

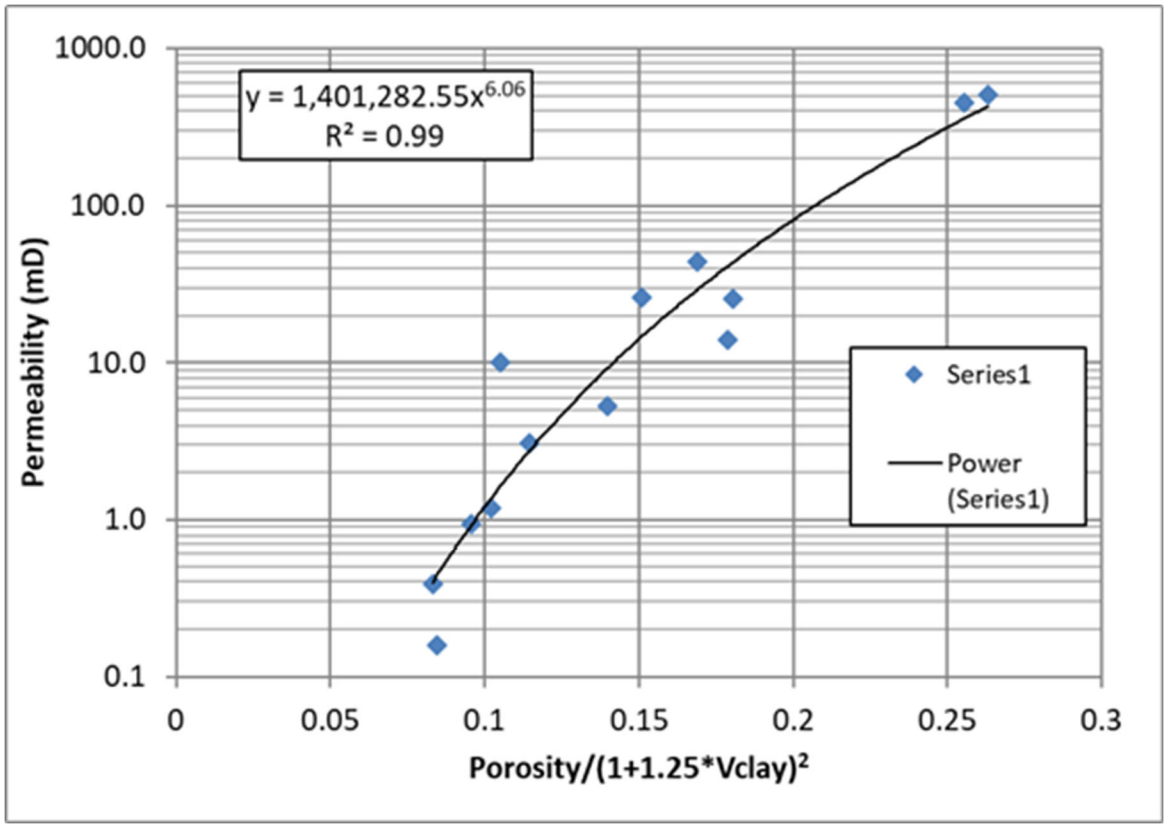

Figure B-8. Porosity and permeability data from capillary pressure analysis for Injection Zone sand. A permeability transform calculates permeability from log-based porosity.

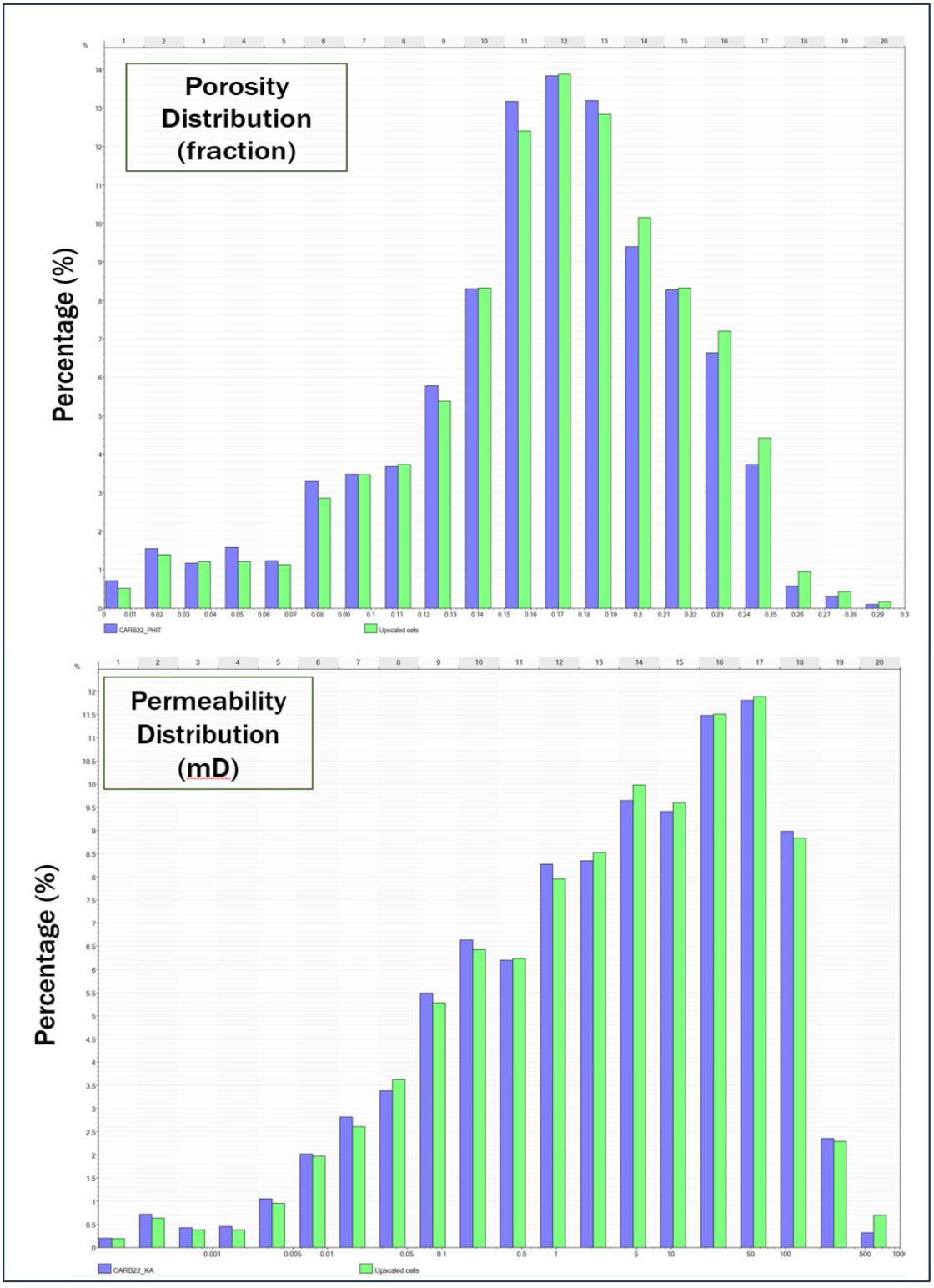

Figure B-9. Injection Zone porosity and permeability distribution in the static model.

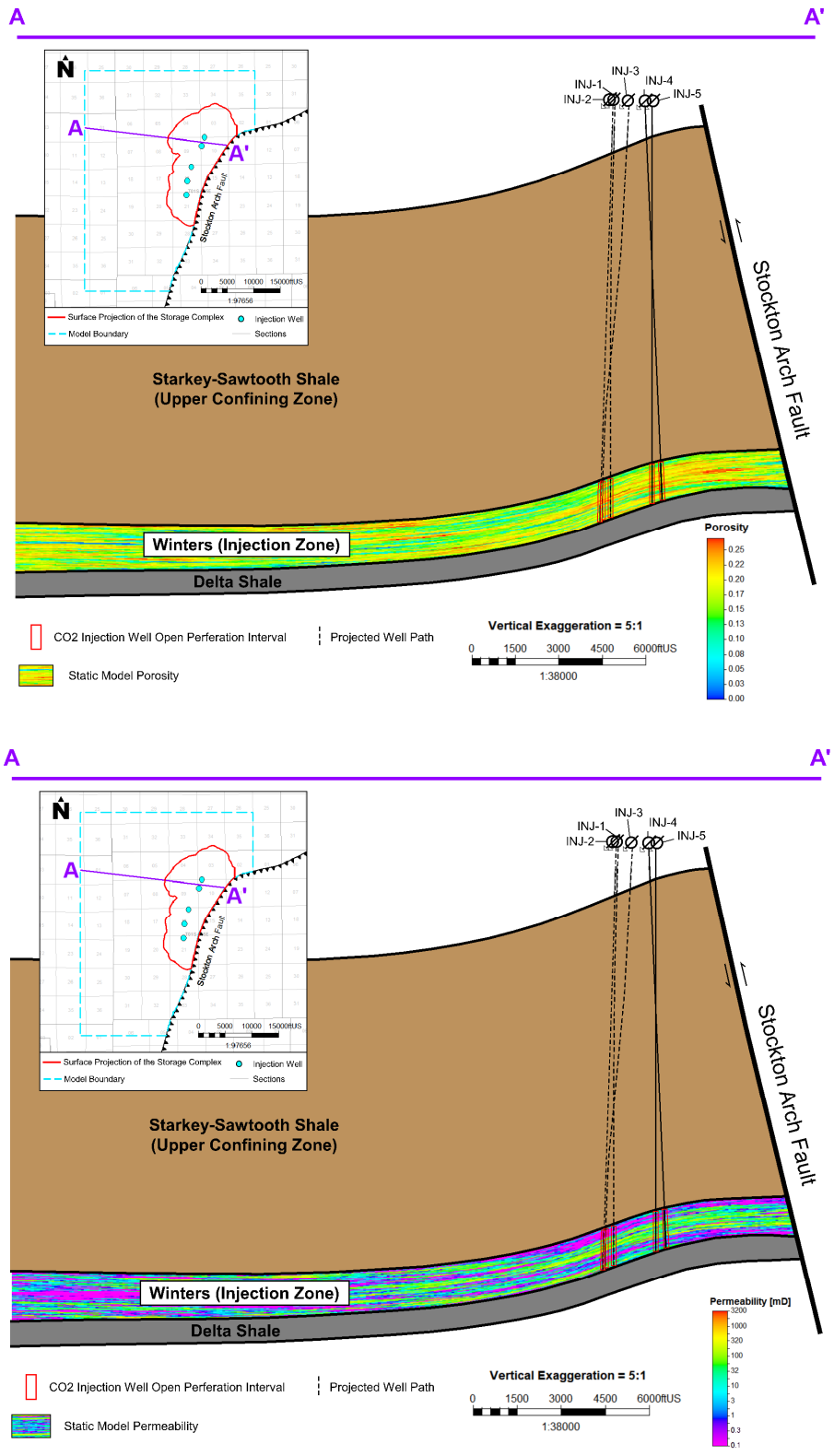

Figure B-10a. Dip (east-west) section through the static grid. Shows the distribution of porosity and permeability in the reservoir with all injectors projected onto section to show relative depth in reservoir structure.

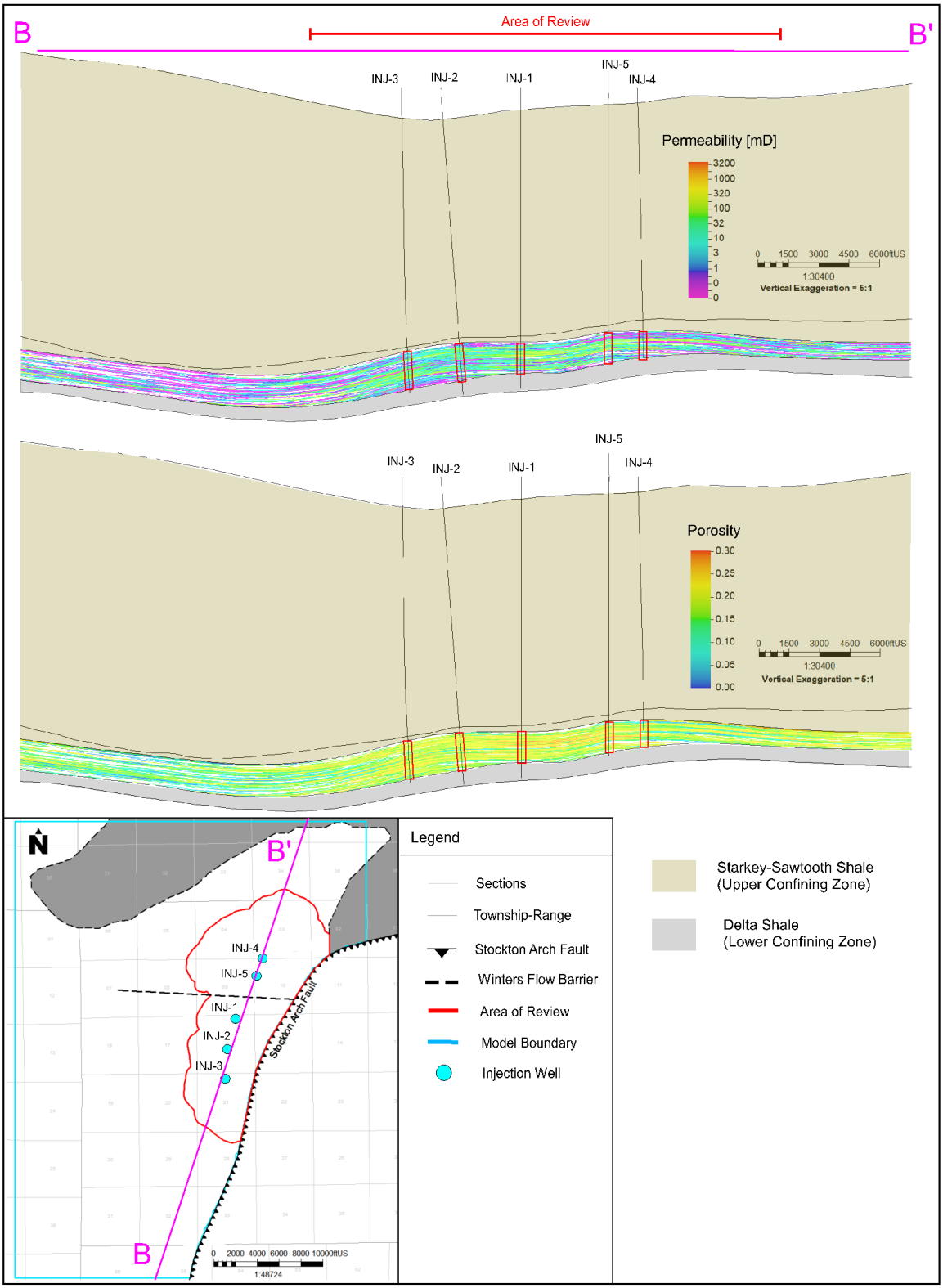

Figure B-10b. Strike (north-south) section through the static grid. Shows the distribution of porosity and permeability in the reservoir with all injectors projected onto section to show relative depth in reservoir structure.

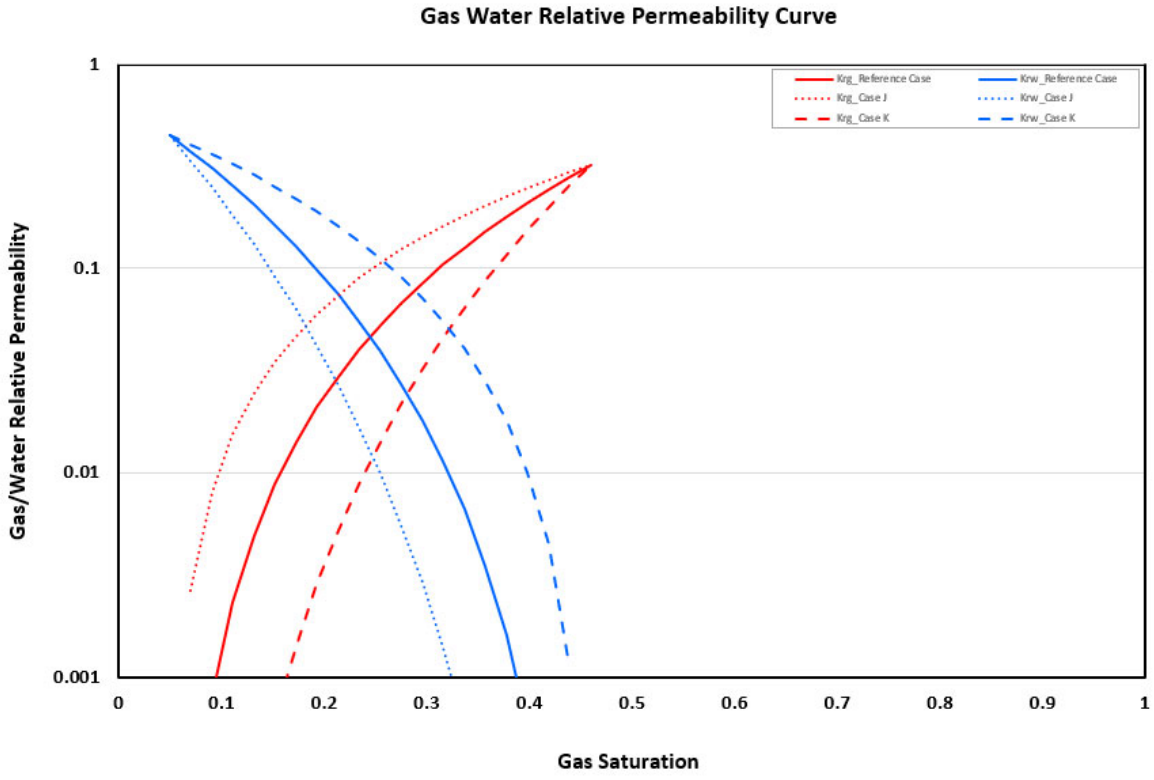

Figure B-11a. Relative permeability curves for gas-water system.

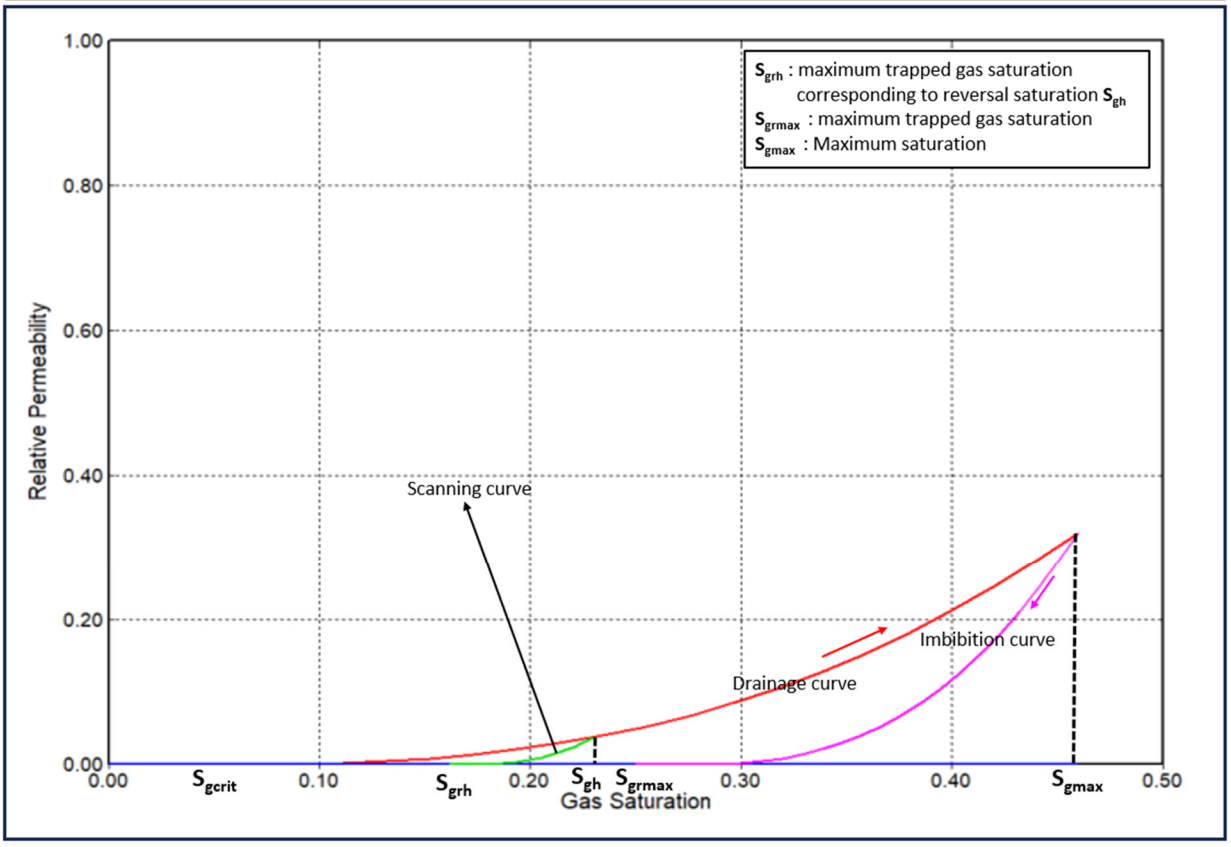

Figure B-11b. Hysteretic gas-phase relative permeability plot.

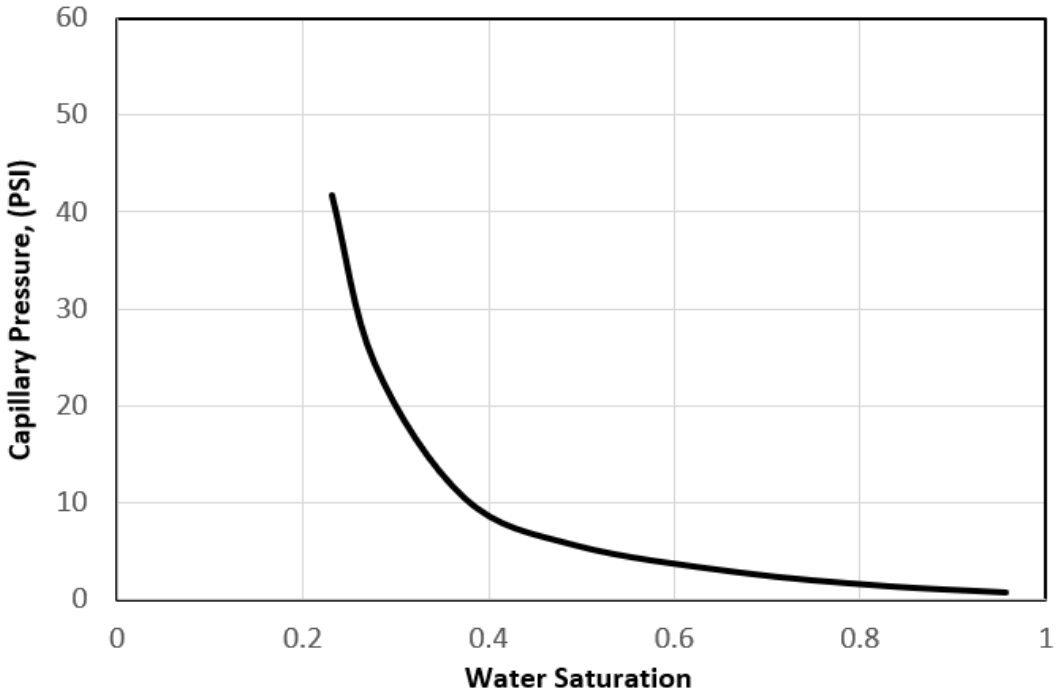

Figure B-12. Capillary pressure curve.

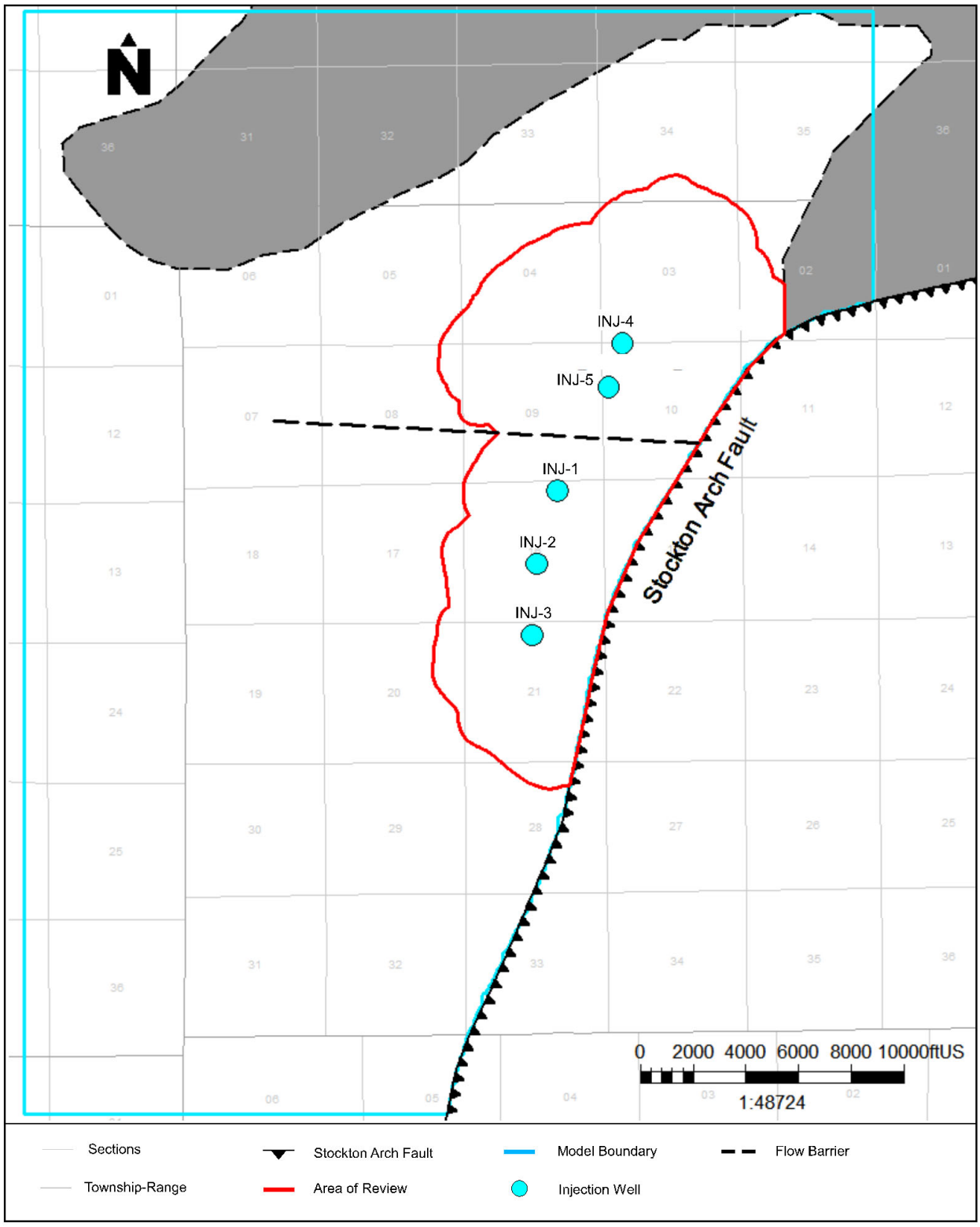

Figure B-13. Partial flow barrier between the northern and southern sections of the modeled area. The flow barrier transmissibility is set to 0.

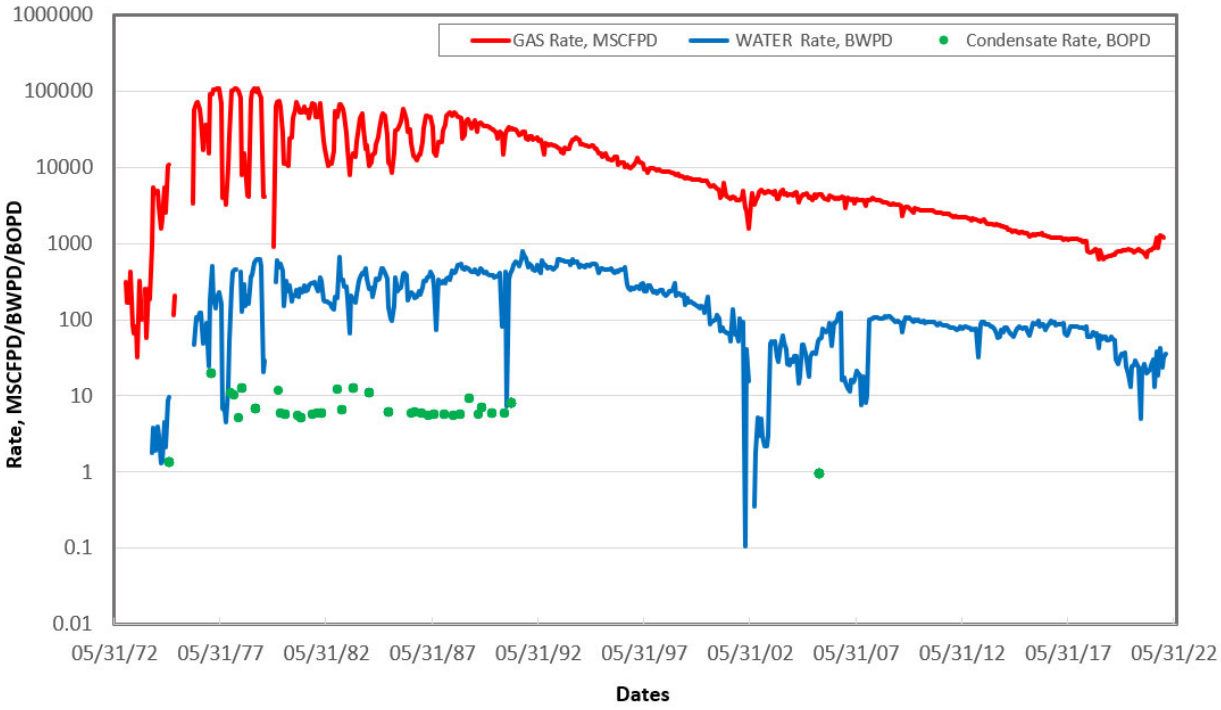

Figure B-14. Field production graph.

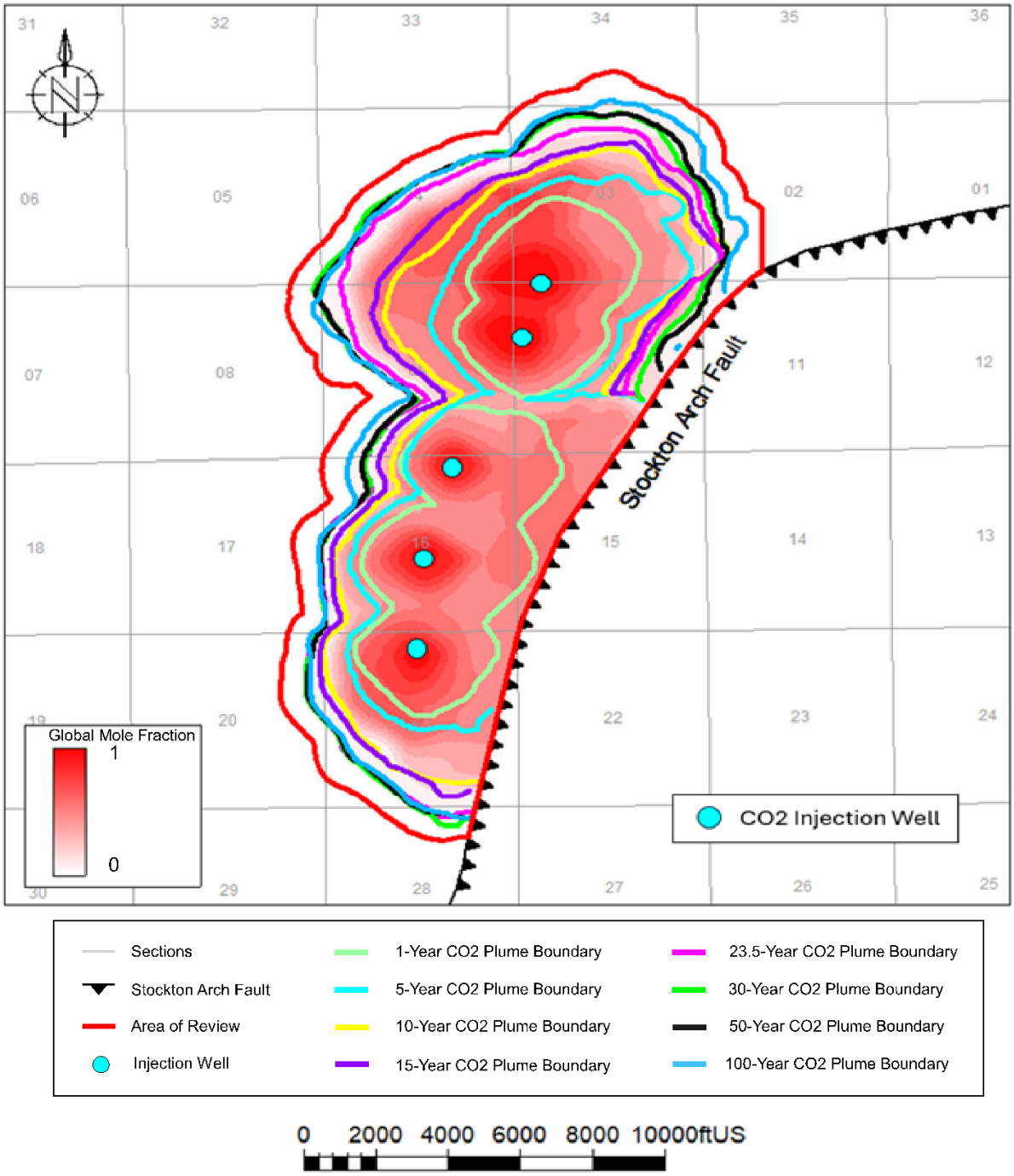

Figure B-15a. Injectate 1 plume development through time. 1-year, 5-year, 10-year, 15-year, 23.5-year (end of injection), 30-year post injection, 50-year post injection, and 100-year post injection.

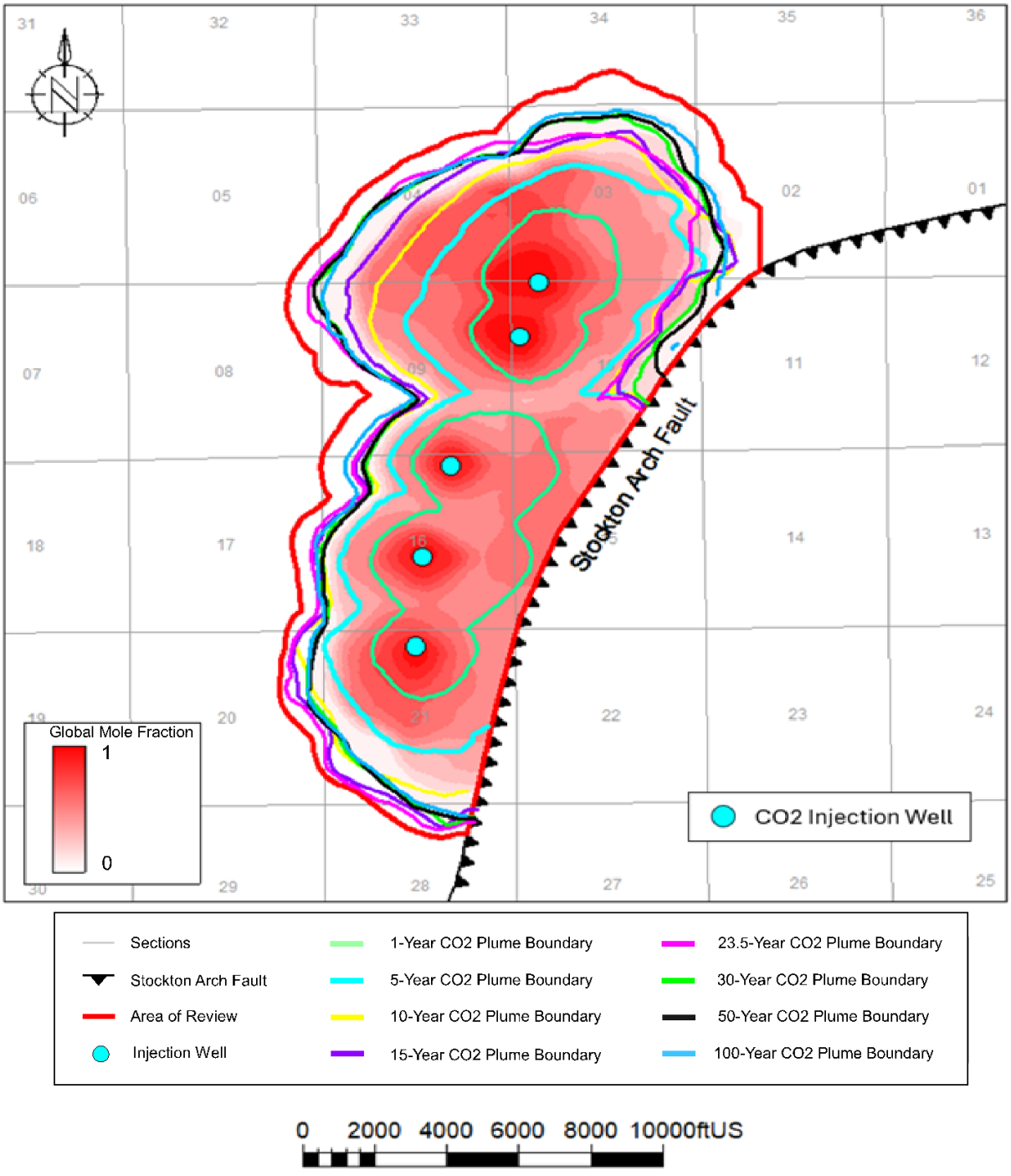

Figure B-15b. Injectate 2 plume development through time. 1-year, 5-year, 10-year, 15-year, 20-year, 23.5-year (end of injection), 32-year post injection, and 100-year post injection.

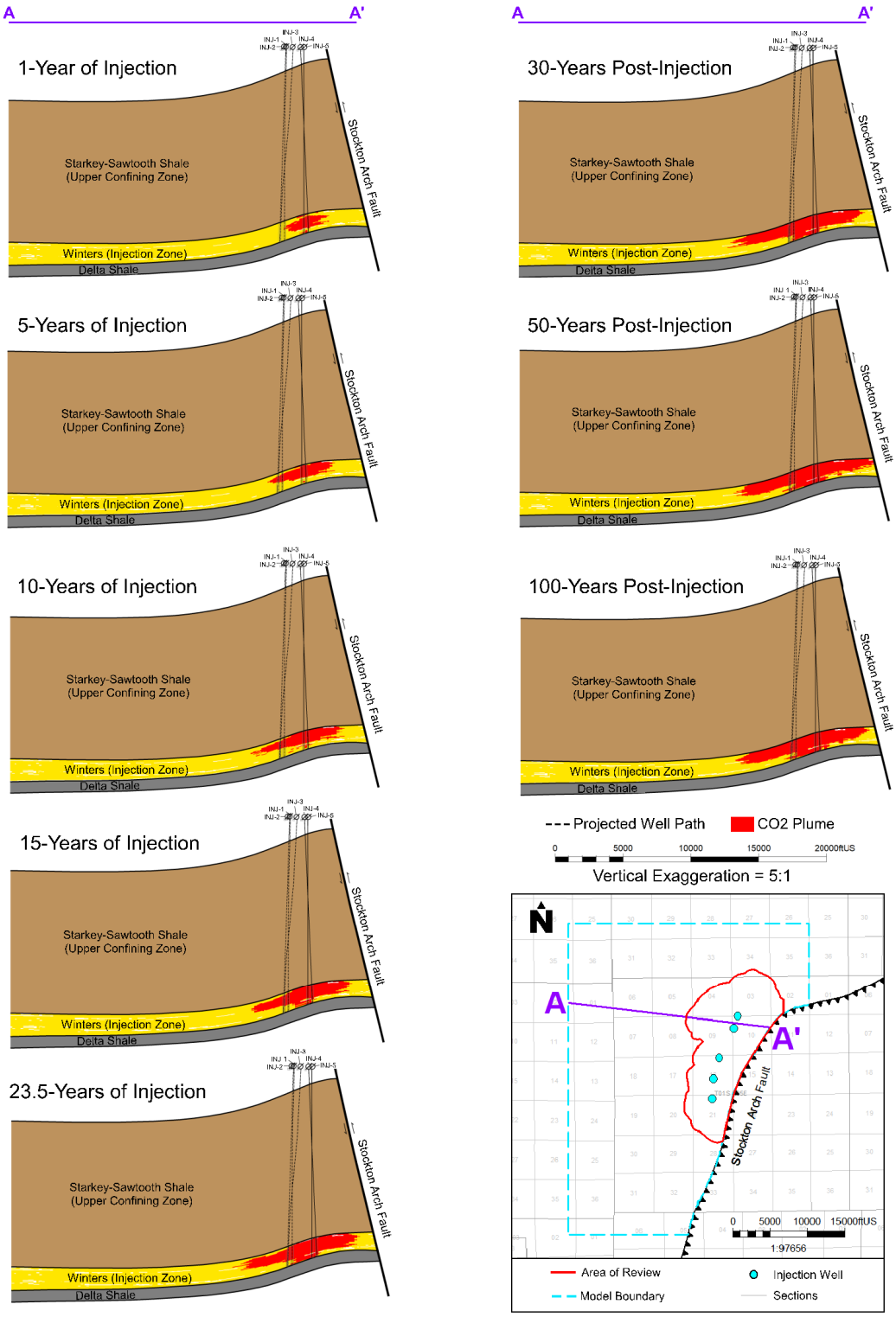

Figure B-16a. Section showing proximity of CO_2 (Injectate 1) to the Stockton Arch Fault and lateral dispersion of CO_2 throughout time and confinement under the overlying Starkey-Sawtooth through time for the five injector modeled Base scenario. As the sections show, plume growth over time is driven by the reservoir anticlinal structure, and is thus representative of the plume growth at all injector locations.

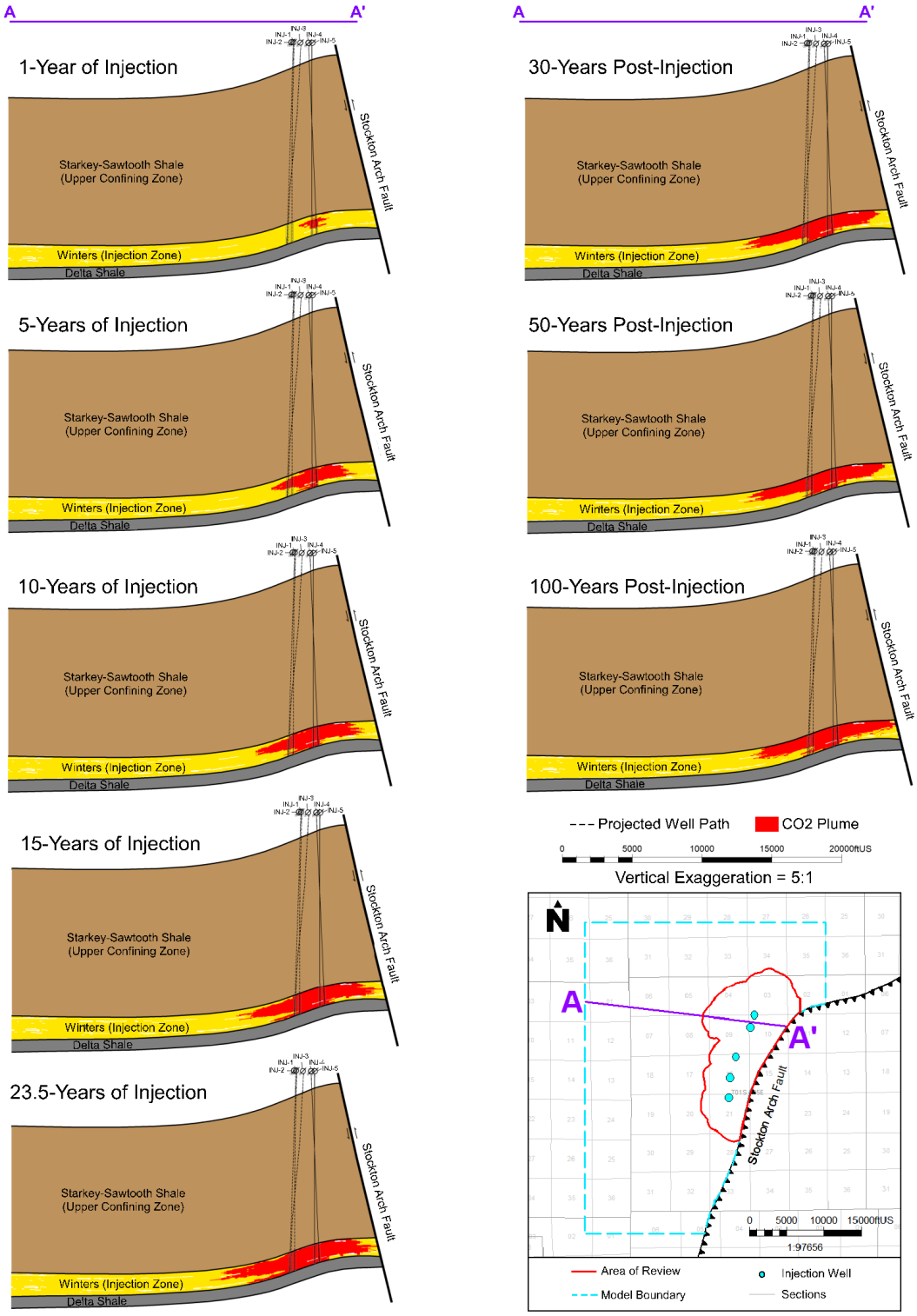

Figure B-16b. Section showing proximity of CO_2 (Injectate 2) to the Stockton Arch Fault and lateral dispersion of CO_2 throughout time and confinement under the overlying Starkey-Sawtooth through time for the five injector modeled Base scenario. As the sections show, plume growth over time is driven by the reservoir anticlinal structure, and is thus representative of the plume growth at all injector locations.

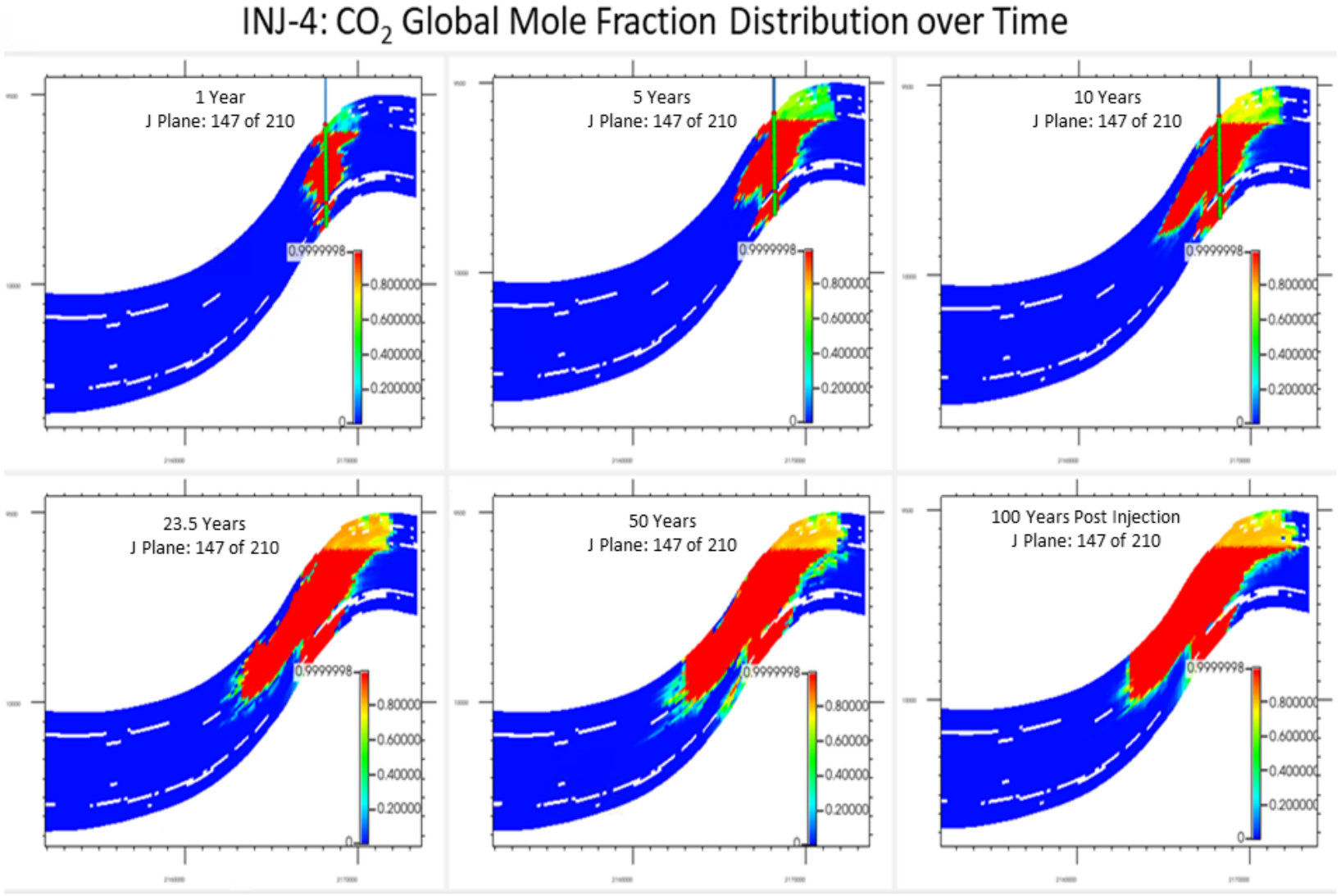

Figure B-17a. 100% CO_2, INJ-4, CO_2 Global Mole Fraction Distribution at 1 year, 5 years, 10 years, 23.5 years (end of injection), 50 years (Since start of the injection) and 100 years post injection.

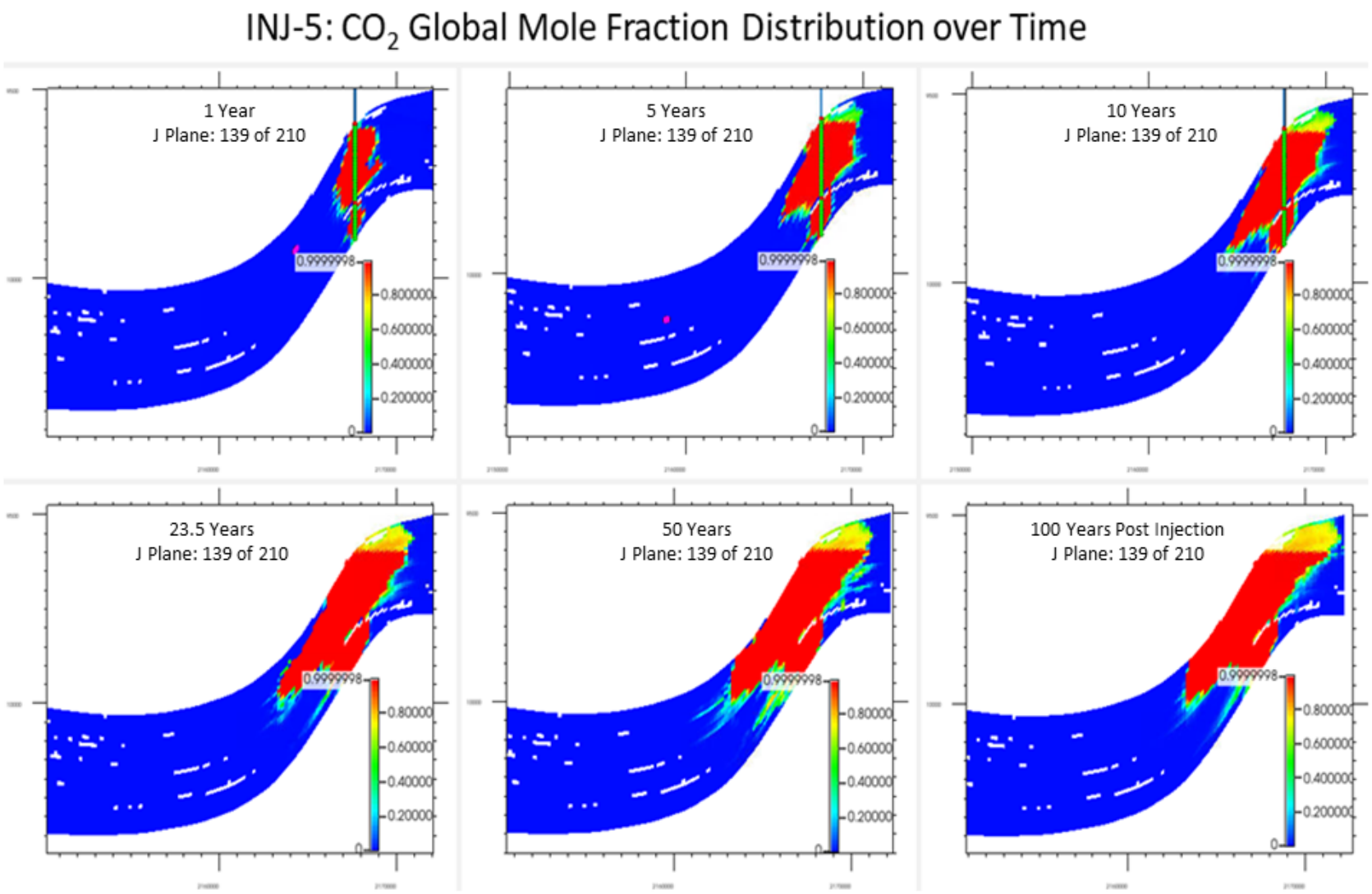

Figure B-17b. 100% CO_2, INJ-5, CO_2 Global Mole Fraction Distribution at 1 year, 5 years, 10 years, 23.5 years (end of injection), 50 years (Since start of the injection) and 100 years post injection.

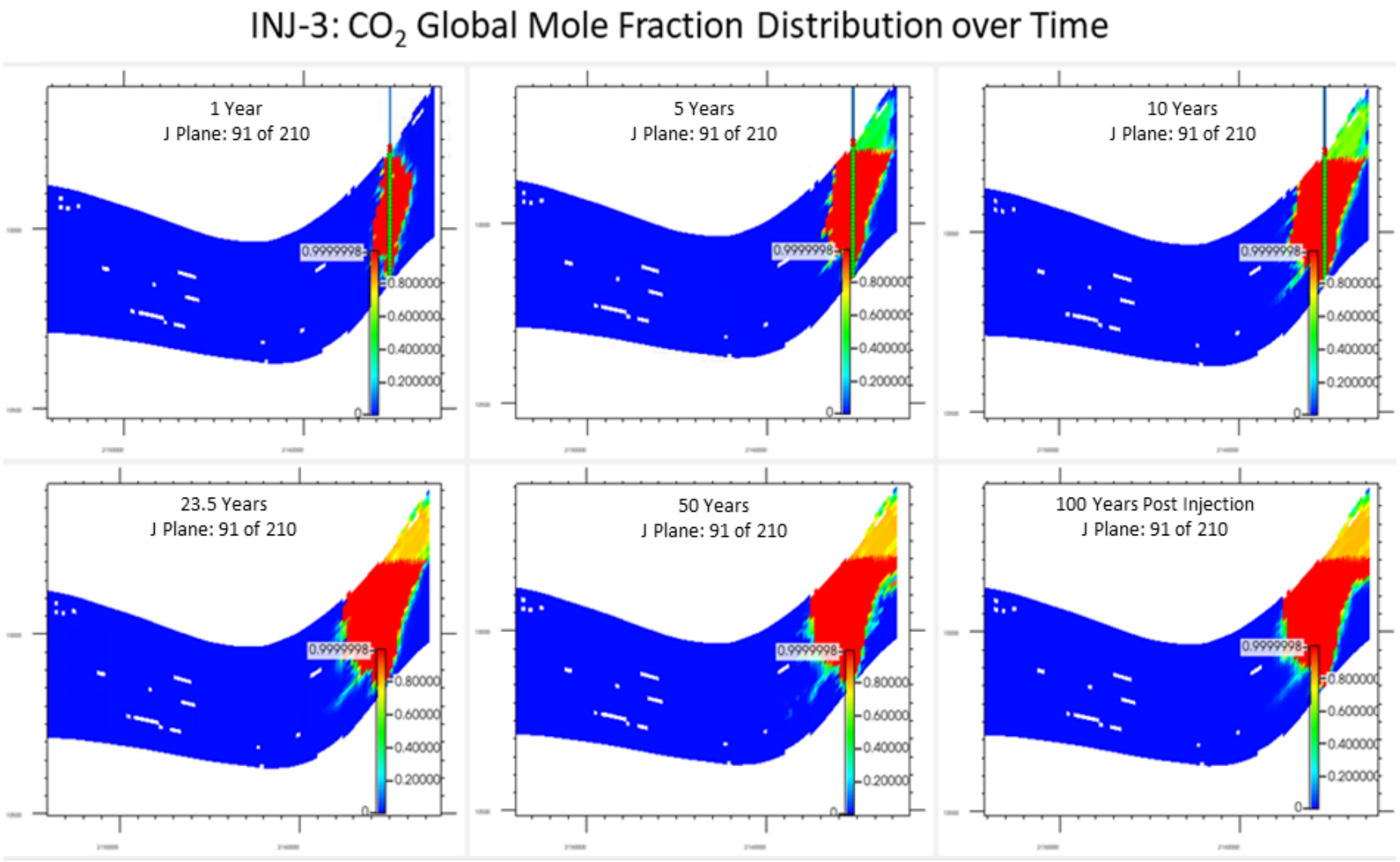

Figure B-17c. 100% CO_2, INJ-3, CO_2 Global Mole Fraction Distribution at 1 year, 5 years, 10 years, 23.5 years (end of injection), 50 years (Since start of the injection) and 100 years post injection.

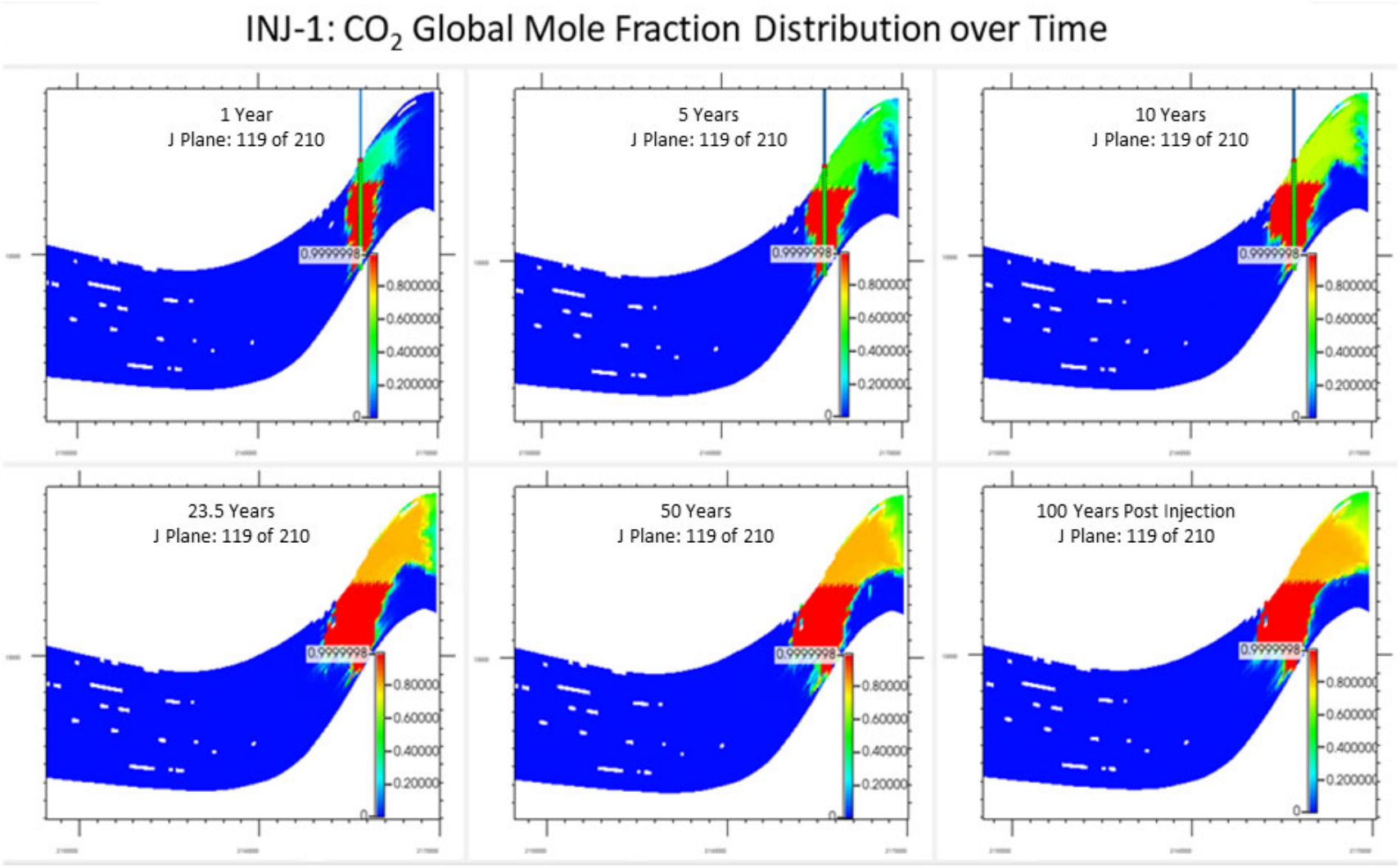

Figure B-17d. 100% CO_2, INJ-1, CO_2 Global Mole Fraction Distribution at 1 year, 5 years, 10 years, 23.5 years (end of injection), 50 years (Since start of the injection) and 100 years post injection.

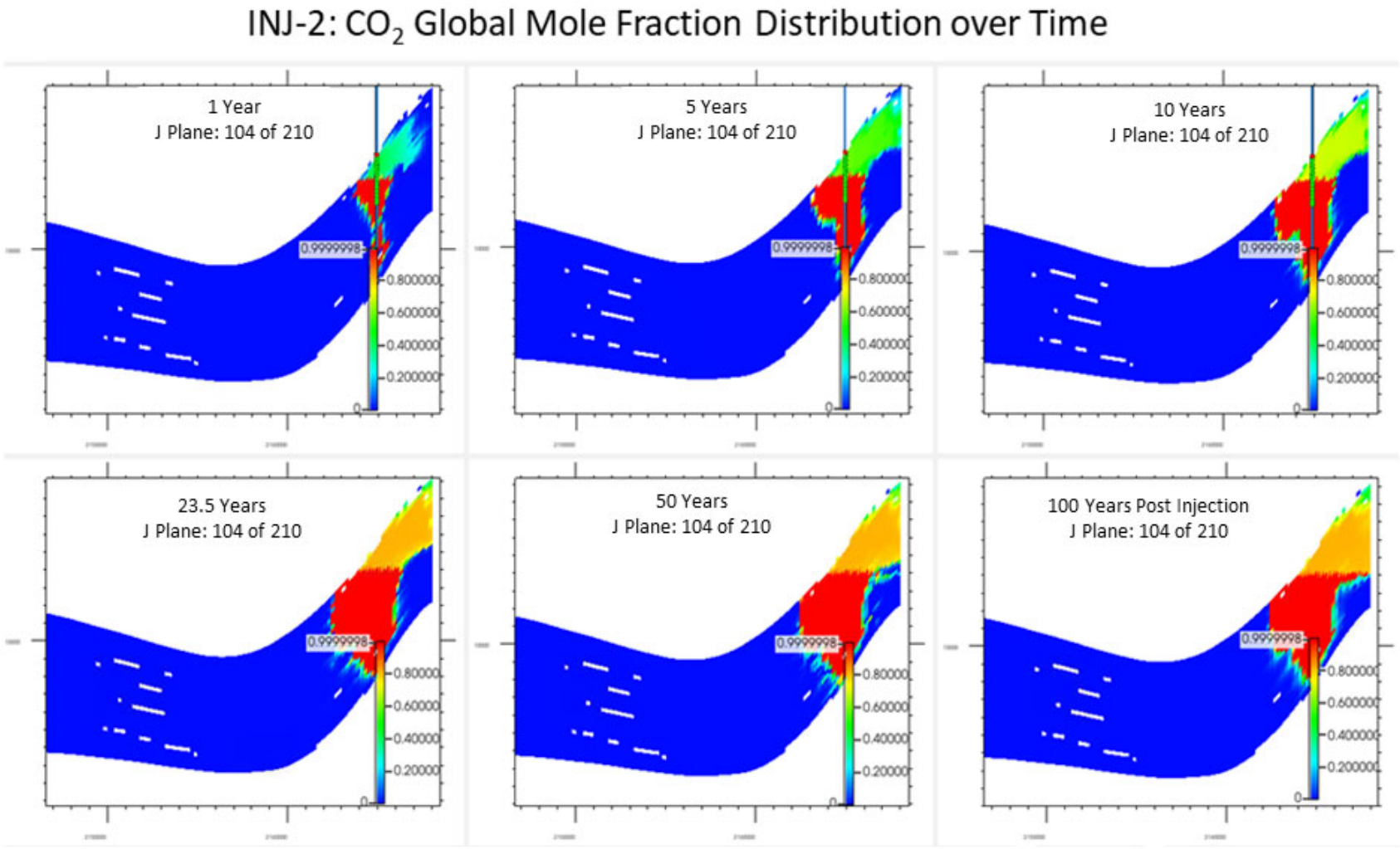

Figure B-17e. 100% CO_2, INJ-2, CO_2 Global Mole Fraction Distribution at 1 year, 5 years, 10 years, 23.5 years (end of injection), 50 years (Since start of the injection) and 100 years post injection.

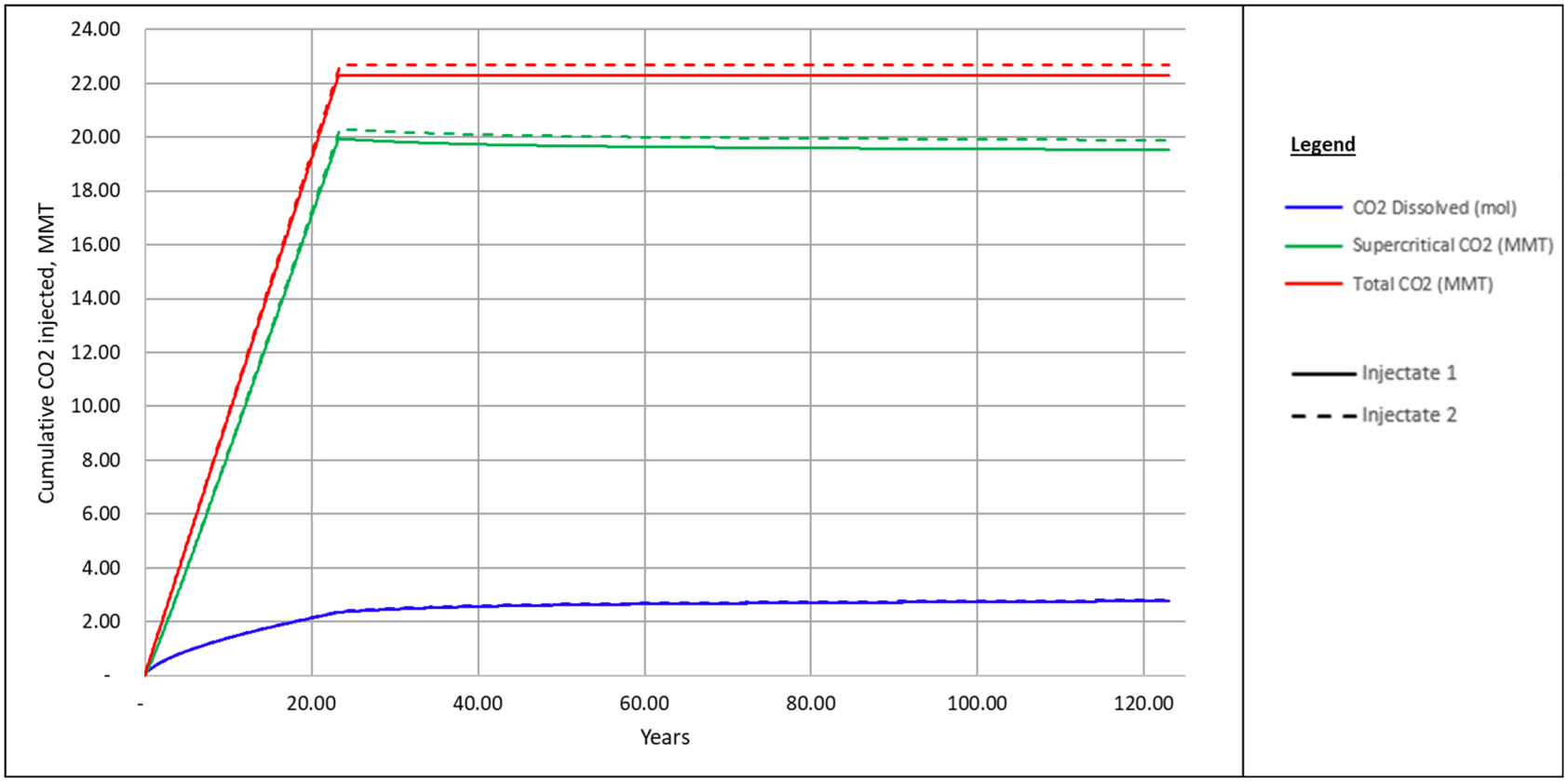

Figure B-18. CO_2 storage mechanisms in the reservoir. Results shown for Base cases with Injectate 1 (solid lines) and Injectate 2 (dashed lines).

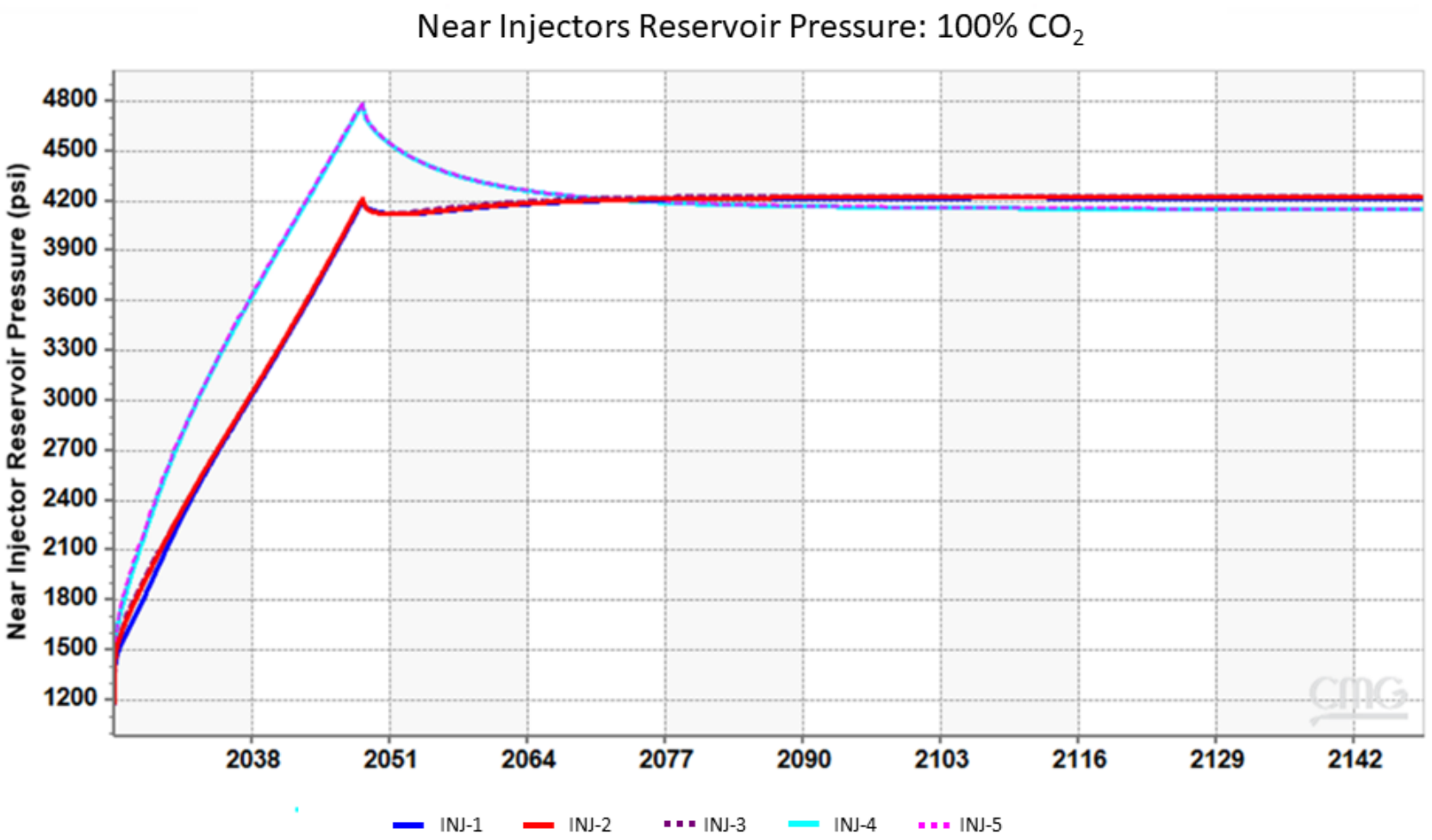

Figure B-19a. Near injectors reservoir pressure for 100% CO_2 case.

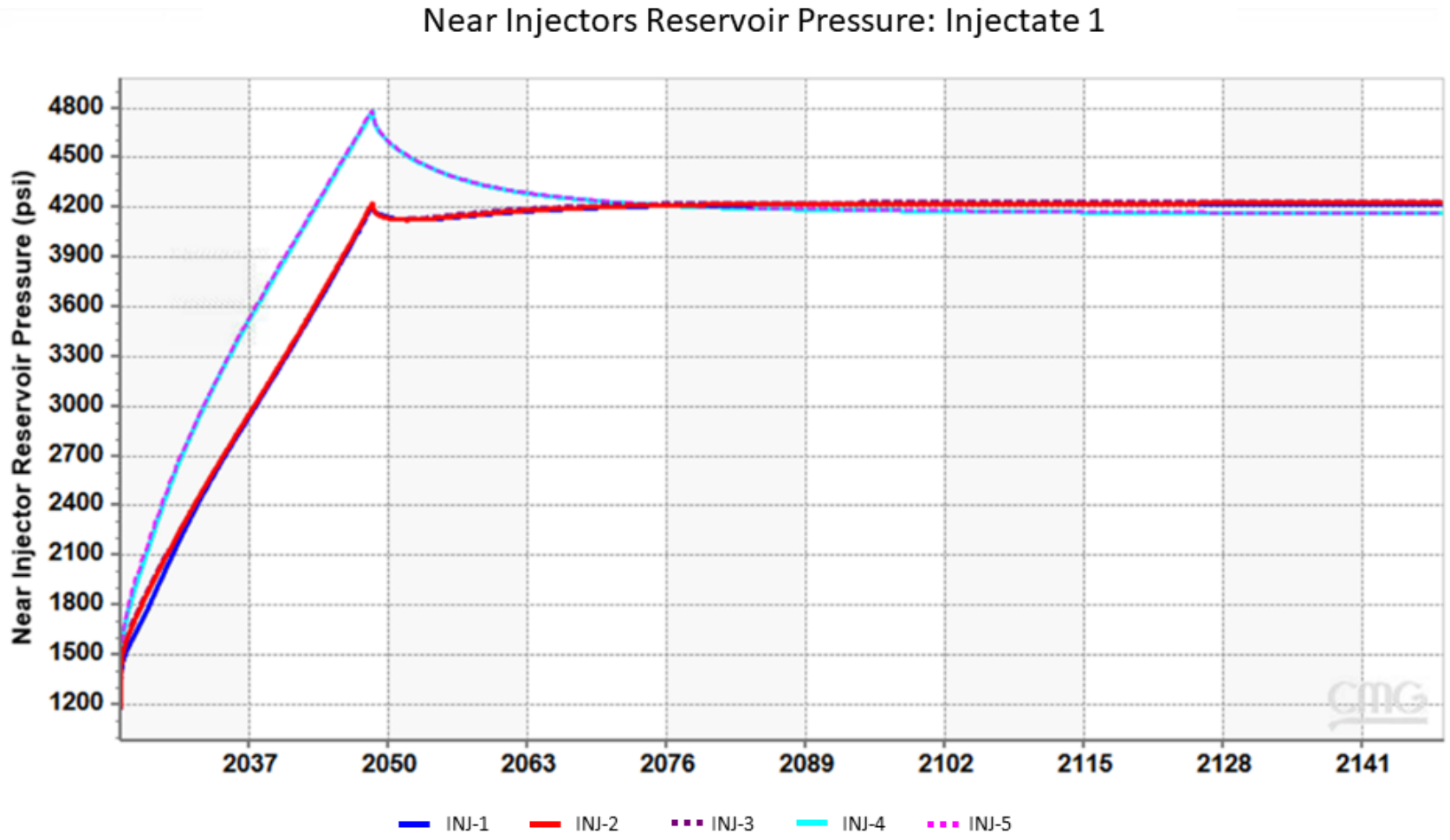

Figure B-19b. Near injectors reservoir pressure for Injectate 1.

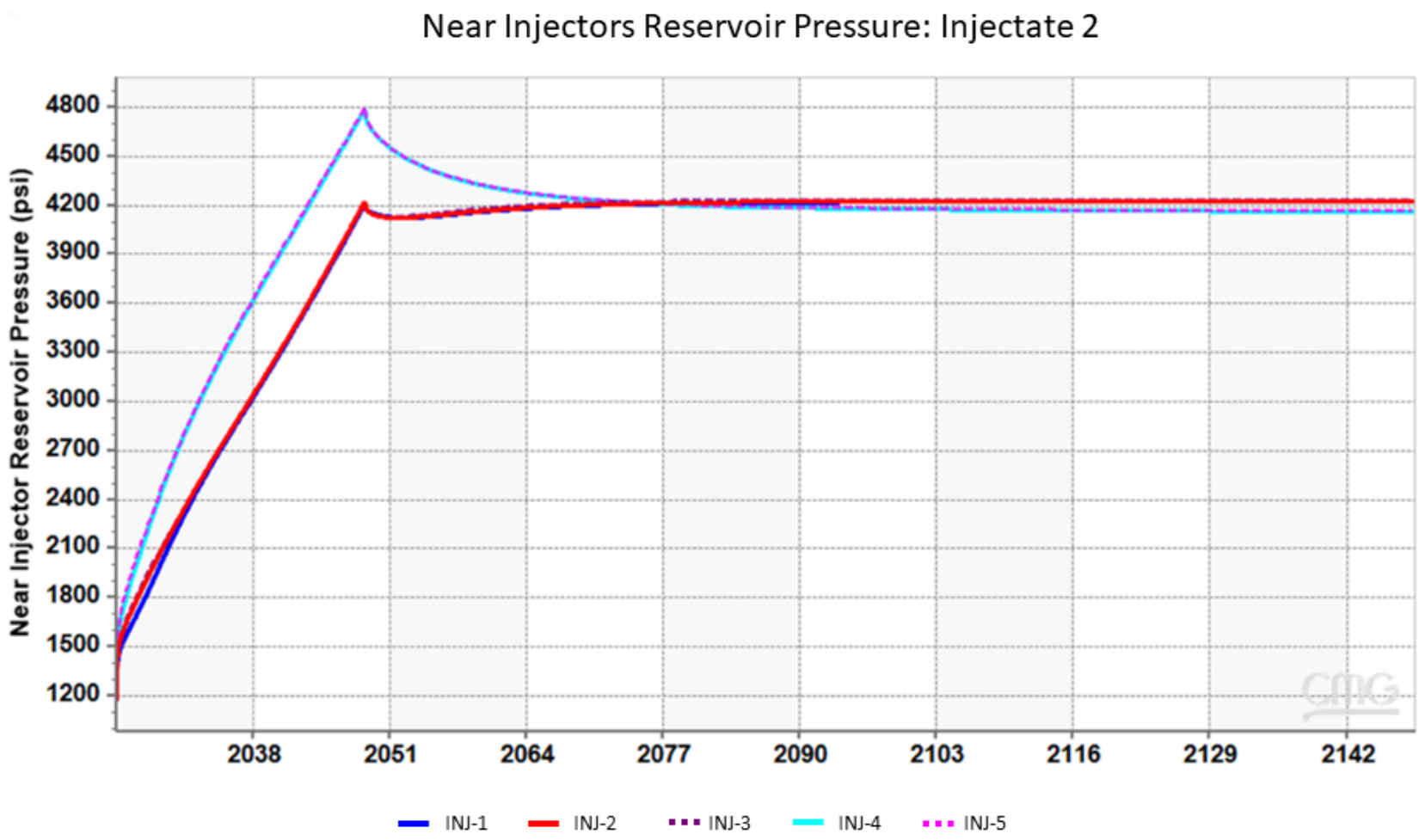

Figure B-19c. Near injectors reservoir pressure for Injectate 2.

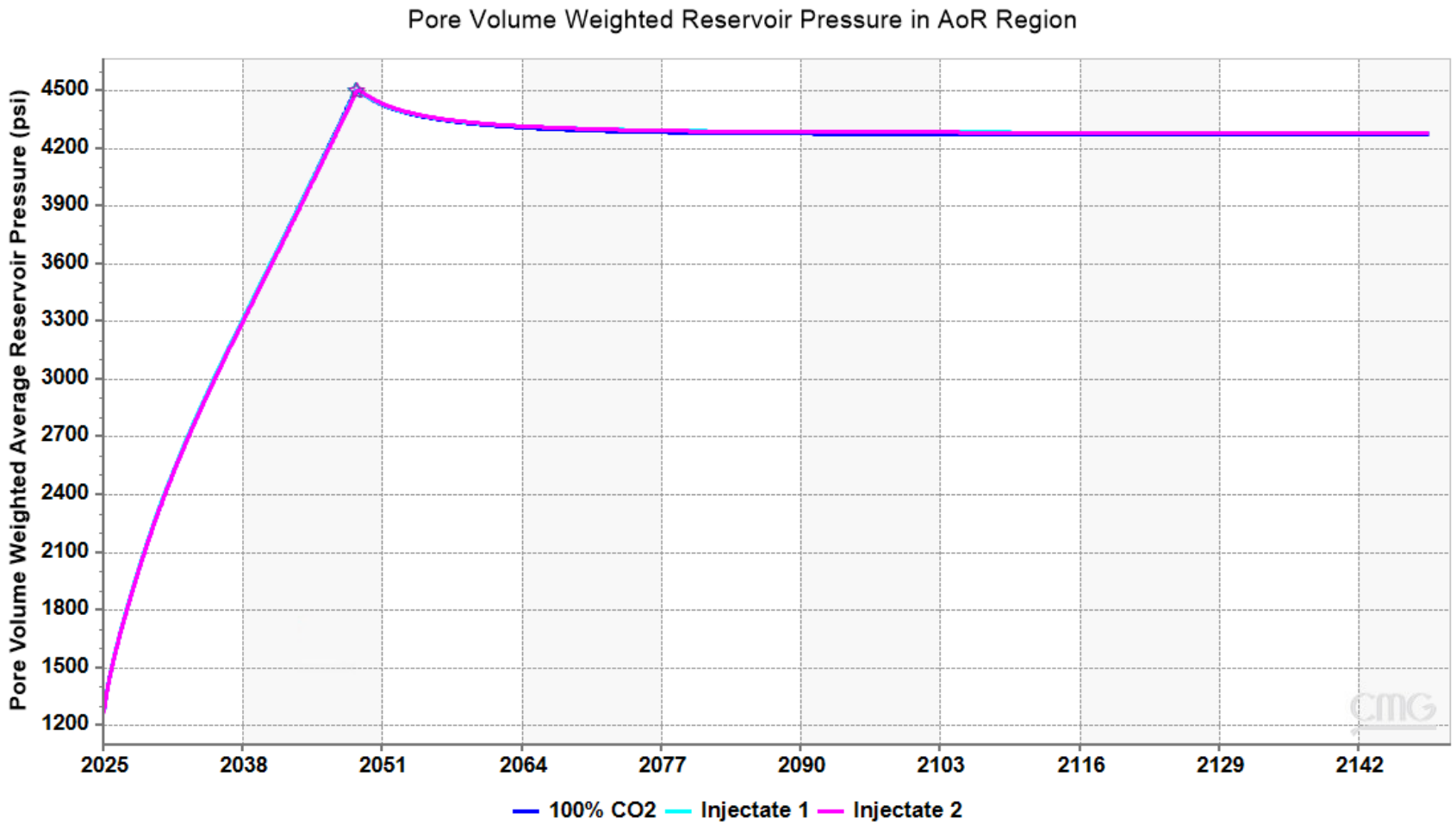

Figure B-20a. Average reservoir pressure within approximate AoR for Injectate 1, Injectate 2 and 100% CO2 cases. 100% CO_2 case and Injectate 2 case pressure trends plot almost on top of each other.

(A) Project Cumulative CO_2 Injection

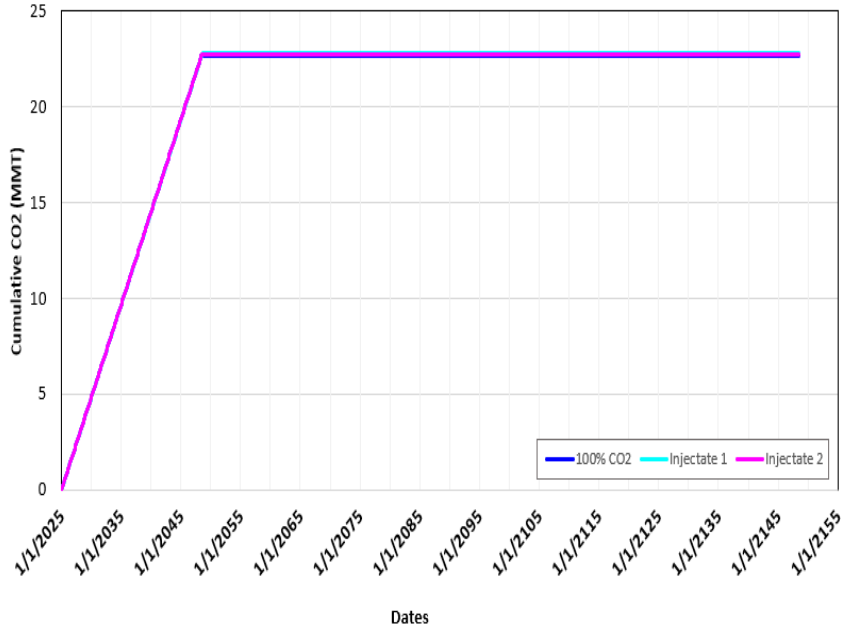

(B) Project CO_2 Injection Rate

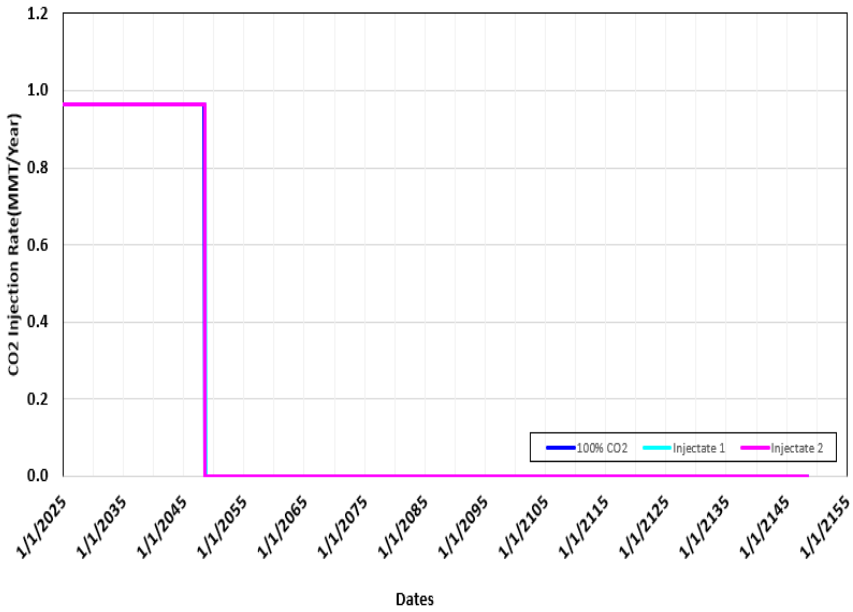

Figure B-20b. Project CO_2 cumulative injection and injection rate summary. Injectate 1 (Light Blue), Injectate 2 (Pink) and 100% CO_2 Cases (Dark Blue). They are overlay for all the 3 cases.

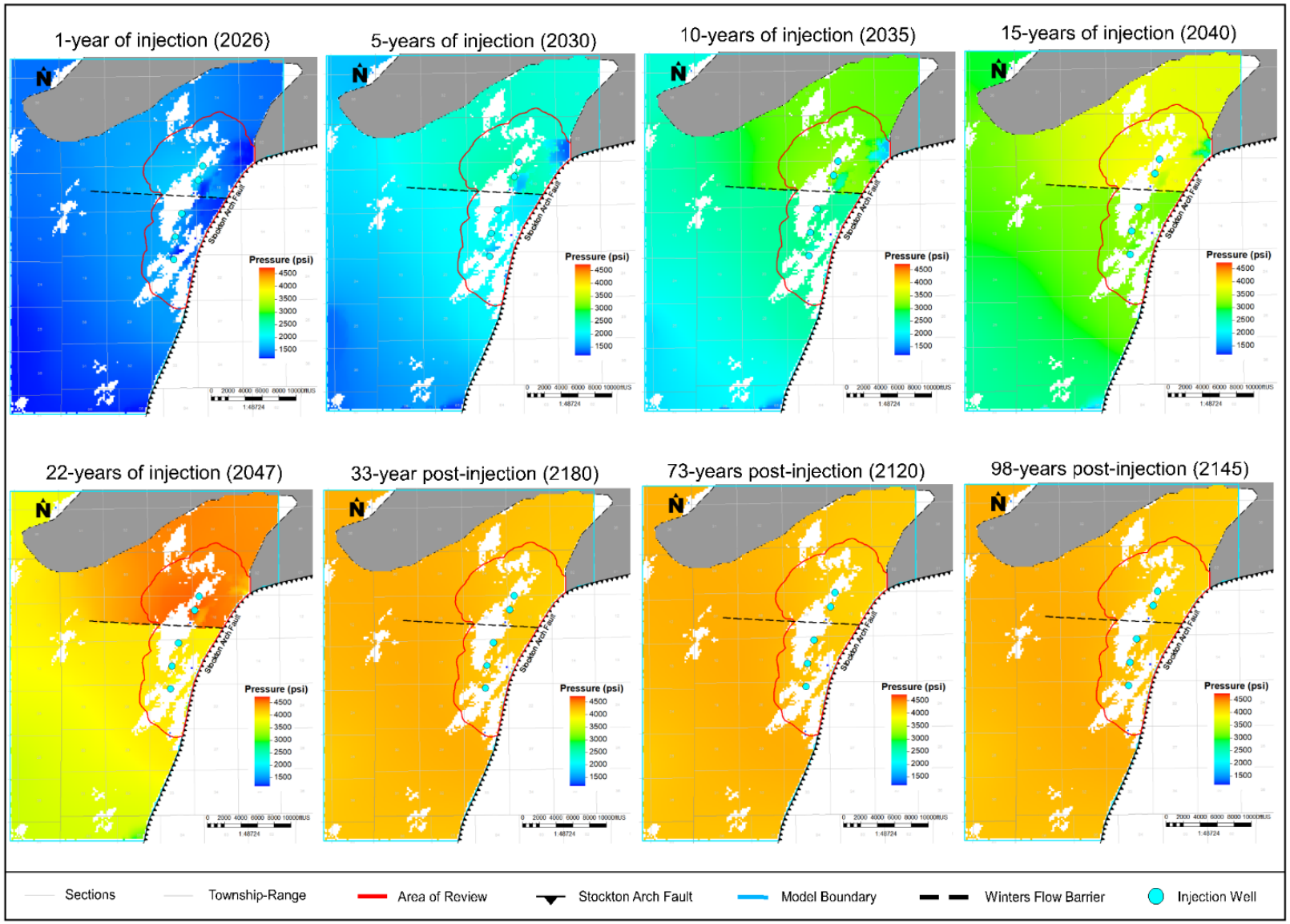

Figure B-21. Pressure through time.

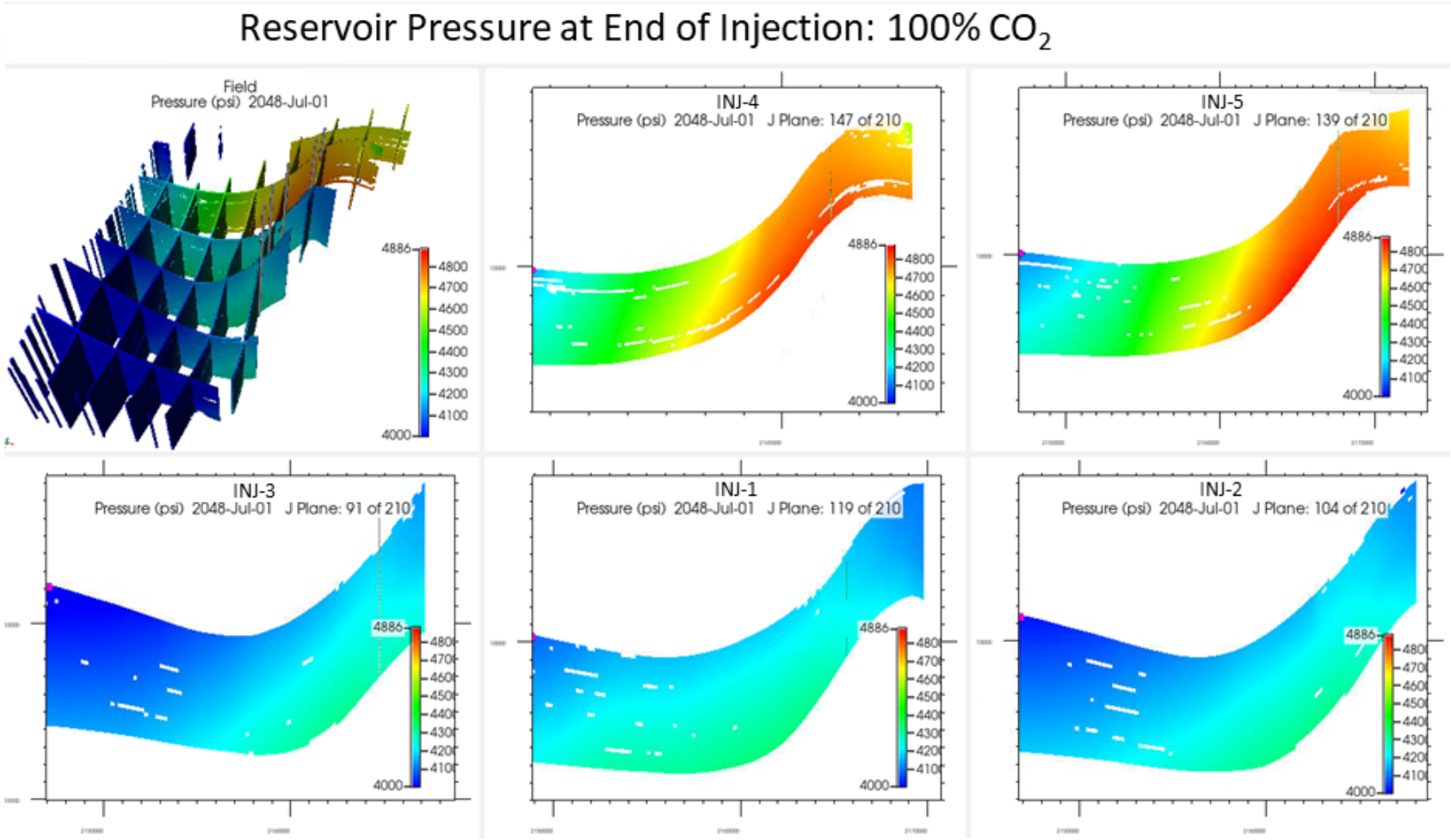

Figure B-22a. 100% CO_2 case field reservoir pressure. Each injector reservoir pressure cross section against the Stockton Arch Fault.

(A) Trapped CO_2

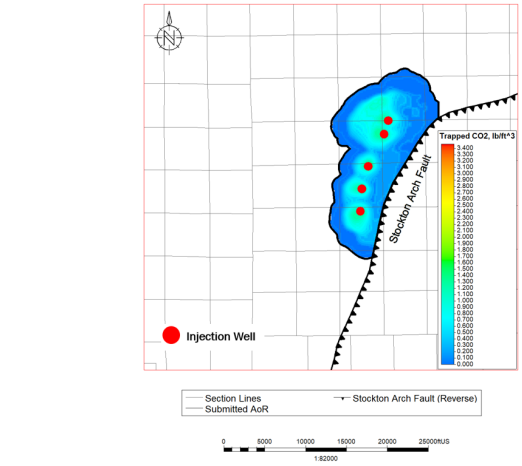

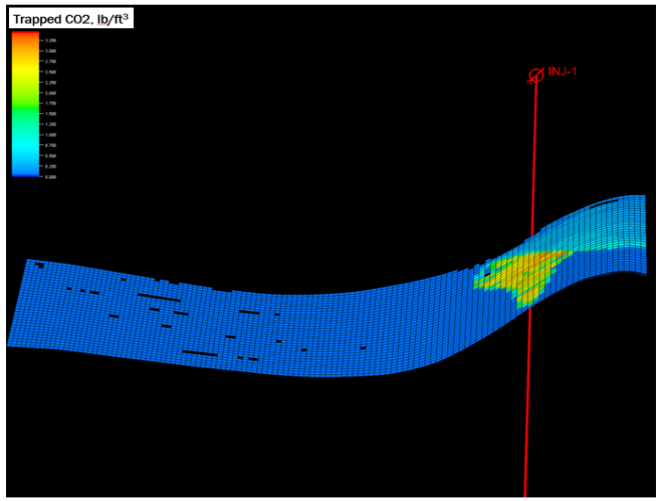

(B) Dissolved CO_2

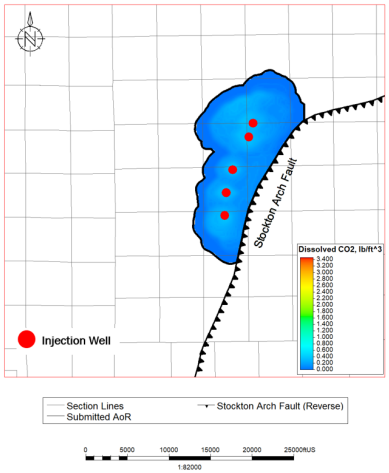

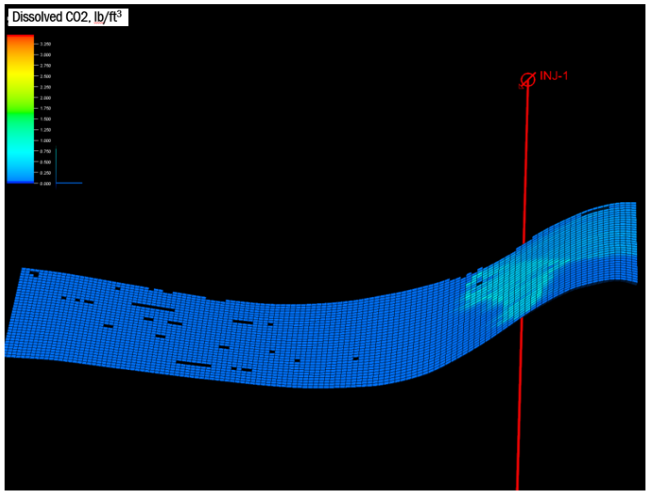

Figure B-22b. 100% CO_2 case trapped CO_2 and dissolved CO_2 distributions at 100 years post injection, lb/ft^3.

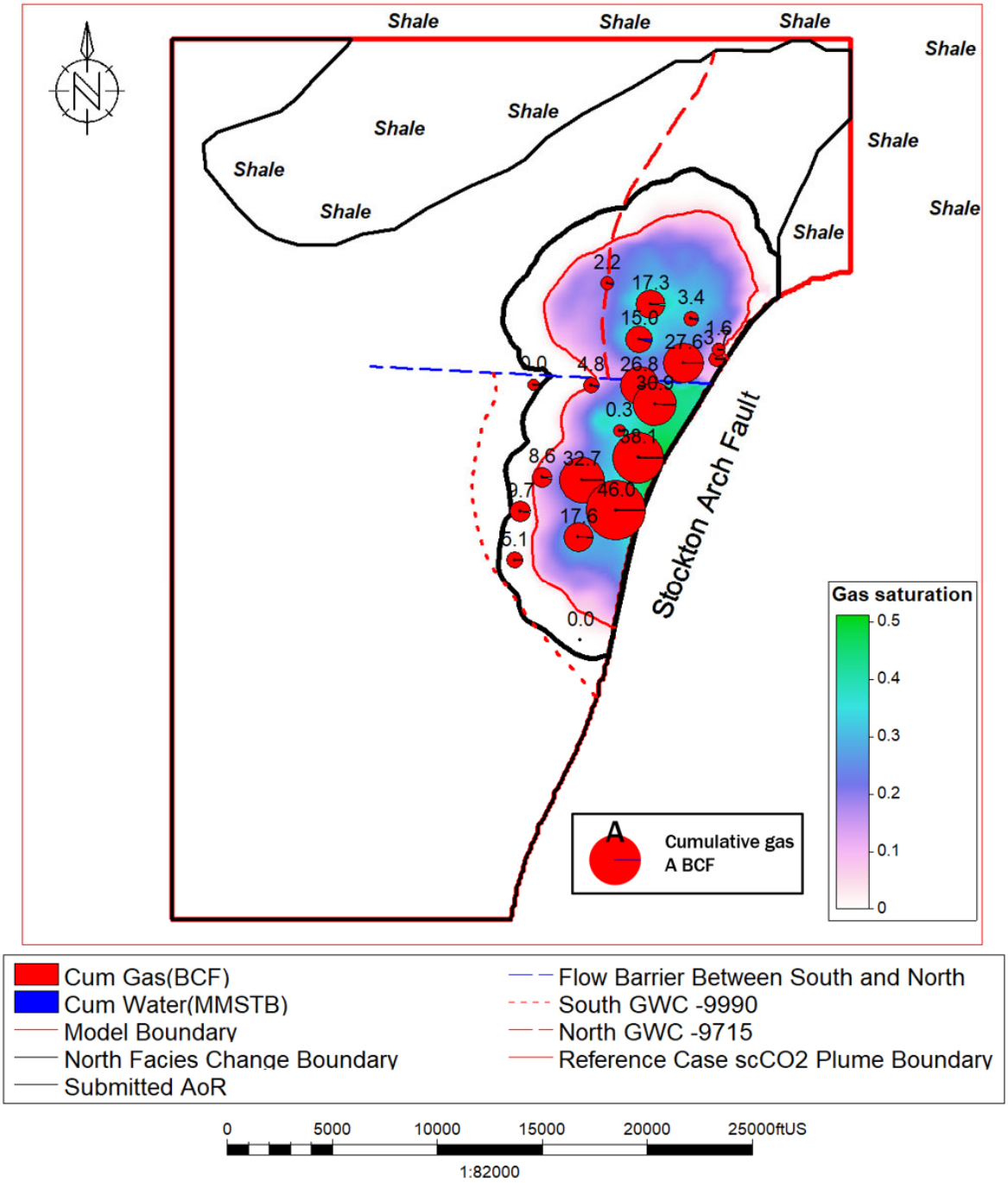

Figure B-23. Cumulative production, $scCO_2$ plume boundary and original gas-water contact (GWC) summary. $scCO_2$ plume boundary is defined by 0.05 gas saturation cutoff 100 years post injection. CO_2 plume is defined by 0.01 CO_2 global mole fraction cutoff 100 years post injection.

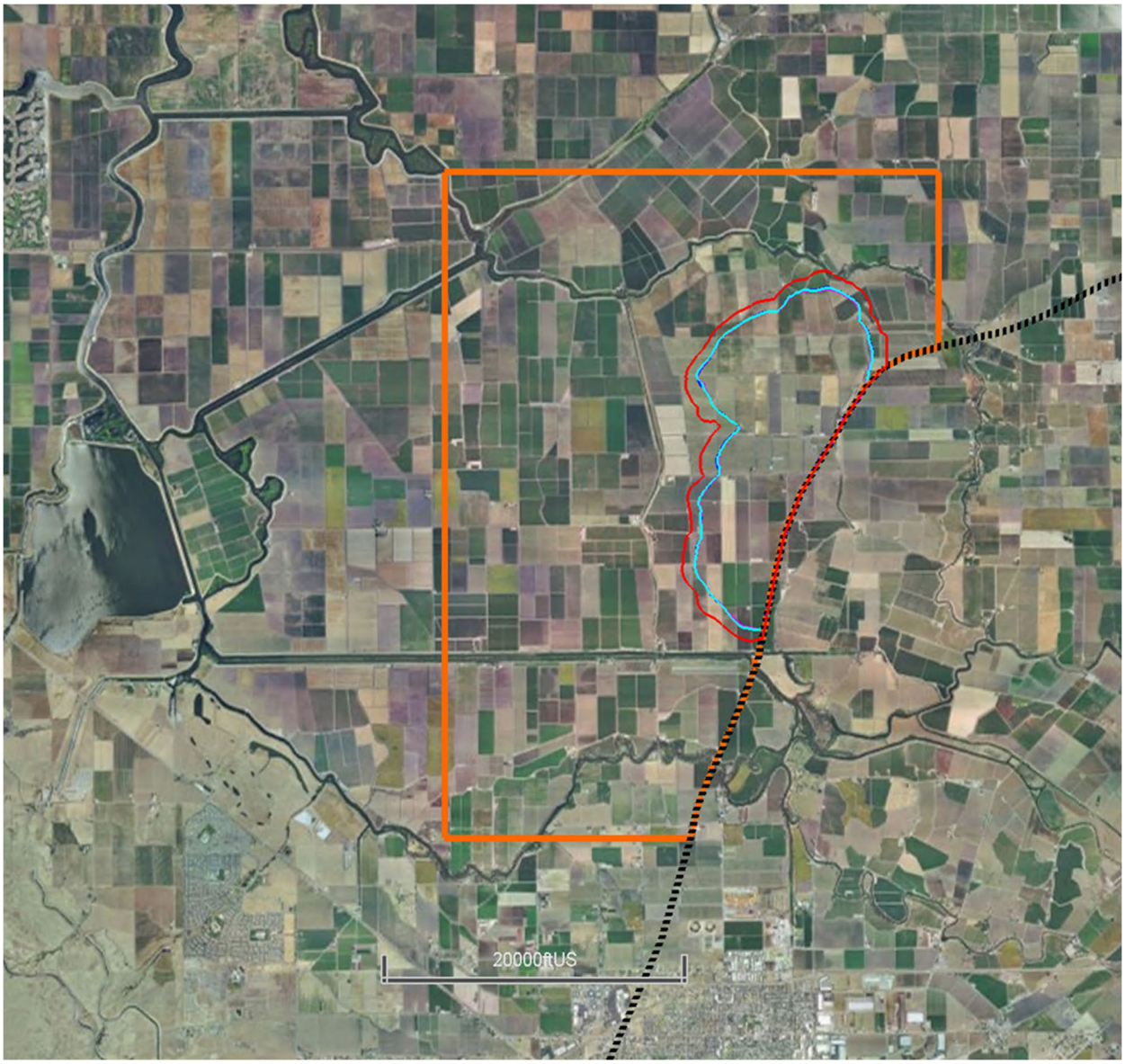

Figure B-24a. Submitted AoR boundary and CO_2 plume outlines. Injectate 1 (Light Blue), Injectate 2 (Pink) and 100% CO_2 Cases (Dark Blue). Larger orange outline is the model boundary. Minimal difference in plume boundaries between the 3 cases with the boundaries overlying each other for the most part. AoR (red) is plume boundary plus 500 feet buffer. CO_2 plume is defined by 0.01 CO2 global mole fraction cutoff, 100 years post injection.

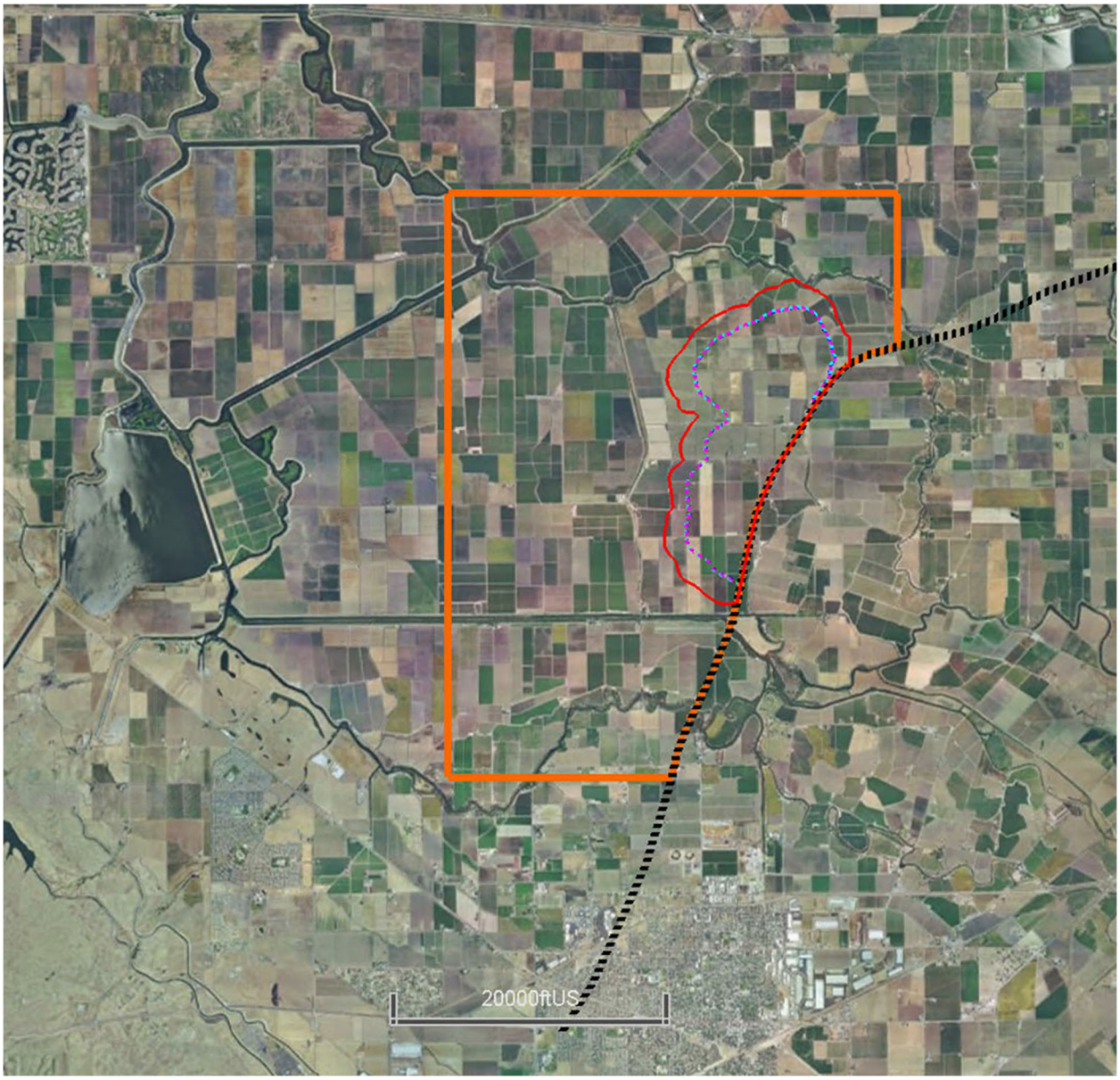

Figure B-24b. Submitted AoR boundary and $scCO_2$ plume outlines. Injectate 1 (Light Blue), Injectate 2 (Pink) and 100% CO_2 Cases (Dark Blue). Larger orange outline is the model boundary. Minimal difference in $scCO_2$ plume boundaries between the 3 cases with the boundaries overlying each other for the most part. AoR (red) is plume boundary plus 500 feet buffer. scCO2 plume boundary is defined by 0.05 gas saturation cutoff, 100 years post injection.

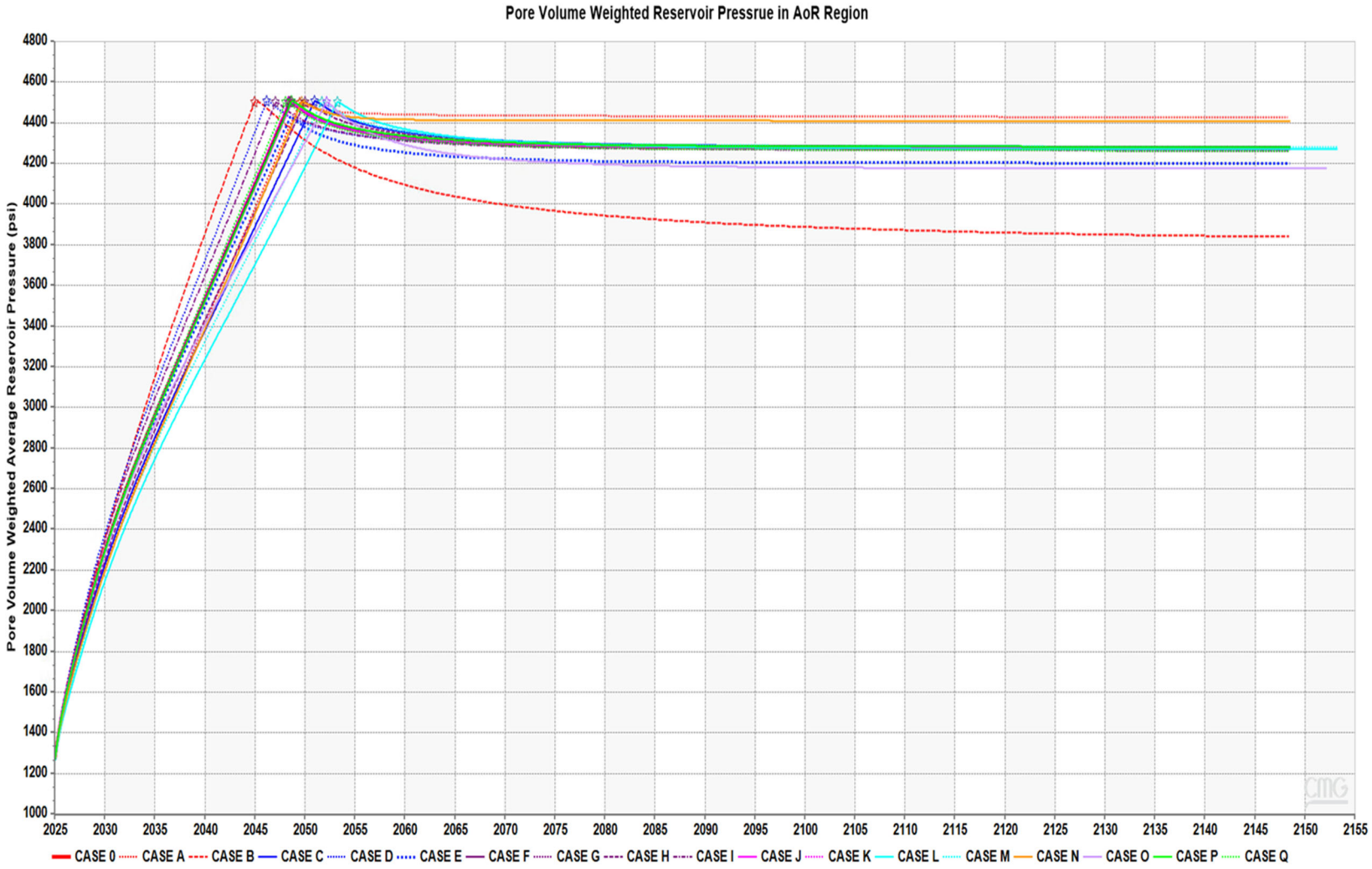

Figure B-25. Average reservoir pressure within approximate AoR for sensitivity analysis CASE A to CASE Q vs. reference case.

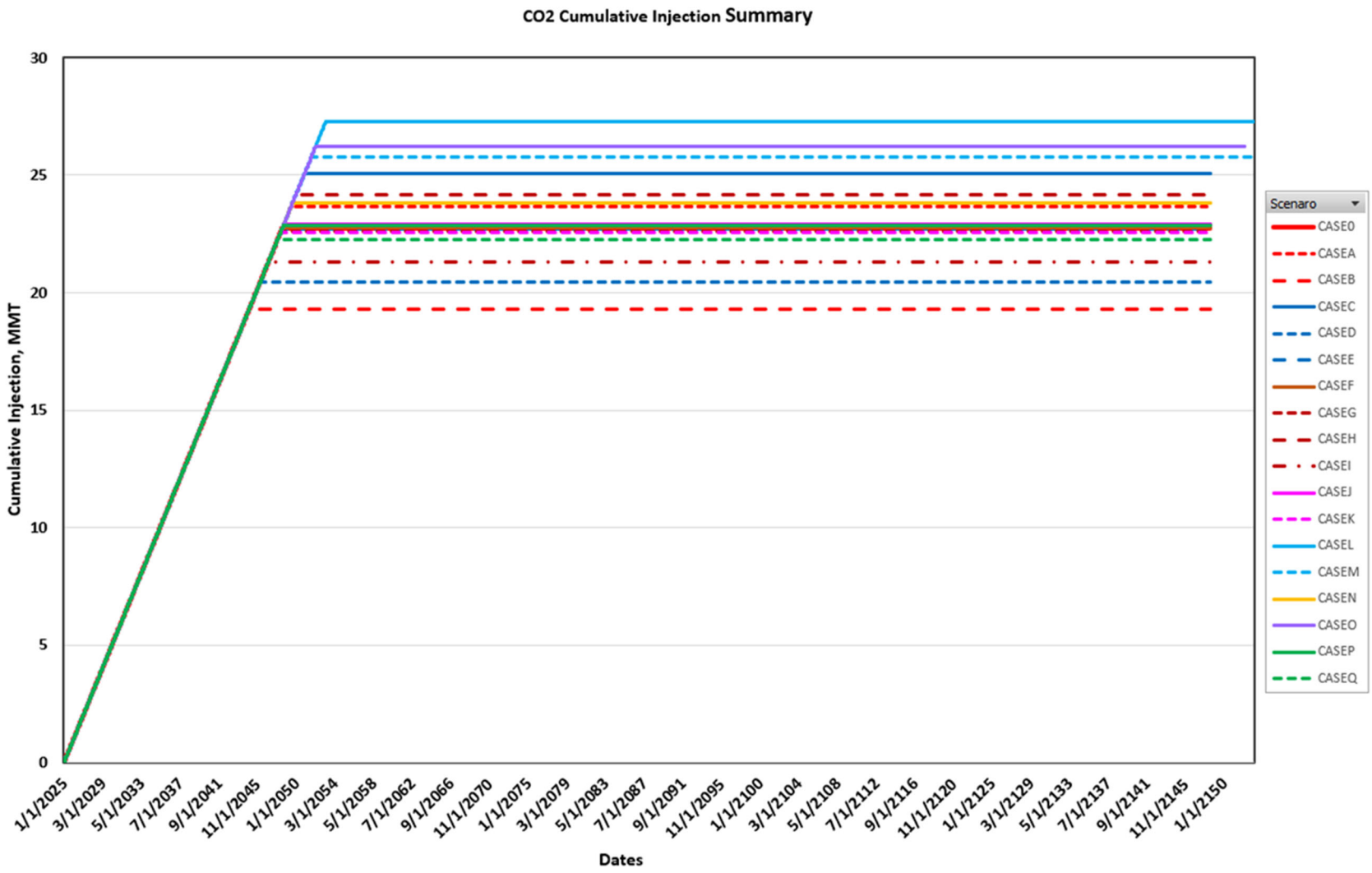

Figure B-26. Project CO_2 cumulative injection comparison for sensitivity analysis CASE A to CASE Q vs. reference case.

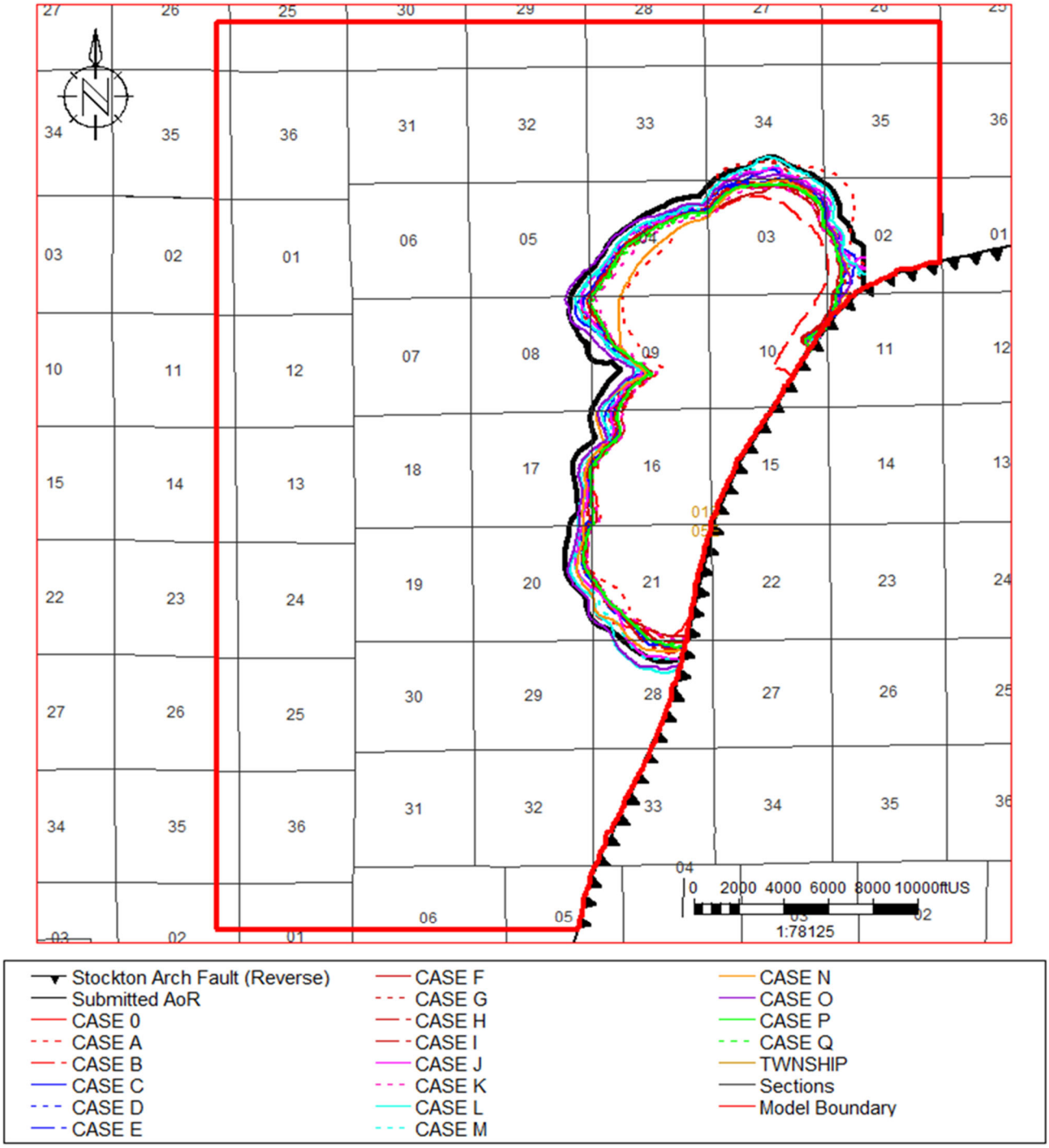

Figure B-27a. Submitted AoR boundary and CO_2 plume outlines for CASE A to CASE Q vs. reference case with 100% CO_2. Larger red outline is the model boundary. Minimal difference in plume boundaries for most scenarios except a couple extreme parameters case. AoR is plume boundary plus 500 feet buffer. CO2 plume is defined by 0.01 CO_2 global mole fraction cutoff 100 years post injection.

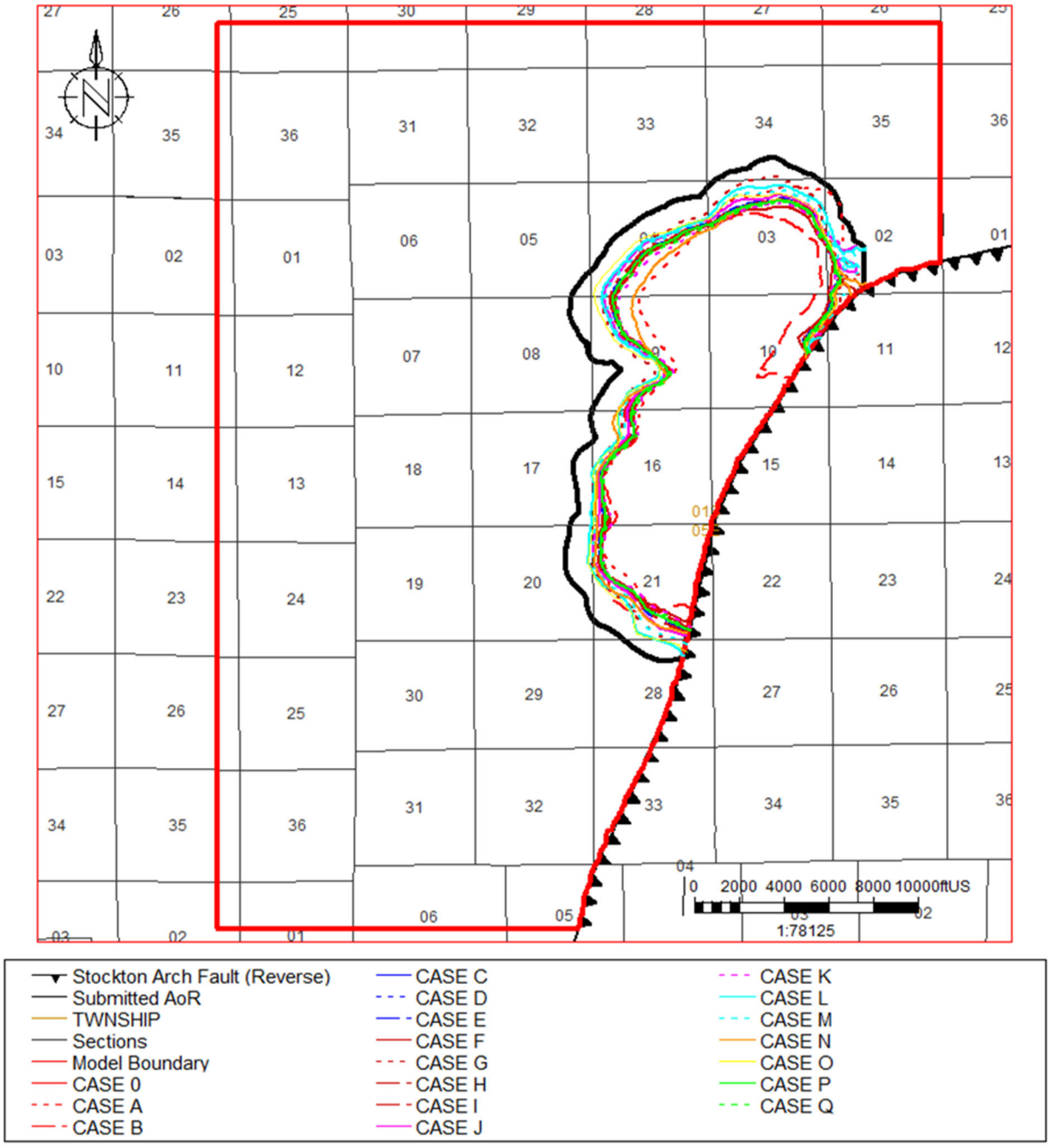

Figure B-27b. Submitted AoR boundary and scCO$_2$ plume outlines for CASE A to CASE Q vs. reference case with 100% CO$_2$. Larger red outline is the model boundary. Minimal difference in scCO2 plume boundaries for most scenarios except a couple extreme parameters case. AoR is plume boundary plus 500 feet buffer. scCO2 plume boundary is defined by 0.05 gas saturation cutoff 100 years post injection.

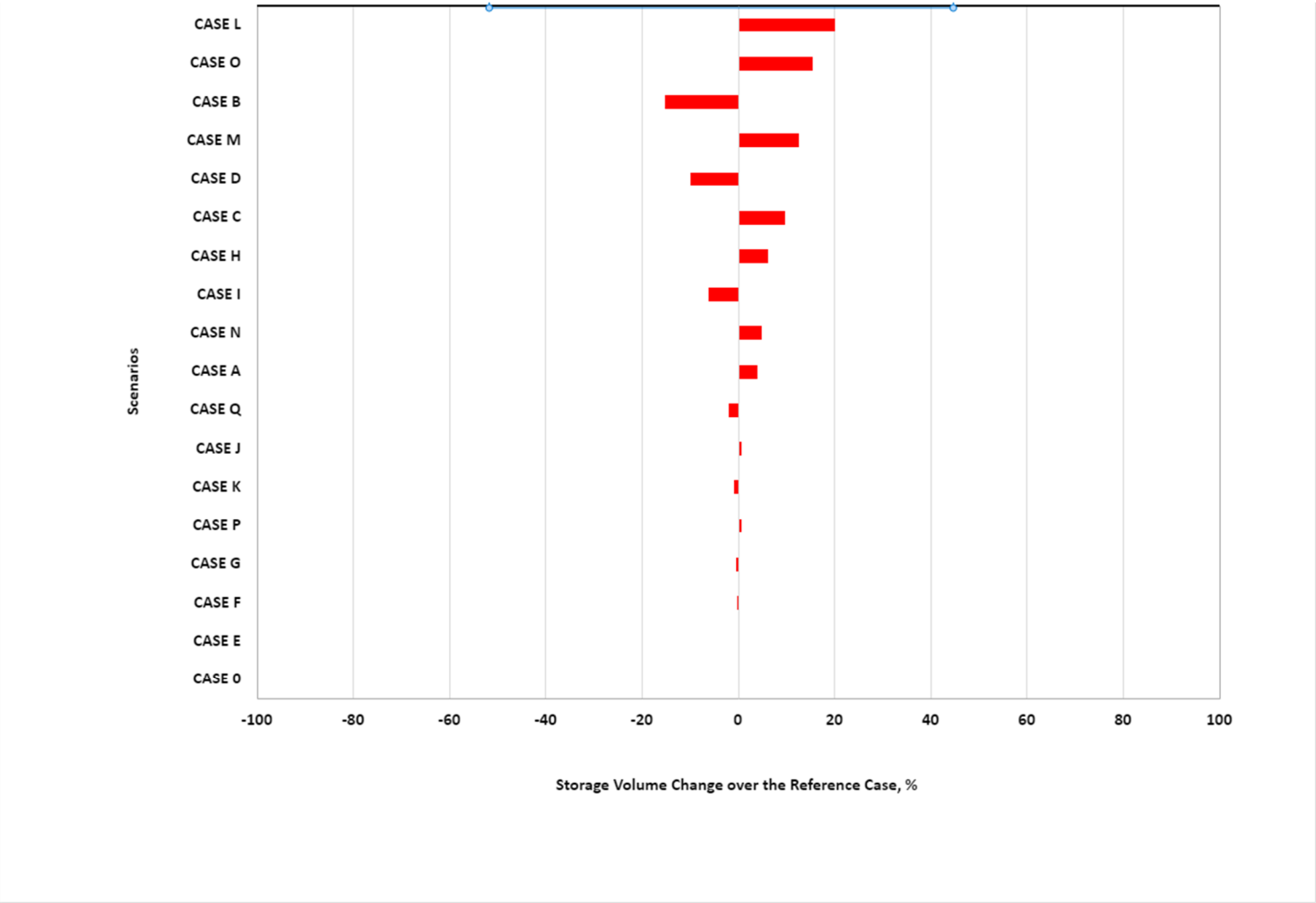

Figure B-28a. Sensitivity analysis Tornado chart for storage volume.

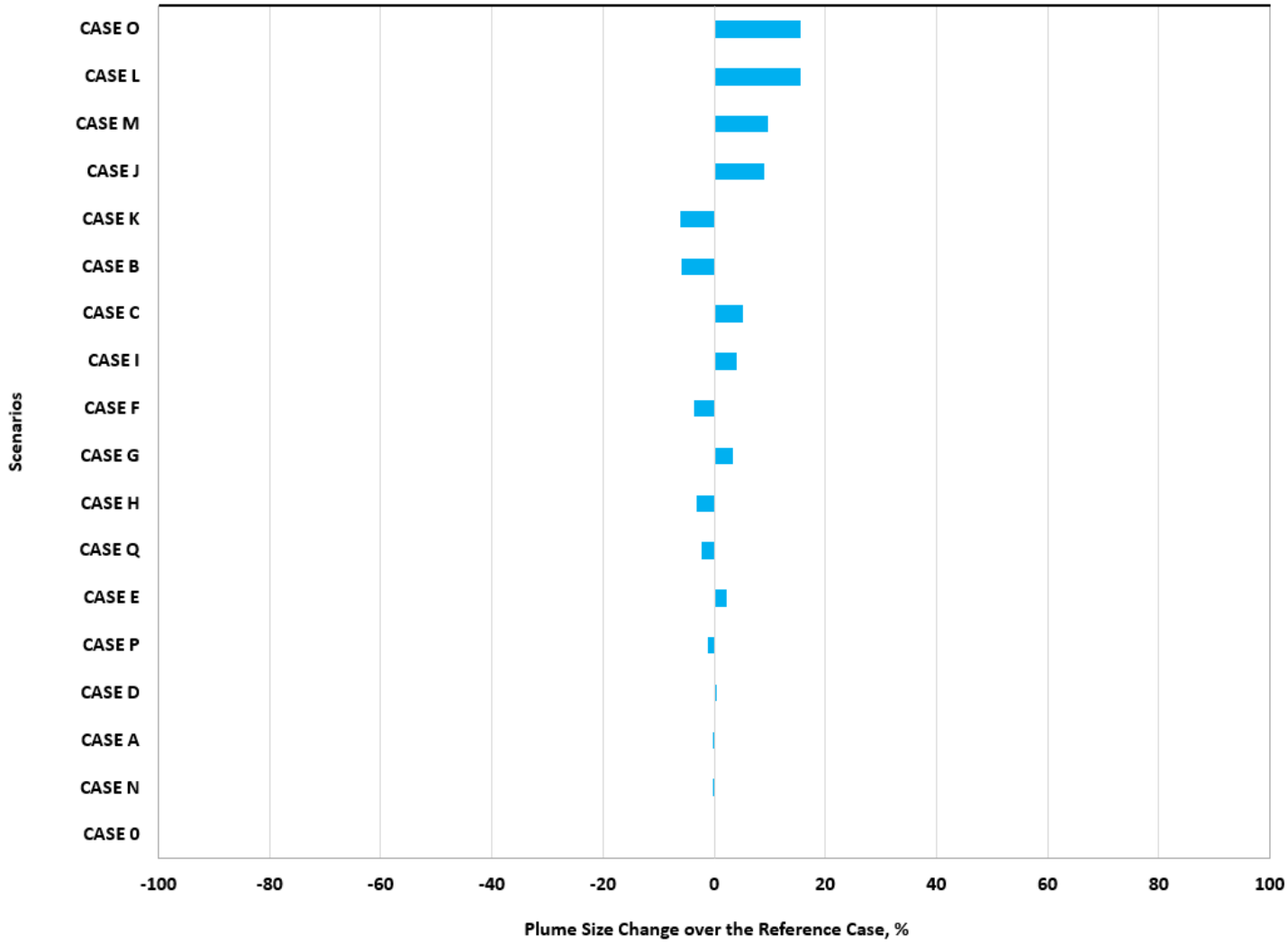

Figure B-28b. Sensitivity analysis Tornado chart for plume size.

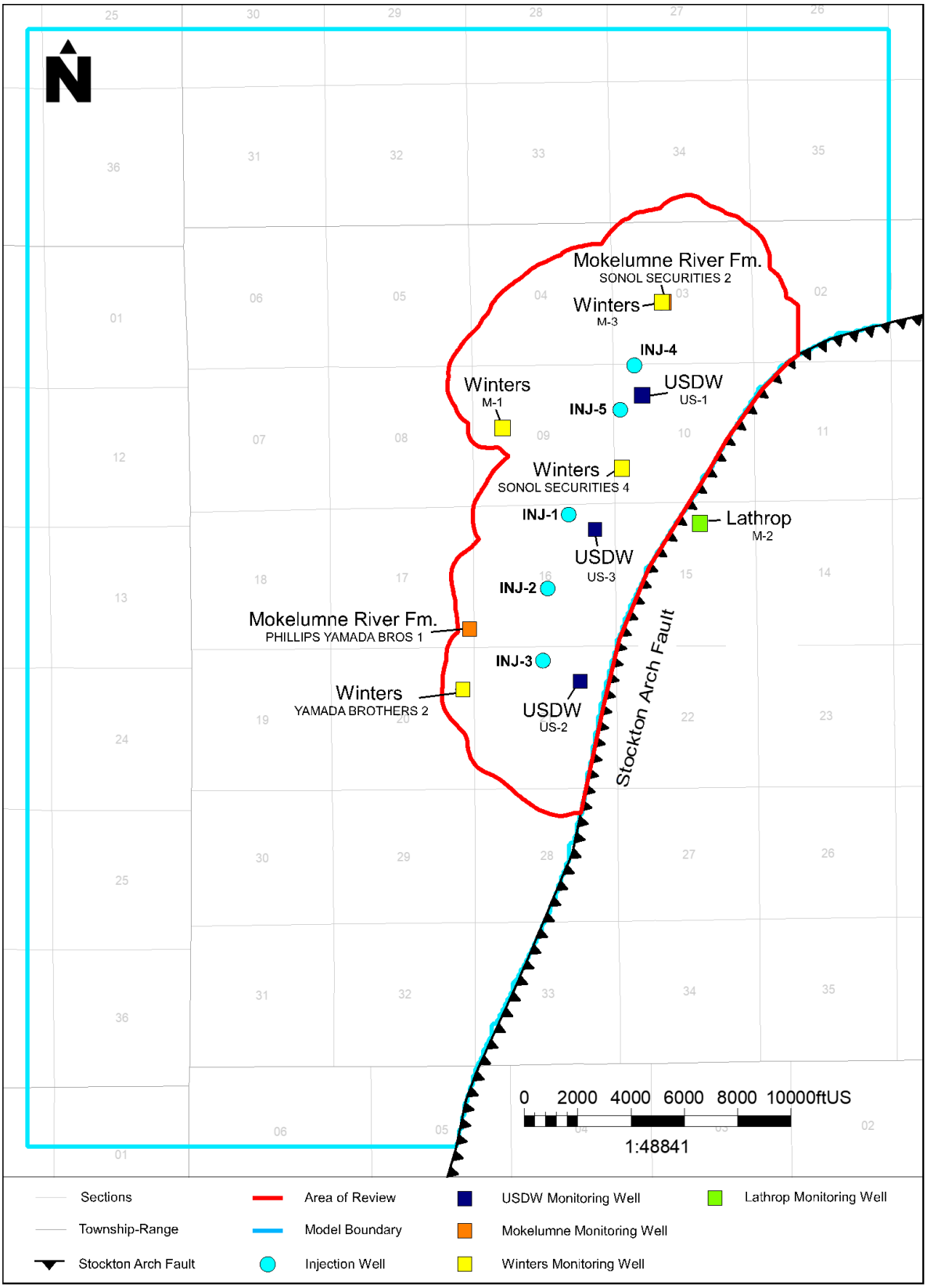

Figure B-29. Map showing the locations of injection wells and plume monitoring wells.

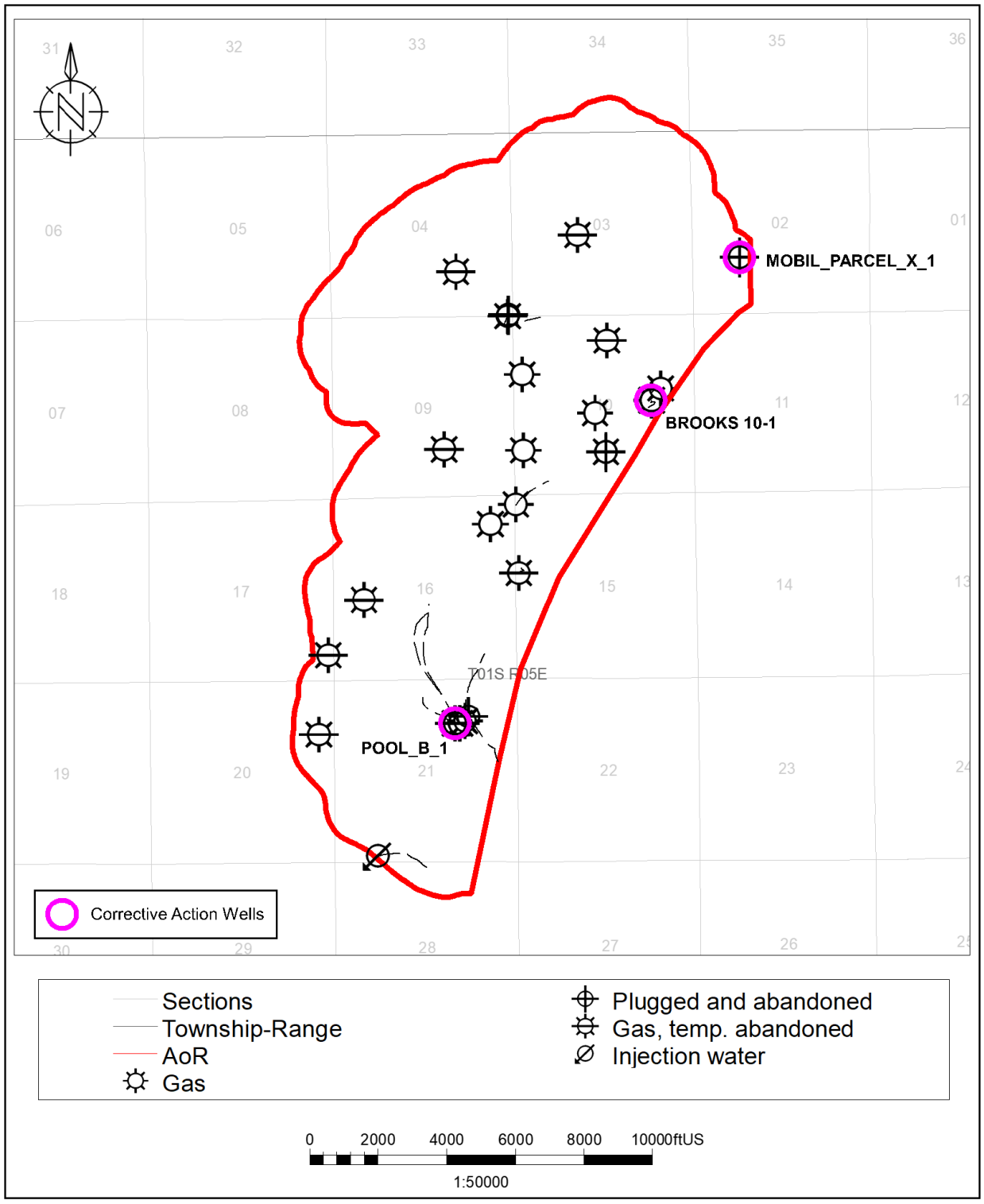

Figure B-30. Wells penetrating the Upper Confining Layer and the Injection Zone reviewed for corrective action. The wells requiring corrective action prior to injection are identified by a magenta circle.

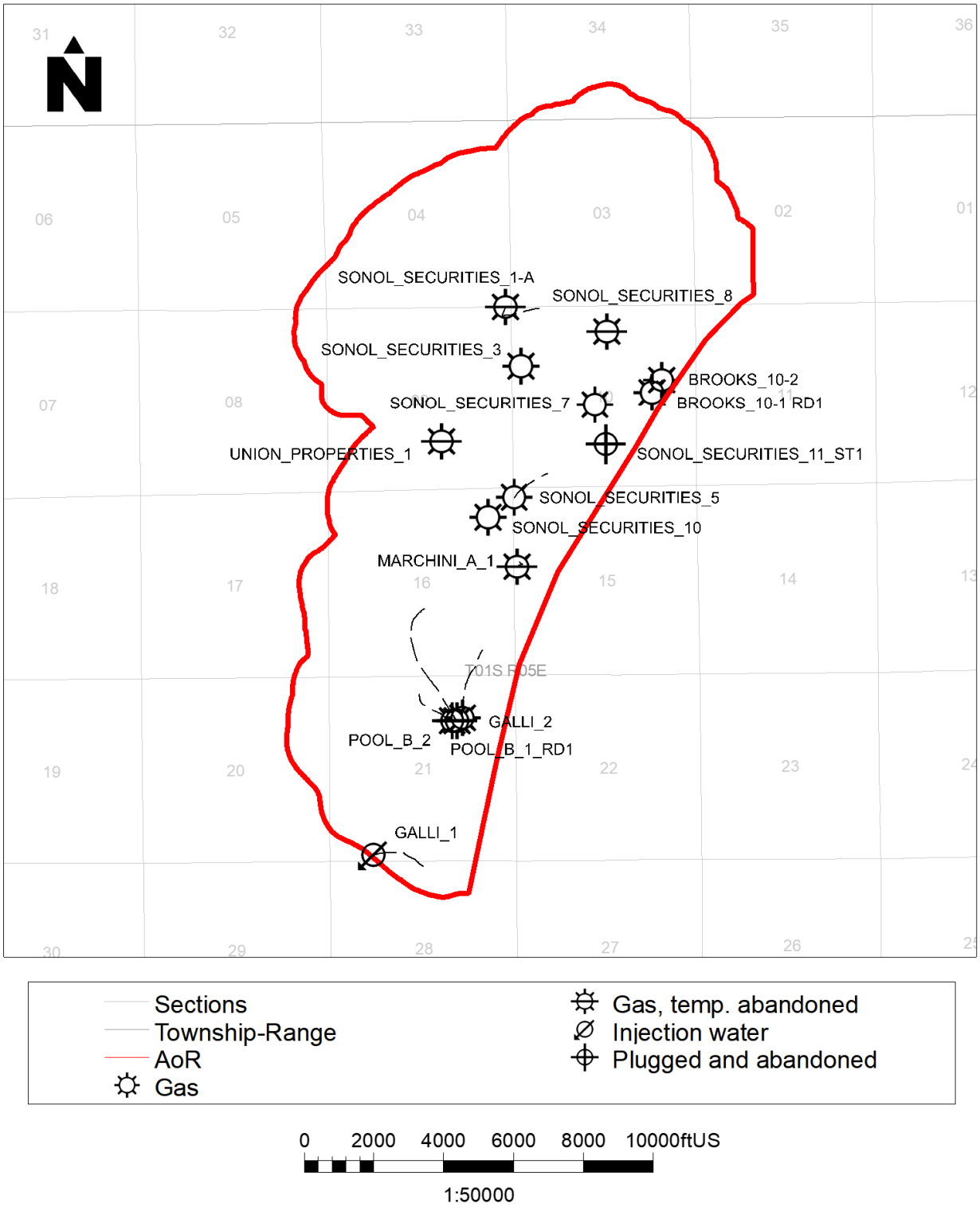

Figure B-31. Wells to be abandoned prior to injection.

Tables

Table B-1. Production Volumes for the Proposed Injection Zone at the Union Island Gas Field

Process	Phase	Volume
Production	Gas	292 billion cubic feet
	Water	3.4 million barrels

Table B-2. Model Domain Information

Coordinate System	California State Plane		
Horizontal Datum	North American Datum (NAD) 27		
Coordinate System Units	Feet		
Zone	Zone 2		
FIPSZONE	0402	ADSZONE	3301
Coordinate of X min	2,145,400.00	Coordinate of X max	2,177,700.00
Coordinate of Y min	44,800.00	Coordinate of Y max	86,700.00
Elevation of bottom of domain	-10,375	Elevation of top of domain	-9,492

Table B-3. Computational Model Input Parameters for Reference Case

Material	Parameters		Value	Notes
Winters Formation	Structure		Static Modeling	
	Porosity, fraction		Based on log and core data	
	Net to Gross Ratio		Facies analysis	
	Permeability, horizontal(md)		Based on transform	
	Permeability, vertical (md)		50% of horizontal permeability	
	Gas composition		SONOL_SECURITIES_5, 2022 fluid analysis	
	Component properties		Equation of state modeling	
	Relatve permeability and Capillary Pressure	Sgc	0	Connate gas saturation
		Sgcrit	0.05	Critical gas saturation
		Sgrmax, maximum residual gas saturation for Hysteresis	0.25	Maximum residual gas saturation(fraction), adjustable parameters which determins the imibiiiton krg curve as a function of the given drainage curve.
		SWCR, residual water saturation	0.34	During dynamic model, relative permeability and capillary pressure will scale up to the end point to each grid block.
		Krw at Sgc	0.447	
		Krg at Swc	0.32	
		NW	3.5	Water relative permeability curvature to gas displacement of Corey Model
		NG	2.6	Gas relative permeability curvature to water displacement of Corey Model
	Sg above current gas water contact		0.66	
	Sg below current gas water contact		0	Conservative case used based on delpleted dry gas reservoir with limited aquifer, reservoir pressure from 5040 psi to current 1200 psi. Sensitivity analysis done.

Table B-4. Gas and Water Contacts Used in the Computational Modeling Study

	North	South	Water Zone
Contact (depth in feet sub-sea)	Gas–water 9,600	Gas–water 9,800	
Saturation (fraction)	Water: 0.34 Gas: 0.66	Water: 0.34 Gas: 0.66	Water: 1.0

Values derived by open hole well logs, material balance analysis production analysis.

Table B-5. Initial Conditions (Start of CO_2 Injection)

Parameter	Value or Range	Units	Corresponding Elevation (ft msl)	Data Source
Temperature	218	degrees Fahrenheit	9,600	Pool B-2 pressure and temperature gradient measured in 2022; DOGGR (1998) for Union Island Field
Formation pressure	1,200	pounds per square inch	9,600	Pressure test; Pool B-2 pressure and temperature gradient measured in 2022.
Gas density	11.254	pounds per cubic foot	9,600	Equation of state (EOS) modeling
Water density	61	pounds per cubic foot	9,600	Equation of state (EOS) modeling
Salinity	15,000	parts per million	9,600	Water analysis (Sonol 4)

Table B-6. Operating Details

Operating Information	UI-INJ-4	UI-INJ-5	UI-INJ-3	UI-INJ-1	UI-INJ-2
Location (global coordinates) LAT/LONG	37.8690/ –121.4177	37.8636/ –121.4194	37.8383/ –121.4291	37.8533/ –121.4262	37.8457/ –121.4288
Model coordinates (ft) X/Y	2168121.14/ 74221.99	2167636.16/ 72273.25	2164903.30/ 63024.34	2165702.95/ 68502.85	2164946.41/ 65731.55
Perforated Interval (ft MD | TVD | msl) Z top Z bottom	9,618 | 9,577 | 9,576 9,891 | 9,848 | 9,847	9,601 | 9,597 | 9,596 9,907 | 9,903 | 9,902	9,833 | 9,749 | 9,746 10,231 | 10,142 | 10,139	9,905 | 9,782 | 9,760 10,173 | 10,049 | 10,027	10,465 | 9,755 | 9,732 10,845 | 10,103 | 10,080
Wellbore diameter (inches)	8.75	8.75	8.75	8.75	8.75
Planned injection period Start / End	2025 / 2048	2025 / 2048	2025 / 2048	2025 / 2048	2025 / 2048
Injection duration (years)	23.5	23.5	23.5	23.5	23.5
Injection rate (t/day)	530–794	530–794	530–794	530–794	530–794

Table B-7. Injection Pressure Details

Injection Pressure Details	UI-INJ-4	UI-INJ-5	UI-INJ-3	UI-INJ-1	UI-INJ-2
Fracture gradient (psi/ft)	0.70	0.70	0.70	0.70	0.70
Maximum bottomhole injection pressure (90% of fracture pressure) (psi)	6,033	6,046	6,142	6,163	6,146
Elevation corresponding to maximum injection pressure (ft TVD)	9,577	9,597	9,749	9,782	9,755
Elevation at the top of the perforated interval (ft TVD)	9,577	9,597	9,749	9,782	9,755
Average bottom hole injection pressure at top of perforations (psi)	3,344	3,352	3,009	2,960	3,005
Average bottom hole injection gradient at top of perforations (psi/ft)	0.35	0.35	0.31	0.30	0.31

Table B-8. Simulation Sensitivity Scenarios

Case	Description	Reference	Perturbation
0	Reference case		NA
A	Increased permeability based on transform 90th percentile; maintain anisotropy ratio	1, multiplier	3, multiplier
B	Decreased permeability based on transform 10th percentile; maintain anisotropy ratio	1, multiplier	0.3, multiplier
C	Increased porosity of Winter sands based on 75th percentile of measured values	1, multiplier	1.1, multiplier
D	Decreased porosity of Winter sands based on 25th percentile of measured values	1, multiplier	0.9, multiplier
E	Decreased porosity and increased compressibility based on compaction effects	1, multiplier	0.99, multiplier
		Compressibility, 2.5E-6 1/psi	Compressibility, 2.95E-6 1/psi
F	Increased phase trapping by increasing critical gas saturation of Winters sands	S_{gcrit} = 0.05	S_{gcrit} = 0.15
G	Reduced phase trapping by reducing residual gas saturation of Winters sands	S_{grmax} = 0.25	S_{grmax} = 0.05
H	Increased phase trapping by reducing residual water saturation of Winters sands	Sw_{cr} = 0.34	Sw_{cr} = 0.25
I	Decreased phase trapping by increasing residual water saturation of Winters sands	Sw_{cr} = 0.34	Sw_{cr} = 0.43
J	Changed the shape for relative permeability of Winters sand based on core data	NG=2.6	NG=1.6
		NW=3.5	NW=5.5
K	Changed the shape for relative permeability of Winters sand based on core data	NG=2.6	NG=4.5
		NW=3.5	NW=2.0
L	Gas trapping between the original GWC to current GWC	Sg=0	Sg=0.05
M	Gas trapping between the original GWC to current GWC	Sg=0	Sg=0.03
N	Grid orientation effects spatial discretization	Five-point spatial discretization	Nine-point spatial discretization
O	Boundary conditions	No-flow side boundary conditions	West and South are open boundary
P	Geothermal gradient effect	Constant temperature, 218 F	Temperature gradient, 0.0159561 F/ft
Q	Thermal effects	Isothermal	Non-Isothermal

Table B-9. Wellbores in the AoR by Status

Status	Count
Active Producer	5
Idle Producer	15
Plugged and Abandoned Producer	8
Total	**28**